UNIVERSITÉ DU QUÉBEC À CHICOUTIMI

MÉMOIRE PRÉSENTÉ À

L'UNIVERSITÉ DU QUÉBEC À CHICOUTIMI

COMME EXIGENCE PARTIELLE

DE LA MAÎTRISE EN SCIENCES DE LA TERRE

PAR

ALEXANDRE AUBIN

BSc. Ing

THE SCHAKALSBERG SEAMOUNT: PHYSICAL VOLCANOLOGY, STRUCTURE, ALTERATION AND MINERALIZATION

FÉVRIER 2004

Bibliothèque
Paul-Émile-Boulet

UQAC
Université du Québec
à Chicoutimi

Mise en garde/Advice

Afin de rendre accessible au plus grand nombre le résultat des travaux de recherche menés par ses étudiants gradués et dans l'esprit des règles qui régissent le dépôt et la diffusion des mémoires et thèses produits dans cette Institution, **l'Université du Québec à Chicoutimi (UQAC)** est fière de rendre accessible une version complète et gratuite de cette œuvre.

Motivated by a desire to make the results of its graduate students' research accessible to all, and in accordance with the rules governing the acceptation and diffusion of dissertations and theses in this Institution, the **Université du Québec à Chicoutimi (UQAC)** is proud to make a complete version of this work available at no cost to the reader.

L'auteur conserve néanmoins la propriété du droit d'auteur qui protège ce mémoire ou cette thèse. Ni le mémoire ou la thèse ni des extraits substantiels de ceux-ci ne peuvent être imprimés ou autrement reproduits sans son autorisation.

The author retains ownership of the copyright of this dissertation or thesis. Neither the dissertation or thesis, nor substantial extracts from it, may be printed or otherwise reproduced without the author's permission.

RÉSUMÉ

Les montagnes du Schakalsberg du Sperrgebiet en Namibie sont considérées comme partie intégrante de la Ceinture Néo protérozoïque de Gariep (745-550 Ma), qui est connue pour le gisement de métaux de base de Rosh Pinah (30 millions de tonnes, Zn-Pb-Cu-Ag). La zone étudiée, propriété EPL 2757 acquise par la compagnie sud-africaine Kumba Resources, fait partie du terrane de Marmora et s'étend de 28°00'00" à 28°07'30" sud, et de 16°30'00" à 16°37'30" est. La zone cartographiée représente un segment des montagnes du Schakalsberg dont la superficie est de 225 km^2. La cartographie par lithofaciès a révélé une succession à dominance volcanique d'une épaisseur d'environ 1.4 km qui présente les caractéristiques d'un mont sous-marin. La stratigraphie composite du secteur montre une séquence de haut fond dont la base est dominée par les roches volcaniques mafiques et où la partie supérieure est dominée par les roches volcanoclastiques.

Deux principaux lithofaciès et un lithofaciès subordonné sont associés avec le mont sous-marin du Schakalsberg et incluent : 1) lithofaciès volcanique mafique, 2) lithofaciès volcanoclastique, et 3) lithofaciès de brèche sédimentaire. Le lithofaciès de carbonates, identifié dans la zone à l'étude, est probablement l'équivalent latéral de la séquence de mont sous-marin, mais est séparé par une faille de chevauchement majeure. Le lithofaciès volcanique mafique, allant jusqu'à 1 km d'épaisseur, qui est composé exclusivement de coulées mafiques et roches intrusives mafiques, a été divisé en multiples faciès en se basant sur la nature des phénocristaux, la composition chimique et les relations de recoupement. Les faciès (i) aphanitique, (ii) microporphyrique, (iii) feldspath-phyrique, (iv) pyroxène±feldspath-phyrique, et (v) phonolitique sont des coulées sous-marines massives, cousinées, et bréchiques. Des joints columnaires ont été observés dans la portion massive des coulées et de gros tubes sont visibles par endroits. Les unités de brèche de coussins sont restreintes au faciès aphanitique qui est situé dans la partie supérieure du mont sous-marin. À l'opposé, les faciès à phénocristaux se retrouvent principalement à la base de la séquence. Le faciès volcanique intrusif de gabbro est considéré comme contemporain avec le volcanisme effusif sous-marin et se distingue par la géochimie des éléments majeurs, traces et terre rares.

Le lithofaciès volcanoclastique est la contrepartie autoclastique remaniée et explosive des coulées sous-marines et est divisé selon les faciès de (i) tuf, (ii) tuf à lapilli, et (iii) tuf à bloc. Le faciès de tuf d'une épaisseur de 0.10 à 90 m, composé de fins lits parallèles et granoclassés qui peuvent être dérivés d'explosions sous-marines ou d'un processus de granulation thermique, a été déposé via des courants de turbidité dilués et des dépôts de suspension. Le faciès de tuf à lapilli, d'épaisseur de 0.20 à 1.5 m, est composé de lits massifs à granoclassés et des lits à lamination parallèle à entrecroisée, le premier étant le résultat de (re)déposition de coulées trubiditiques de haute concentration et de coulées de masse, tandis que le dernier est considéré comme un dépôt pyroclastique primaire produit par des courants de densité alimentés par les éruptions. Le faciès de tuf à bloc, ayant une population hétérolithique de fragments, est un dépôt volcanoclastique remanié que a été transporté du sommet vers les pentes par un processus de coulée de débris laminaire. Le

lithofaciès de brèche sédimentaire est observé seulement dans le faciès de tuf de 90 m et est considéré comme un dépôt de coulée de masse relié à du glissement synsédimentaire.

La caractéristique frappante des montagnes du Schakalsberg est l'altération hydrothermale pénétrante en carbonate qui peut être tracée sur au moins 20 km. L'altération est bien développée dans la partie supérieure de la séquence stratigraphique en raison de la prédominance du lithofaciès volcanoclastique. L'organisation d'altération semi-conforme est commune aux dépôts de sulfures massifs archéens de type Mattabi. L'assemblage d'altération est composé de calcite ($CaCO_3$), dolomite [$CaMg(CO_3)_2$] dolomite ferrifère [$Ca(Mg,Fe)(CO_3)_2$], avec une augmentation du contenu en Mg et Fe du nord-ouest au sud-est à l'échelle de la propriété. Cet assemblage, considéré comme l'équivalent du halo d'altération distale (calcite) à intermédiaire (clacite-dolomite ferrifère) des gisements de type Mattabi, est compatible avec les patrons d'altération de fonds sous-marin anciens et modernes. L'altération en carbonates a été produite par la circulation dans l'édifice du mont sous-marin de fluides hydrothermaux riches en CO_2. La source supposée pour le $(CO_3)^{-2}$ est le lithofaciès de carbonate, car il est l'équivalent latéral du mont sous-marin du Schakalsberg .

Deux types de minéralisation ont été identifiés: 1) minéralisation en Fe composée de (i) aiguilles, μm à mm, d'hématite (Fe_2O_3) disséminées dans la matrice des roches volcaniques, et (ii) remplacement de la magnétite (Fe_3O_4) par de l'hématite (Fe_2O_3) le long des plans de clivage, et 2) minéralisation en manjiroite, [$(Na,K)(Mn^{4+}, Mn^{2+})_8O_{16}\cdot n(H_2O)$], oxyhydroxydes de Mn, en amas massifs ou bréchiques de 2 à 6m d'épais et traçable jusqu'à 1 km en longueur. La minéralisation en Fe est une minéralisation de basse température qui a été déposée dans un environnement oxydant, avec les roches carbonatisées agissant comme scellant. Cette minéralisation pourrait représenter une phase distale, de basse température, d'un gisement de SMV. La minéralisation en Mn est supergène et a été produite par la percolation de fluide et le lessivage des roches avoisinantes après la déformation du mont sous-marin (quaternaire?).

L'évolution structurale du segment des Montages du Schakalsberg est compatible avec une ceinture de plissement et de chevauchement qui a été subséquemment sujette à une transpression senestre. La structure dominante est la faille de chevauchement des Red Dunes qui sépare le lithofaciès de carbonate d'avec la séquence à prédominance volcanique des montagnes du Schakalsberg. Cette faille de chevauchement a une attitude et des linéations d'étirement compatibles avec un mouvement du sud sur le nord. La zone à l'étude a été divisée selon la schistosité principale (Sp) en trois domaines structuraux: (i) domaine 1 avec un Sp moyen de 158/84, (ii) domaine 2 de 355/65 et (iii) domaine 3 de 149/40.

La zone à l'étude du Schakalsberg montre l'évolution d'un mont sous-marin précambrien pendant l'ouverture de la mer d'Adamastor (proto-Atlantique). Une altération hydrothermale pénétrante en carbonates avec des zones locales de minéralisation en Fe a été observée. La minéralisation est principalement restreinte aux unités volcanoclastiques poreuses qui forment supposément la partie de haut-fond de la séquence de mont sous-marin. La zone étudiée est le premier exposé détaillé d'une séquence volcanique-volcanoclastique dans le Sperrgebiet de Namibie.

ABSTRACT

The Schakalsberg Mountains of the Sperrgebiet in Namibia are considered an integral part of the ca. 740-550 Ma Neoproterozoic Gariep Belt, which is renowned for the ca. 30 million tonne Zn-Pb-Cu-Ag Rosh Pinah base metal deposit. The study area is part of the Marmora terrane and the concession EPL 2757, acquired by Kumba Resources, South Africa, is located at 28°00'00" to 28°07'30" S, 16°30'00" to 16°37'30" E. The mapped area represents a segment of the Schakalsberg Mountains that covers 225 km^2. Lithofacies mapping revealed a ca. 1.4 km-thick volcanic-dominated succession that displays the salient characteristics of an oceanic seamount. The composite stratigraphy of the Schakalsberg area represents an upward shoaling sequence in which mafic volcanic flows dominate the base and volcaniclastic rocks are prevalent at the top of the succession.

Two principal lithofacies and one subordinate lithofacies are associated with Schakalsberg seamount construction including: 1) a mafic volcanic lithofacies, 2) a volcaniclastic lithofacies, and 3) a sedimentary breccia lithofacies. A carbonate lithofacies recognized in the study area is probably the lateral equivalent of the seamount sequence, but they are now separated by a major thrust fault. The up to 1 km-thick mafic volcanic lithofacies, composed of lava flows and mafic intrusive rocks, has been divided into several facies based on phenocryst content, chemical composition and cross-cutting relationships. The (i) aphanitic, (ii) microporphyritic, (iii) feldspar-phyric, (iv) pyroxene±feldspar-phyric, and (v) phonolitic volcanic facies are submarine massive, pillowed, and pillow breccia flows. Columnar joints, observed in massive portions of flows and large pillow tubes, represent master tubes, and are locally exposed and traceable for 10's of metres. Extensive pillow breccia units are characteristic of the aphanitic volcanic facies, which is located in the upper part of the seamount succession. In contrast, the phenocryst-rich volcanic facies are predominant at the base of the sequence. The intrusive gabbro volcanic facies is considered coeval with effusive submarine volcanism as is borne out by the major, trace element and rare earth element geochemistry.

The volcaniclastic lithofacies is the reworked autoclastic and explosive fragmental counterpart of the subaqueous lava flows and is divided into (i) tuff, (ii) lapilli tuff, and (iii) lapilli tuff breccia facies. The 0.10-90 m-thick tuff facies, composed of thin parallel laminated and graded beds that may be derived from subaqueous explosions or thermal granulation processes, was deposited via dilute turbidity currents and suspension deposits. The 0.20-1.50 m-thick lapilli tuff facies contains both massive to graded beds and planar to cross beds. The former facies resulted from (re)deposition of high-concentration turbidites and mass flows, whereas the latter is considered a primary pyroclastic deposit produced by subaqueous eruption-fed density currents. The lapilli tuff breccia facies, which has a heterolithic clast population, is a reworked volcaniclastic deposit from the summit of the edifice that has been transported downslope via laminar debris flow processes. The sedimentary breccia lithofacies with angular tuff rip-up clasts is only observed in the 90 m-thick tuff facies and is considered a mass flow deposit, related to synsedimentary slumping.

The striking characteristic of the Schakalsberg Mountains is the pervasive hydrothermal carbonate alteration that can be traced for at least 20 km along strike. The alteration is well-developed in the upper part of the stratigraphy where the volcaniclastic lithofacies is predominant.The semi-conformable alteration pattern is common to Archean massive sulphide deposits, referred to as Mattabi-type. The carbonate alteration assemblage consists of calcite ($CaCO_3$), dolomite [$CaMg(CO_3)_2$] and Fe-dolomite [$Ca(Mg,Fe)(CO_3)_2$], with an increase in Mg and Fe content from the northwest to the southeast. This assemblage, considered the equivalent of the distal calcite and dolomite to intermediate calcite-Fe-dolomite carbonate alteration halo found in Mattabi-type deposits, is consistent with modern and ancient seafloor alteration patterns. The carbonate alteration was produced by circulating CO_2-rich hydrothermal fluids within the seamount. The inferred source for $(CO_3)^{-2}$ is the carbonate lithofacies, because it is the lateral platformal continuation of the Schakalsberg seamount.

Two types of mineralization were identified: 1) Fe-mineralization consisting of (i) μm-to-mm hematite (Fe_2O_3) needles disseminated in the volcanic rock matrix, and (ii) replacement of primary magnetite (Fe_3O_4) crystals by hematite (Fe_2O_3) along the cleavage planes, and 2) Mn oxyhydroxide mineralization, manjiroite [$(Na,K)(Mn^{4+}, Mn^{2+})_8O_{16}\cdot n(H_2O)$], in brecciated or massive zones, 2-6 m-thick and traceable for up to 1 km along strike. The Fe-mineralization is a low-temperature mineralization, which was deposited in an oxidizing environment, with the carbonatized rocks acting as cap rocks. The mineralization precipitated in the porous volcaniclastic units that were already carbonatized. This mineralization could represent a distal, lower temperature phase of a VMS deposit. The Mn mineralization is supergene and was produced by percolation of fluids and leaching of the surrounding rocks after the deformation of the Schakalsberg seamount (Quaternary?).

The structural evolution of the Schakalsberg Mountain segment is consistent with a fold and thrust belt that was subsequently subjected to sinistral transpression. The prominent structure is the Red Dunes thrust, which separates the marine carbonate lithofacies from the volcanic-dominated sequence of the Schakalsberg Mountains. The Red Dunes thrust trends and has a stretching lineation consistent with a south over north movement. The study area was divided into three structural domains according to the principal schistosity (Sp): (i) domain 1 has a mean Sp of 158/84, (ii) domain 2 of 355/65 and (iii) domain 3 of 149/40.

The Schakalsberg study area is consistent with evolution of a Precambrian seamount that formed during the opening of the proto-Atlantic Adamastor Sea. The pervasive hydrothermal carbonate alteration zone with local intense Fe-mineralization is primarily restricted to the porous volcaniclastic lithofacies that presumably forms the shoaling part of the seamount sequence. The study area is the first detailed account of a volcanic-volcaniclastic sequence in the Sperrgebiet of Namibia.

ACKNOWLEDGEMENTS

I would like to thank Kumba Resources, without whom the project could not have been conducted, and who provided logistical and financial support. I would also like to express my gratitude toward my supervisor (Dr Wulf Mueller) who never lost faith in me and who greatly helped me, often during his personal and family time, especially in the end. His knowledge of literature and his field experience was also a big advantage for me. I would also like to thank my committee (Dr Jacques Carignan and Dr Réal Daigneault) for their help and their continuous input. I am also thankful to my friends at the university (Henrik, Hugues, Marie-Line, Michaël, Pierre and Sébastien) who made my stay at the university joyful and relaxing, especially on certain Friday afternoons. I would also like to thank them for the animated geological discussions. Last but not least, I would like to thank my family, who supported me throughout the process, who cheered me up when I was down, and who stuck together in hard times.

TABLE OF CONTENTS

LIST OF FIGURES

LIST OF PLATES

LIST OF TABLES

LIST OF APPENDICES

LIST OF MAPS (IN POCKET)

CHAPTER 1

INTRODUCTION

1.1 Introduction and Problem

Seamounts are subaqueous volcanic edifices located near or at mid-oceanic ridges, occur in intra-oceanic plate settings, or are parts of volcanic arc sequences (Schmidt and Schmincke 2000). Guyots are more evolved versions of seamounts composed of fringing submerged carbonate reefs (Schmidt and Schmincke 2000). Although readily identified in modern settings, ancient ocean floor sequences that contain seamounts remain enigmatic and have only recently been recognized in the Archean Slave craton, based on detailed facies analysis (Corcoran 2000). Intra-oceanic seamounts are commonly mafic-dominated sequences, such as the Canary Islands (Staudigel and Schmincke 1984) and the Emperor seamount chain (Clague and Dalrymple 1987), that are hot-spot or plume-generated edifices/volcanic complexes. Ancient seamount sequences are therefore prime candidates for understanding subaqueous volcanic construction, but also first order sites in locating volcanic-hosted massive sulfide (VHMS) deposits.

Ancient VHMS deposits of the Archean Superior craton have been genetically divided into stratiform, mound-shaped Cu-Zn-Pb (±Au ±Ag) deposits of the Noranda-type, or diffuse Cu-Zn deposits of the Mattabi-type (Morton and Franklin 1987; Franklin 1990). Noranda-type deposits have a discordant Cu-rich hydrothermal alteration chimney

(Franklin et al. 1981), whereas the Mattabi-type is a semi-conformable alteration zone (Morton and Franklin 1987; Franklin 1990; Galley 1993). Noranda-type alteration zones feature an inner chlorite core grading into an outer sericitic zone that passes into essentially unaltered footwall rocks (Franklin et al. 1981; Lydon 1984; Chartrand and Cattalani 1990). The inferred shallow-water (<500 m), replacement-type Mattabi deposits (Franklin 1990) display an extensive, pervasive carbonate alteration pattern (Galley 1993) and are characterized by a significant volcaniclastic component, in contrast to the lava flow-dominated, deep-water (>500 m, Franklin 1990) Noranda-type deposits (Chartrand and Cattalani 1990; Gibson and Watkinson 1990).

Alteration and mineralized zones associated with seamounts have not been well-documented. The Schakalsberg Seamount, initially identified by Mueller et al. (2001) and Mueller (2003) but also alluded to by Frimmel et al. (1996a), offers a unique opportunity to test the economic potential of the Schakalsberg area (Exclusive Prospecting Licence, EPL-2757 to Kumba Resources, South Africa), located in the Sperrgebiet of Namibia. Emphasis of this thesis is placed on the pervasive hydrothermal carbonate alteration as well as the mineralization in a selected area of the Sperrgebiet that includes the Schakalsberg Mountains.

Carbonatization is a hydrothermal process that occurs when CO_2-rich fluids interact with the host rock and replace the existing mineral phases with carbonates (Foucault et Raoult 1995). Carbonates with varying Fe-Mg ratios in Mattabi-type deposits display a zoning pattern that creates a regional and local pattern generally conformable at the regional scale but discordant at the local scale. The aim of this thesis is to discern the

alteration pattern and establish the mineralization in the concession EPL-2757, and explain both the structural geology and physical volcanology. This study presents the characteristics of an area to which there is little access, but has an enormous economic potential.

1.2 Study area

The Neoproterozoic Gariep Belt (ca. 741 Ma; Frimmel 1996a), located in the southwestern part of Namibia and South Africa, is interpreted to represent a passive margin of the proto-Atlantic Adamastor Sea. The Gariep Belt contains numerous terranes, referred to as complexes by Frimmel (1996b; Figure 1), and includes intrusive volcanic, volcaniclastic, and sedimentary rocks. The study area is located in the Schakalsberg complex near the Upper Gariep Group (Figure 1). The study area (EPL 2757; 28°00'00" - 28°07'30" S, 16°30'00" - 16°37'30" E) is located in the Schakalsberg Mountains in Namibia (Figure 2). The ca. 200km^2 area consists of sand dunes, isolated outcrops (hills) and a chain of mountains in the southwest. Kumba Resources is interested in this area because of its proximity to two important deposits: Skorpion, a zinc oxide deposit and Rosh Pinah, a VMS-SEDEX deposit (30 Mt at 7% Pb, 2% Zn and 0.1% Cu, property of Kumba Resources Inc.). The study area is characterized by a strong carbonate alteration. The probability of finding another deposit in the vicinity of previously exploited region is high because massive sulfide deposits are often grouped together and are referred to as mining camps. Because EPL 2757 was closed for exploration, the geology of the area was unknown and the only existing work showed two rock types: gabbros and greywackes (internal map Kumba Resources).

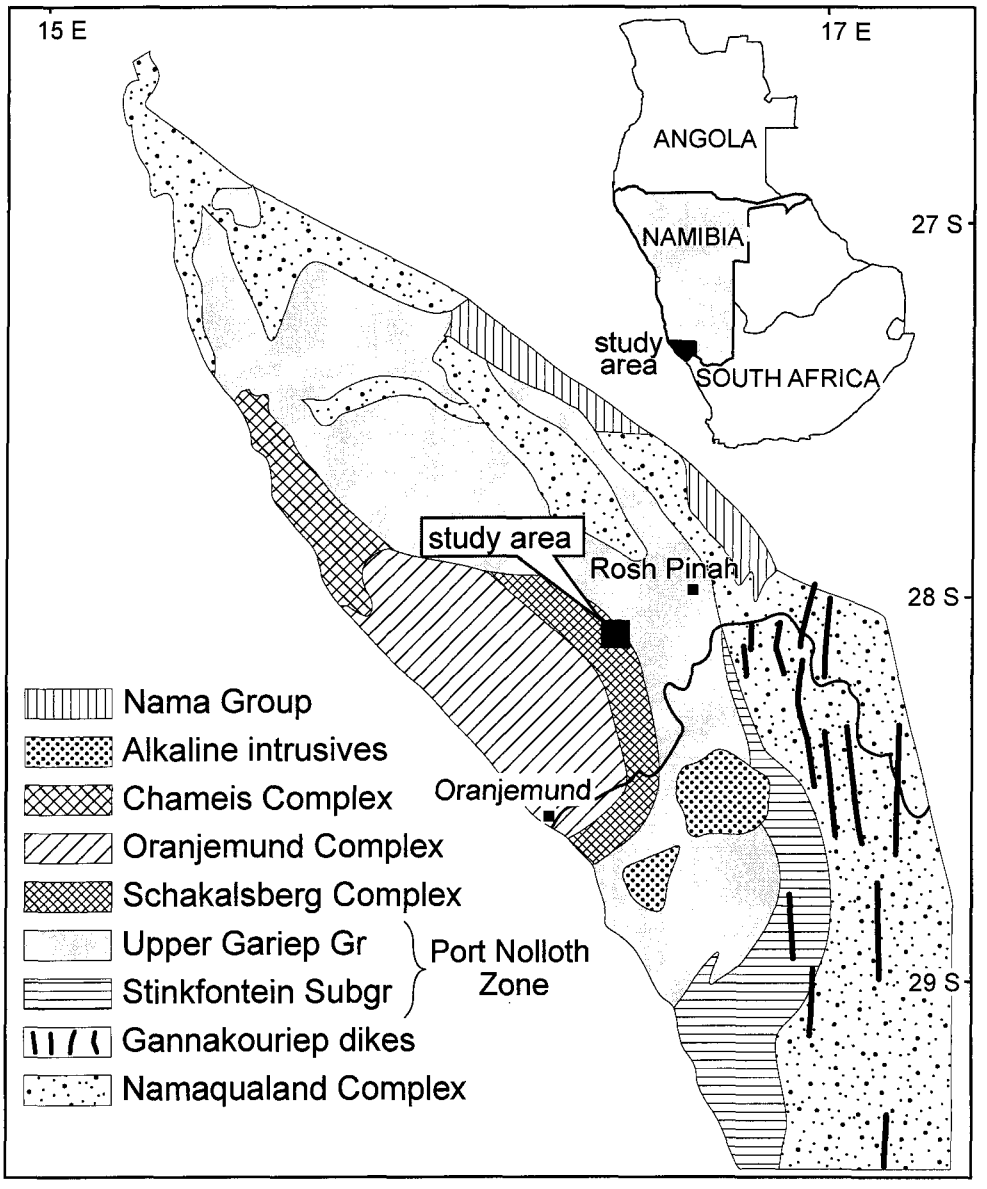

Figure 1: Simplified geological map of the Gariep Belt with tectonic divisions. Modified from Frimmel et al. (1996b).

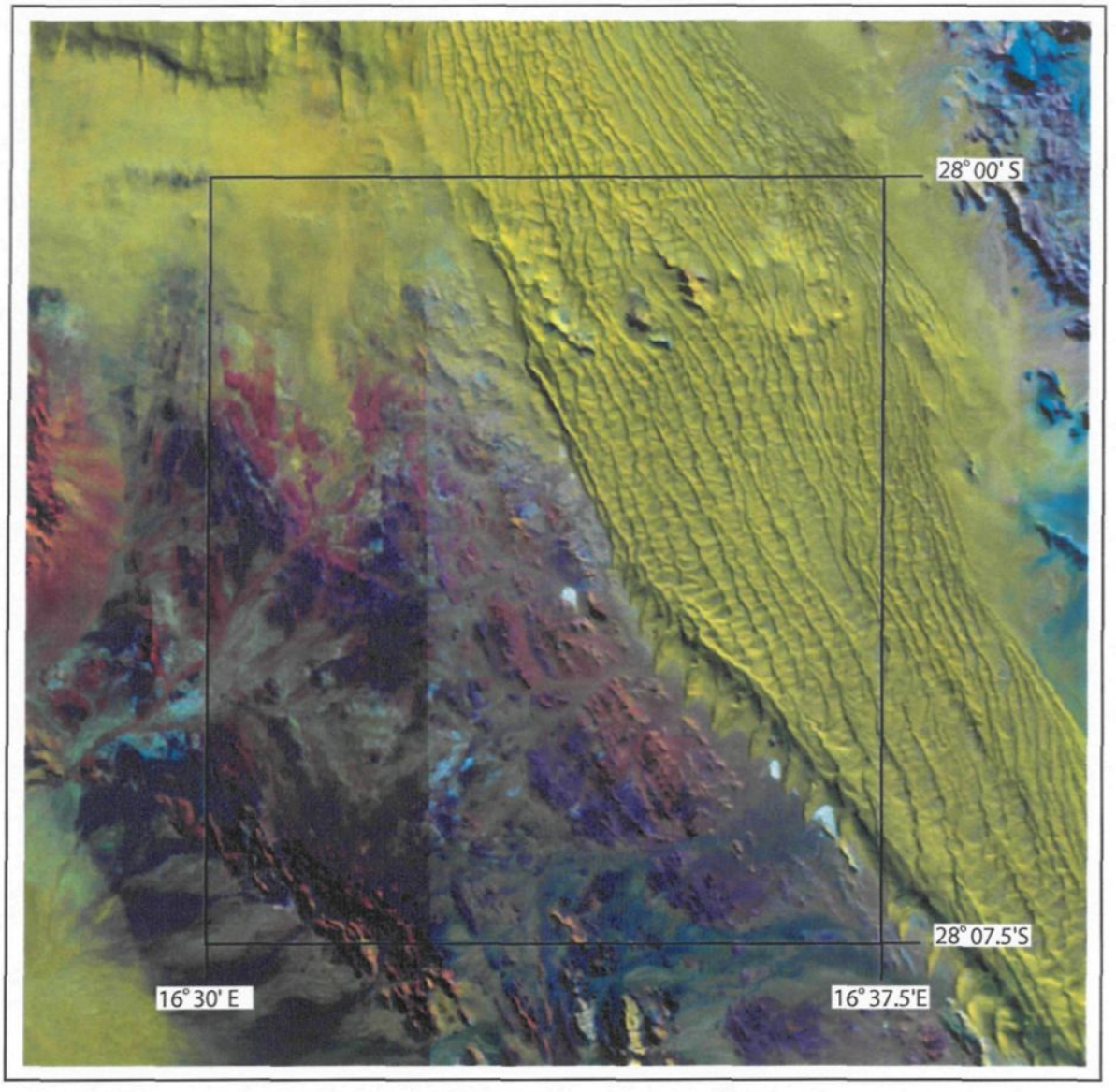

Figure 2: Location of EPL 2757 on a landsat image. The blue to red features represent rocks or gravel (Schakalsberg Mountains) whereas the yellow area represents sand.

1.3 Objectives and methodology

The main objective was the identification of the types of alteration and mineralization present in the EPL 2757, therefore assessing its economic potential. This was attained by doing the following:

1- Characterize the rock types and the mineralization in the area.

2- Establish the stratigraphy of the property.

3- Determine the alteration and the metamorphism affecting the rocks.

4- Characterize the deformation history.

5- Suggest a geological setting for the study area.

In order to attain the objective, a rigorous mapping and sampling program was conducted, which included detailed stratigraphic and lithofacies mapping, structural analysis, and representative sampling of lithological units, altered rocks and mineralization. A detailed petrographic study complemented the field observations. The geochemistry of the volcanic units has been studied by Mueller et al. (2001), and will be discussed in the general geology.

To obtain a coherent data set, the rocks were classified according to physical attributes. Mapping commenced with identification of the principal lithofacies which were subsequently divided into facies, based on volcano-sedimentary structures and composition. Facies mapping focused on the physical characteristics of specific units or subunits. The rocks were divided into 4 categories which include: intrusive mafic rocks, extrusive mafic

volcanic rocks, mafic volcaniclastic rocks, and sedimentary rocks. Igneous rocks were identified according to phenocryst content (% of phenocrysts, type of phenocrysts) and flow form, whereas the volcano-sedimentary rocks were determined based on sedimentary structures such as bedforms, grading, grain-size, and composition of the grains (Miall 1978). The volcanic rocks were grouped according to their field characteristics, such as aphanitic and microporphyritic, and this field classification was retained during geochemical analysis. The structural data, such as bedding (S_0), principal schistosity (S_p), lineations (L) or axial traces of folds were used to define structural domains in the study area.

Mineralized and non-mineralized rocks were sampled systematically for petrological studies. Samples were collected from as many rock types as possible in order to obtain a representative overview (Appendix 1). A tighter sampling grid was used in mineralized areas because of economic significance and larger samples were collected for geochemical analysis. Of the 226 samples, 125 were selected for thin section and polished section analyses. The petrographic study was conducted using a Nikon microscope with transmitted and reflected light. This allowed for identification of the mineral phases, different textures, alteration, mineralization and metamorphic grade.

Ion-microprobe analysis helped distinguish oxide minerals and relict mineral phases that were difficult to determine petrographically due to alteration and metamorphism. A total of 21 samples were analyzed by a Chemica sx-100 electron microprobe at the Université Laval, Québec (Appendix 2).

CHAPTER 2

GENERAL GEOLOGY

2.1 Introduction

The ca. 740 Ma Gariep Belt of Namibia and South Africa is inferred to represent part of a passive margin setting associated with the Adamastor Sea, which is considered to be a precursor to the present-day Atlantic ocean (Frimmel et al. 1996a,b, 2000; Frimmel and Frank 1998; Figure 1). The Neoproterozoic Gariep Belt is divided into the allochthonous Marmora Terrane in the west, and the para-autochthonous Port Nolloth zone in the east. The Marmora Terrane is predominantly volcanic whereas the Port Nolloth Zone is mainly a sedimentary succession; both are separated by the Red Dunes thrust. This volcano-sedimentary succession rests uncomformably on a 1.8 Ga Paleoproterozoic basement.

The Port Nolloth Zone is divided into the Stinkfontein Subgroup and the Upper Gariep Group, containing the Hilda and Holgat Subgroups (Figure 3). Quartzites, limestones and conglomerates dominate the Port Nolloth Zone, and felsic volcanic units are minor. The rocks of the Port Nolloth zone accumulated on the west flank of an actively rising fault scarp, characterized by alluvial fans, alluvial plains, and fan deltas. The volcano-sedimentary Rosh Pinah Formation, located in the Hilda Subgroup of the Port Nolloth Zone, unconformably overlies fluvial siliciclastic deposits (Frimmel et al. 1996a,b).

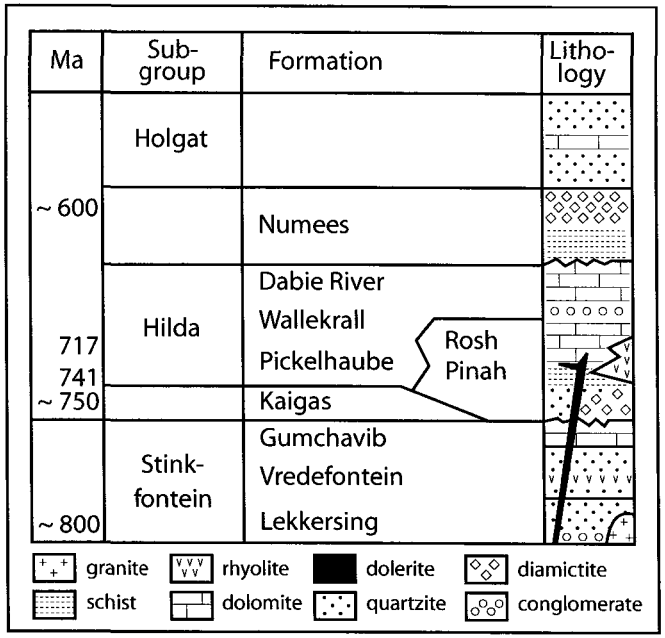

Figure 3: Stratigraphy of the Port Nolloth zone (Frimmel et al. 1996b). The Holgat and Hilda Subgroups and the Numees and Kaigas Formations comprise the Upper Gariep Group.

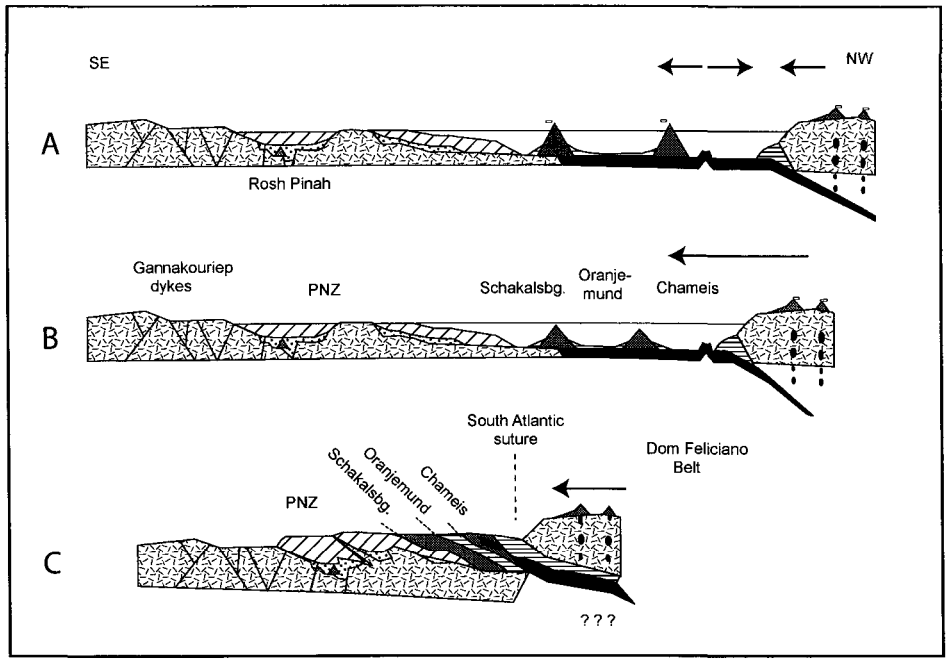

Figure 4: Schematic post-extension tectonic history of the Gariep Belt: A) spreading and subduction underneath South America (after 717 Ma), hotspot-related volcanism, and deposition along a passive continental margin; B) formation of an accretionary wedge (ca. 570 Ma) ; C) closure of the oceanic basin followed by continent-continent collision (545 Ma). PNZ: Port Nolloth Zone (Frimmel et al. 1996a).

The formation consists of felsic volcanic flows and domes and volcaniclastic deposits, but also bedded turbiditic sandstone-pelite sequences and diamictites. The 30-35 million tonne Rosh Pinah deposit, an inferred Sedimentary Exhalative (SEDEX) type deposit with Zn-Pb-Cu-Ag mineralization, is part of this formation. The mineralization is hosted in the turbiditic sequence ± volcaniclastic deposits and the mineralizing system was apparently controlled by the felsic volcanic activity which in turn is responsible for the hydrothermal carbonate alteration. The Port Nolloth zone is inferred to represent the margin of the Adamastor Sea.

The Marmora Terrane is divided into the Chamesis, Oranjemund and Schakalsberg complexes. Based on petrography and geochemistry, Frimmel et al. (1996a,b) considered the Schakalsberg Complex to be an ocean island capped by reef dolomite allocated to an aseismic ridge. The clastic Oranjemund Complex is a turbiditic apron deposit overlying the ocean island, and the Chamesis Complex is a remanant of mid-ocean ridge with ocean islands in an accretionary wedge (Frimmel et al. 1996a,b). The Marmora Terrane represents the outbroad ocean segment of the Adamastor Sea.

In summary, the Gariep Belt is the result of the closing of the Adamastor Sea, which brought together the marine components of the oceanic Marmora Terrane and its coastal counterpart, the Port Nolloth Zone (Figure 4). This is part of the continent-continent collision that resulted in the Pan-African orogeny that culminated around 545 Ma (Frimmel et al. 1996a).

The studied concession EPL 2757, located in the Schakalsberg Complex (Figure 1), is part of the Sperrgebiet, Namibia (see Maps 1 to 4, in pocket). The area consists of a ca.

1.4 km thick volcano-sedimentary sequence with pillowed, massive, and brecciated mafic volcanic flows, co-genetic gabbro sills and dykes, and volcaniclastic units as indicated by the tuffs, lapilli tuffs and lapilli tuff breccias. A pervasive carbonate alteration affects the majority of the volcaniclastic units and numerous volcanic units. The volcanic rocks have undergone greenschist facies metamorphism with chlorite, actinolite, carbonate, quartz, muscovite and epidote (Yardley 1989). Iron and manganese mineralization is present in the southern segment of the property (Maps 1 to 4, in pocket).

2.2 Geochemistry of the Schakalsberg area (concession EPL 2757)

The report by Mueller et al. (2001) elucidates the geochemical affinities of the volcano-dominated Schakalsberg sequence and is used to compliment the observations and results in this study. Physical volcanology is a powerful tool in elucidating flow processes, as documented in the Paleoproterozoic Kangerluluk area, southeast Greenland (Mueller et al. 2002). Mueller et al. (2002) helped establish a depositional setting and discern volcanic process such as flow morphology and explosive activity, but it was the geochemistry that allowed recognition of large-scale driving mechanisms (i.e. rifting or subduction) and helped suggest an overall tectonic setting. Geochemistry is also an important exploration tool that helps explain extensive alteration patterns associated with base metal deposits.

The mafic volcanic lava flows were divided into aphanitic, microporphyritic, feldspar-phyric, pyroxene±feldspar-phyric, gabbro, and phonolitic volcanic facies. A total of 39 samples (31 mafic volcanic rocks and 8 gabbroic rocks) were analyzed using major, trace, and rare earth element (REE) geochemistry. Most rocks plot as subalkaline basalts

and gabbros, with some aphanitic samples plotting in the alkaline basalt field, and one sample, AA-53-2001, in the phonolite field (Figure 5; Winchester and Floyd 1977). The combination of field observations and lithogeochemistry lead to discrimination of one intrusive and two extrusive volcanic suites: 1) transitional to alkali-type basalts (Group I), 2) tholeiitic basalts (Group II), and 3) tholeiitic gabbros (Group III). All 39 samples, with the exception of AA-53-2001, fall into these categories. The REE patterns of the Schakalsberg rocks, Figure 6, permit differentiation between N-, T-, E-(P)-MORB, and ocean island tholeiitic and alkali basalts (Sun and McDonough 1989; Wilson 1989, p. 135; Kerrich and Wyman 1996). With the exception of gabbro sample AA-189-2001 which is not related to the Schakalsberg sequence, all samples display an enrichment in LREE whereby two distinct trends are readily observed: 1) Group I with a pronounced slope, 2) and Group II with a gentle slope. Group III gabbro dykes and sills resemble Group II samples, and are considered comagmatic.

The major element chemistry permits a first order characterisation. Group I mafic volcanic rocks average 3.74% TiO_2 (8 samples; 2.16-4.19%), and 0.81% P_2O_5 (0.45-1.02%), whereas Group II abundances are lower with an average of 2.63% TiO_2 (22 samples; range 2.09-3.45%) and 0.25% P_2O_5 (range 0.18-0.42%). The Group III gabbro suite averaged 2.74% TiO_2 (7 samples; range 2.29-3.06%) and 0.26% P_2O_5 (range 0.23-0.30%), and overlaps favourably with Group II. The $(La/Yb)_n$ and Nb/Y ratios of Group I rocks are 8.72-19.62 (av. 13.74) and 1.50-2.82 (av. 2.12), respectively, whereas the $(La/Yb)_n$ ratio of Group II is significantly lower with 4.85-6.15 (av. 5.35) and the Nb/Y ratio is tightly constrained with a spread 0.60-0.79 (av. 0.68). Group III gabbros have a $(La/Yb)_n$ ratio of

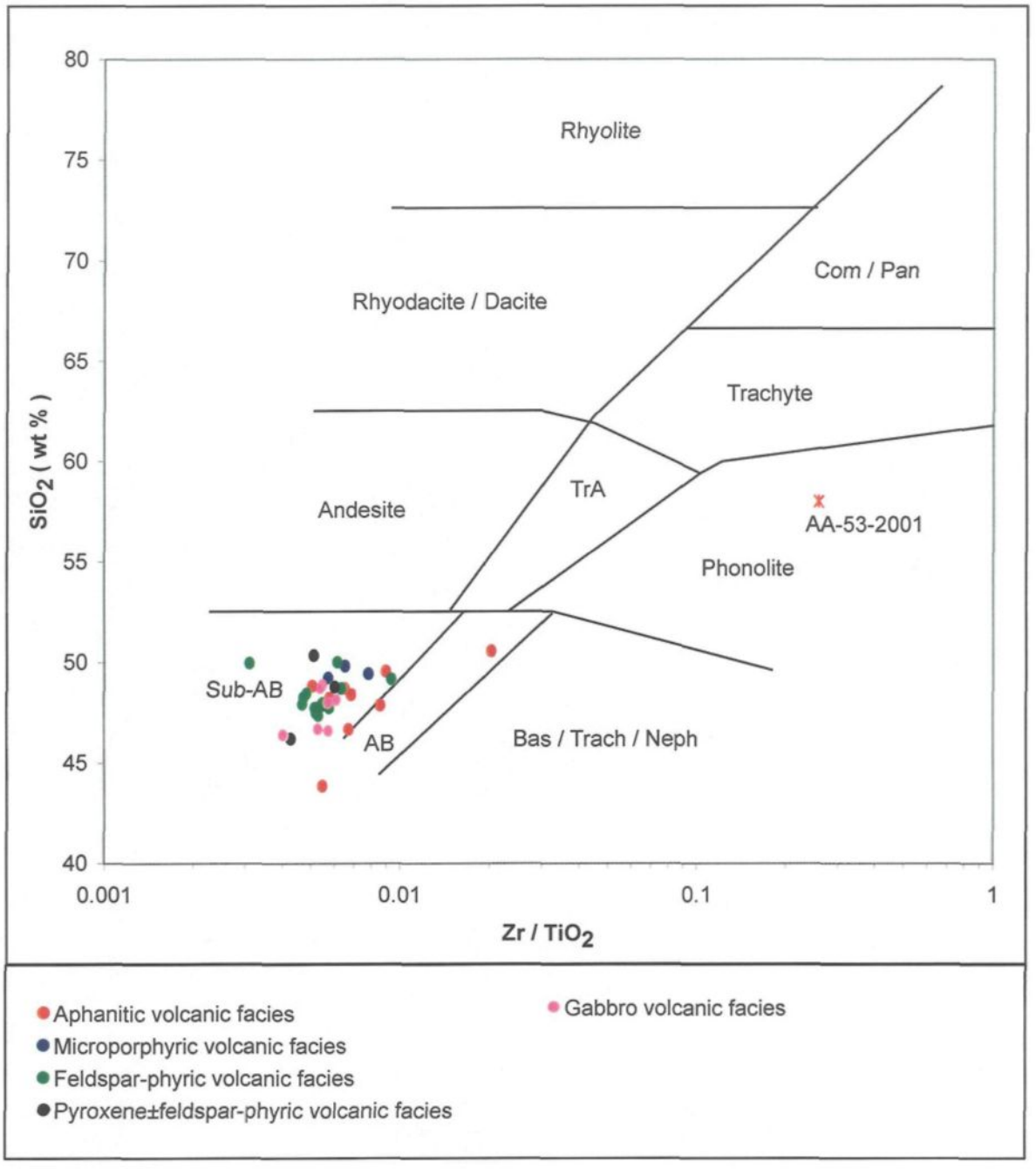

Figure 5: SiO_2 (wt %) vs Zr / TiO_2 diagram of Winchester and Floyd (1977) for the volcanic lithofacies of EPL 2757. Sub-AB, subalkaline basalt; AB, alkaline basalt; TrA, trachyandesite; Bas, basanite; Trach, trachyte; Neph, nephelinite; Com, commendite; Pan, pantellerite.

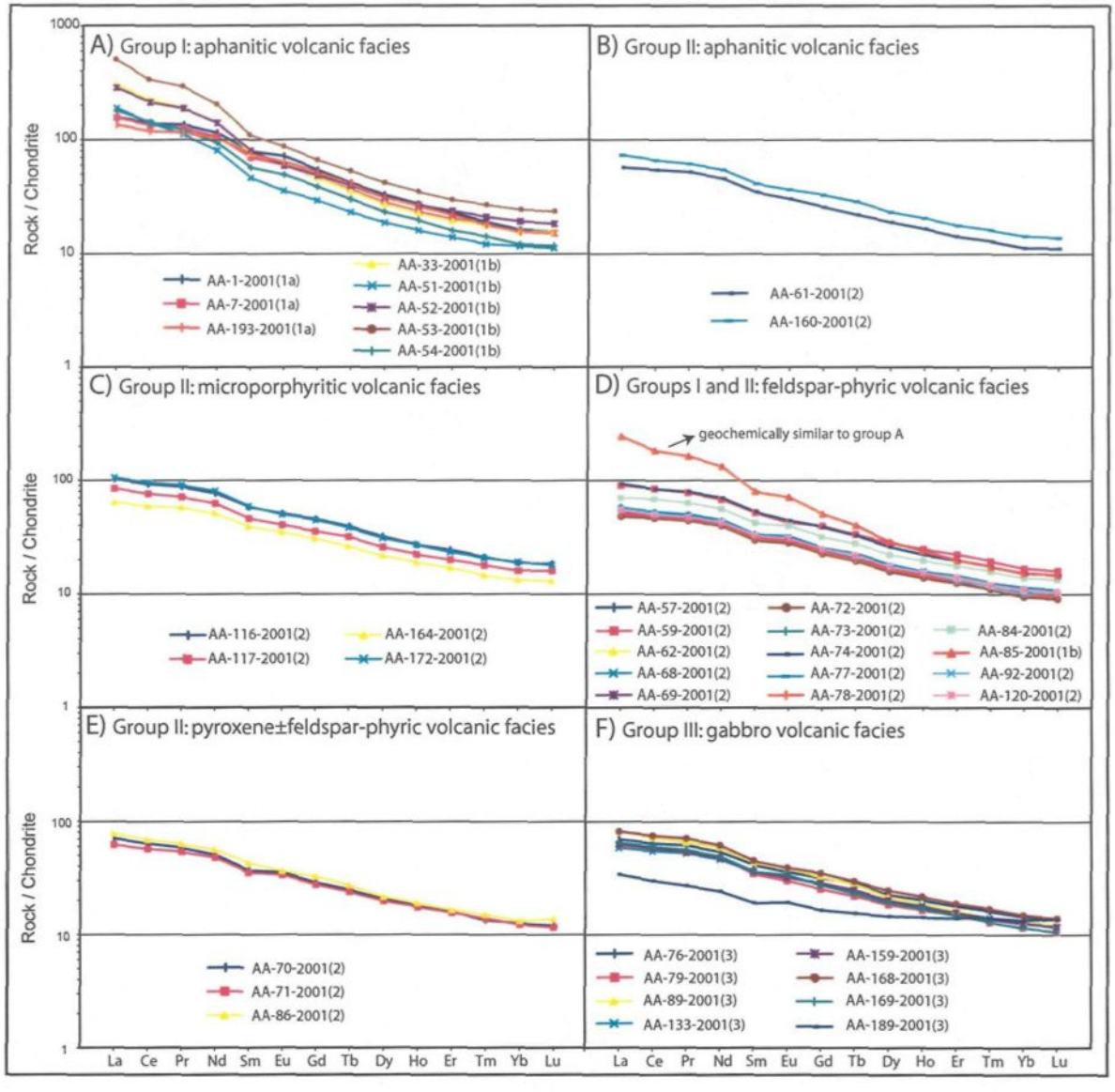

Figure 6: Rare earth elements (REE) diagrams of Schakalsberg mafic volcanic lithofacies.

4.63-6.33 (av. 5.31) and Nb/Y ratios of 0.59-0.82 (av. 0.70), and are geochemically indistinguishable from Group II rocks. Major and REE geochemistry indicate that the Schakalsberg samples are evolved and are either ocean island tholeiites or alkaline basalts (BVSP 1981; Sun and McDonough 1989; Wilson 1989). Using the discrimination diagram of Wood (1980; Figure 7A), Schakalsberg aphanitic volcanic rocks compare favourably with alkaline within-plate basalts whereas the phenocryst-rich volcanic rocks plot in the field of E-type MORB and within-plate tholeiites. Using the diagram of Meschede (1968; Figure 7B) similar results are obtained wherein the aphanitic volcanic rocks fall into the within-plate alkali basalt field and the phenocryst-rich volcanic rocks show a geochemical affinity to within-plate alkali basalts and within-plate tholeiites.

The studied rocks are akin to continental basalts and ocean islands that are related to plume-generated systems or hot spots (BVSP 1981; Chaffey et al. 1989; Davies et al. 1989; Zhao et al. 1994; Pik et al. 1998). The high TiO_2 values of >2% and locally >4% support a hot spot or plume interpretation, and field evidence based on lithofacies mapping argues for an oceanic island or seamount. The geochemical results (Mueller et al. 2001) show that the volcanic-dominated Schakalsberg sequence developed from a Neoproterozoic plume with an enriched mantle source. The two suites in the study area represent either, 1) different levels of melting from a homogeneous mantle source and therefore simply reflect a fractionation trend, or 2) two different sources from a heterogeneous mantle. The latter is preferred, given the significant differences in HFSE and LREE abundances, and trace element characteristics (Mueller et al. 2001).

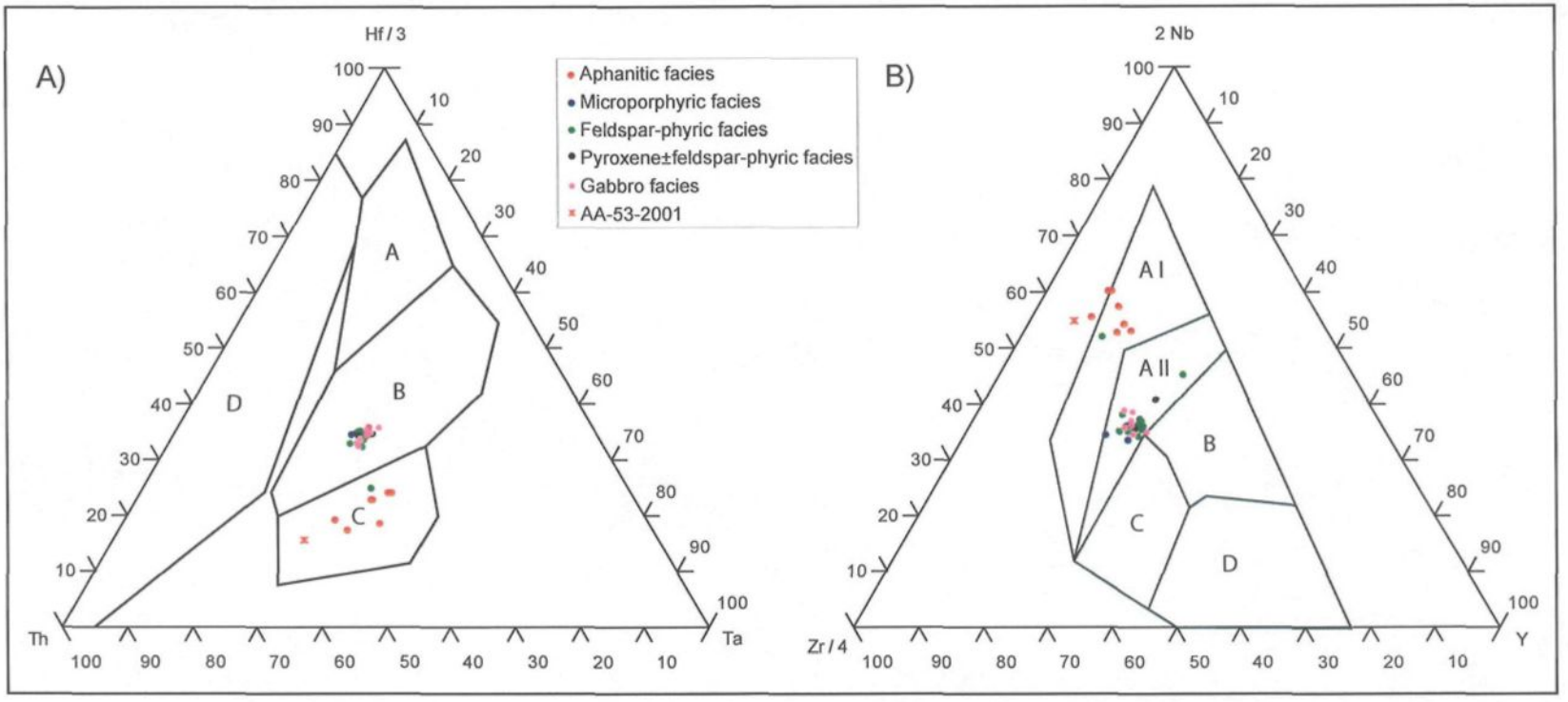

Figure 7: Discrimination diagrams for basaltic rocks. A) The Th-Hf-Ta discrimination diagram (Wood 1980). The fields are: A, N-type MORB; B, E-type MORB and within-plate tholeiites; C, alkaline within-plate basalts; D, volcanic-arc basalts.B) The Zr-Nb-Y discrimination diagram (Meschede 1986). The fields are: A I, within-plate alkali basalts; A II, within-plate alkali basalts and within-plate tholeiites; B, E-type MORB; C, within-plate tholeiites and volcanic-arc basalt; D, N-type MORB and volcanic-arc basalts.

CHAPTER 3

STRUCTURAL GEOLOGY

3.1 Introduction

The structural geology of the area facilitates construction of the local and regional stratigraphy, and helps place the mineralization into a specific context. Bedding (S_0), principal schistosity (Sp), fold axes, axial planes, foliation planes, secondary schistosity and stretching lineations were measured. More than 600 structural elements were measured. The study area was divided into structural domains 1, 2 and 3, according to the general trend of the principal schistosity and the degree of deformation (Figure 8 and Map 1, in pocket). The division of domains according to principal schistosity was used because it was consistently measured throughout the property and present at every outcrop.

3.2 Structural elements

Bedding (S_0) was measured mainly in the volcaniclastic units, where individual beds were readily observed. In the volcanic lithofacies, the bedding was measured according to general pillow attitude. The S_0 helped reconstruct the folding pattern of the study area (Figure 9).

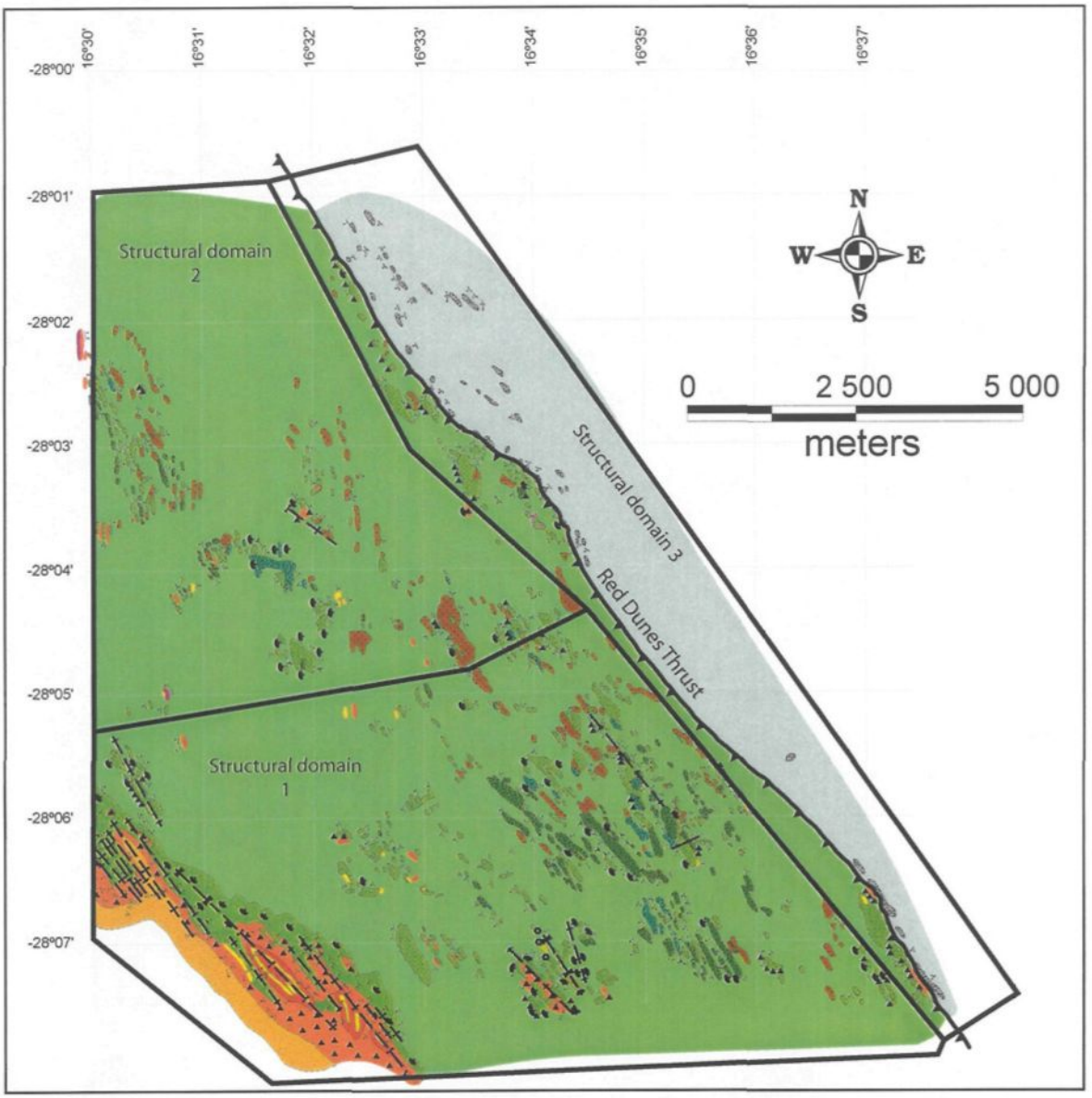

Figure 8: Structural domain divisions of the study area. Domains have been divided according to the general attitude of the principal schistosity (Sp). See Map 1 (in pocket) for more details.

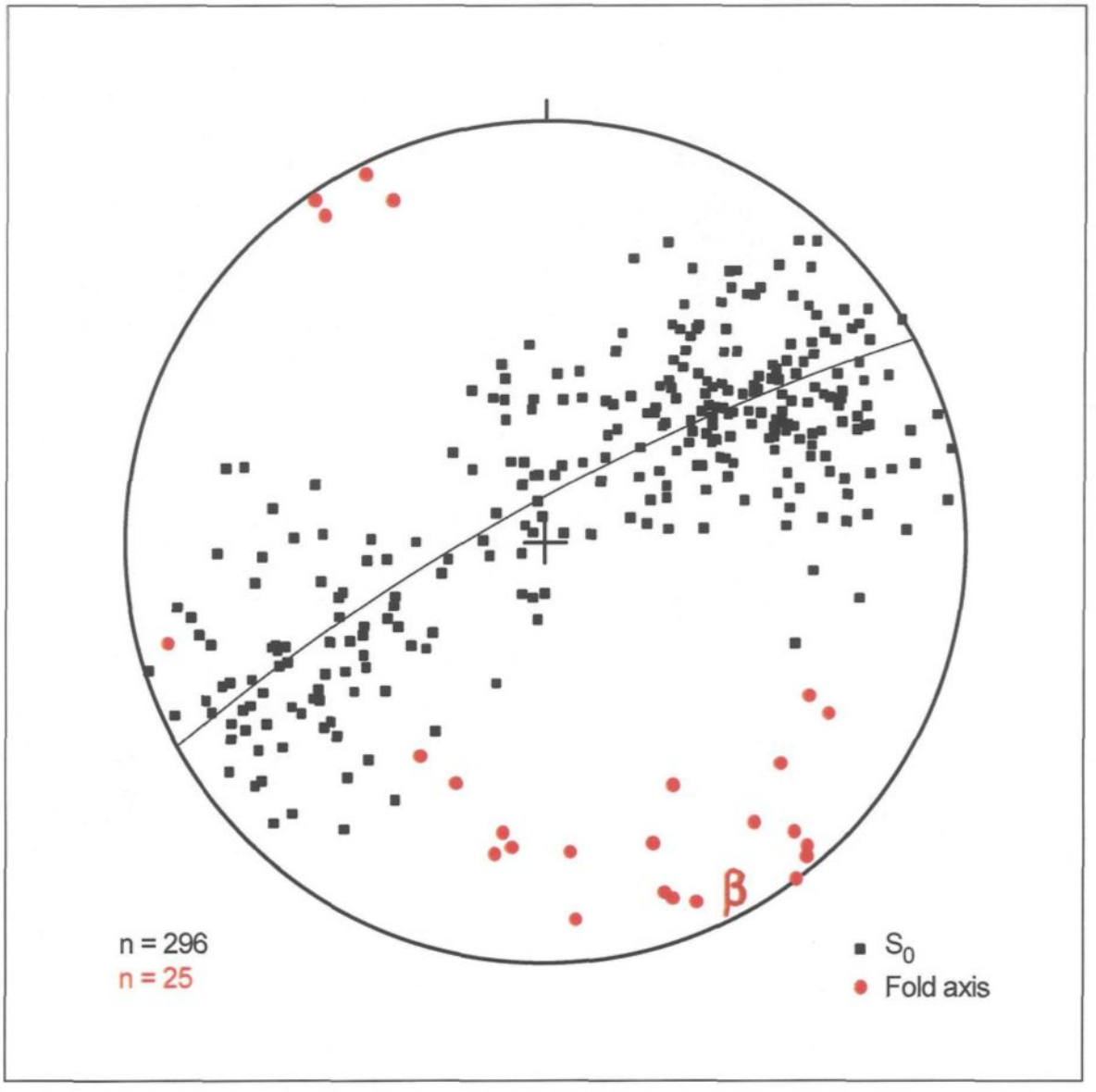

Figure 9: Bedding and fold axes for the 3 structural domains. Projection: Schmidt equal area.

Most of the folding was recognized in the southwest corner of the property (Maps 1 and 2, in pocket). Discerning folds in the mafic volcanic lithofacies was difficult but folding is inferred to be common throughout the property.

Fold axes (Maps 1 and 2, in pocket) trend NW-SE and have 0-10° plunges. Axial planes of the folds are vertical (75-90°, Figure 10), except for the recumbent fold observed near the Red Dunes thrust (Plate 1A). The folds are open, having an amplitude and wavelength of approximately 50 m and 200 m, respectively, that have been estimated according to cross-sections in the Schakalsberg Mountains (Figures 11 and 12). These cross-sections show the general attitude of the folds. Plate 1B illustrates an anticline forming the crest of a mountain; generally anticlines are hills and synclines are valleys. Parasitic folds, observed along the flanks of the main folds (Plate 1C), have parallel axial planes similar to that of the main folds. In contrast, the centimetre to decimetre S and Z folds affecting the bedding (S_0; Plate 1D) have axial planes perpendicular to those of the main folds (fold axes average 200/35).

The principal schistosity (Sp), a planar fabric, affects the volcanic, volcaniclastic and carbonate rocks. Structural domain 1 has a mean Sp of 158/84, structural domain 2 of 355/65, and structural domain 3 of 149/40 (Figure 13), similar to the Red Dunes thrust. The principal schistosity (i.e. the most intense shistosity) is not always parallel to bedding (Plate 2A). Although the schistosity was clear in non-altered rocks, it was difficult to distinguish in the altered, carbonatized rocks, except where unaltered fragments were found within the unit (Plate 2A). In thin section, the schistosity is clearly visible, even in carbonatized rocks (Plate 2B), and underlines the penetrative nature.

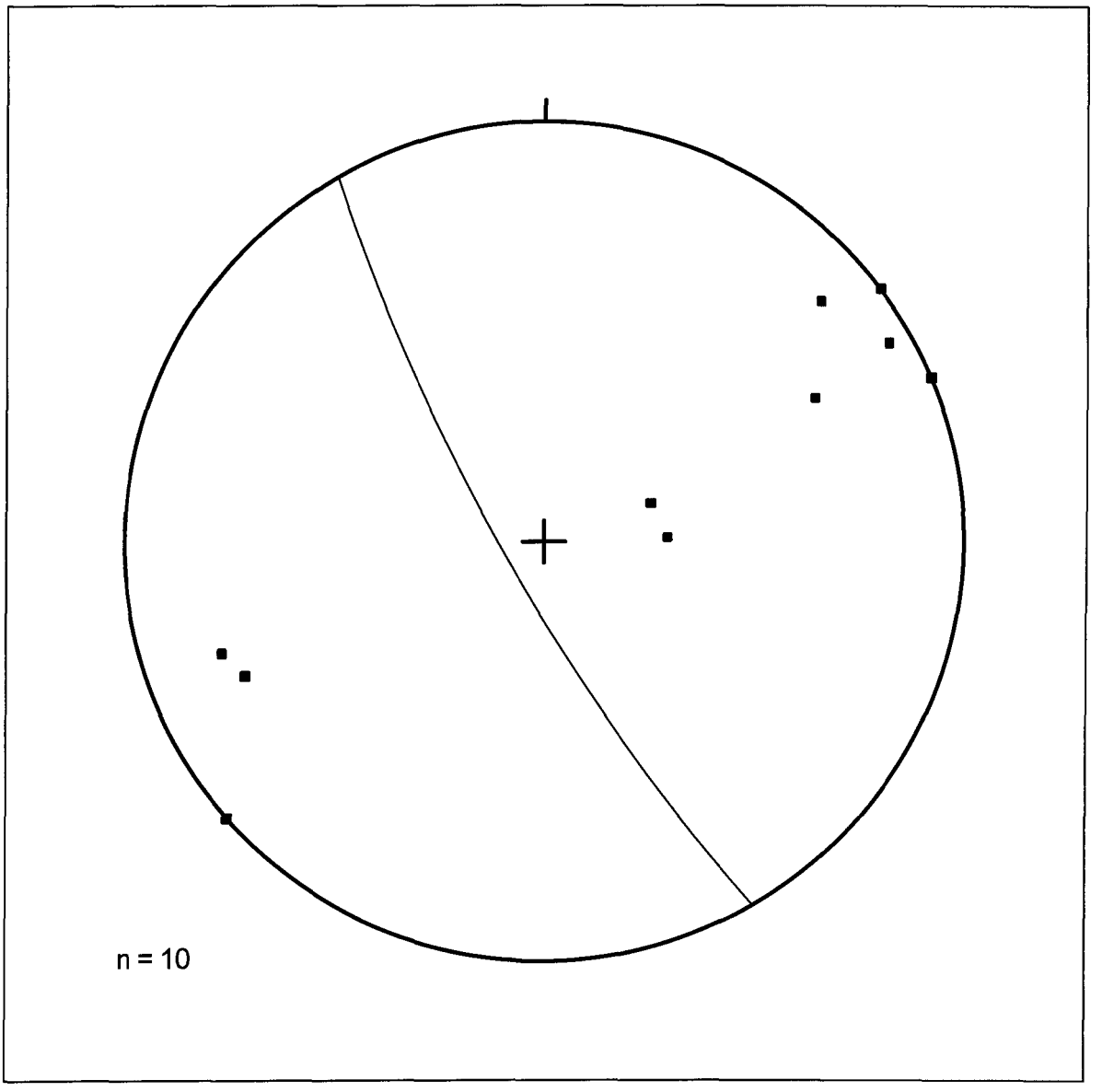

Figure 10: Axial planes of folds from structural domains 1 and 2. Projection: Schmidt equal area.

Plate 1 (A): Recumbent fold in aphanitic mafic volcanic facies, near the Red Dunes thrust. Fold axis: 255/08; axial plane: 178/24. Notebook, 18 cm.

Plate 1 (B): Hinge of an anticline in the Schakalsberg Mountains. Field of view is approximately 100 m.

Plate 1 (C): Anticline on the flank of a larger anticline in the carbonatized volcaniclastic lithofacies. Fold axis: 139/10; axial plane: 139/76. Pen, 14 cm.

Plate 1 (D): Small "Z" fold on the flank of a larger anticline. Facies is a weakly carbonatized tuff. Fold axis: 210/41. Compass, 20 cm.

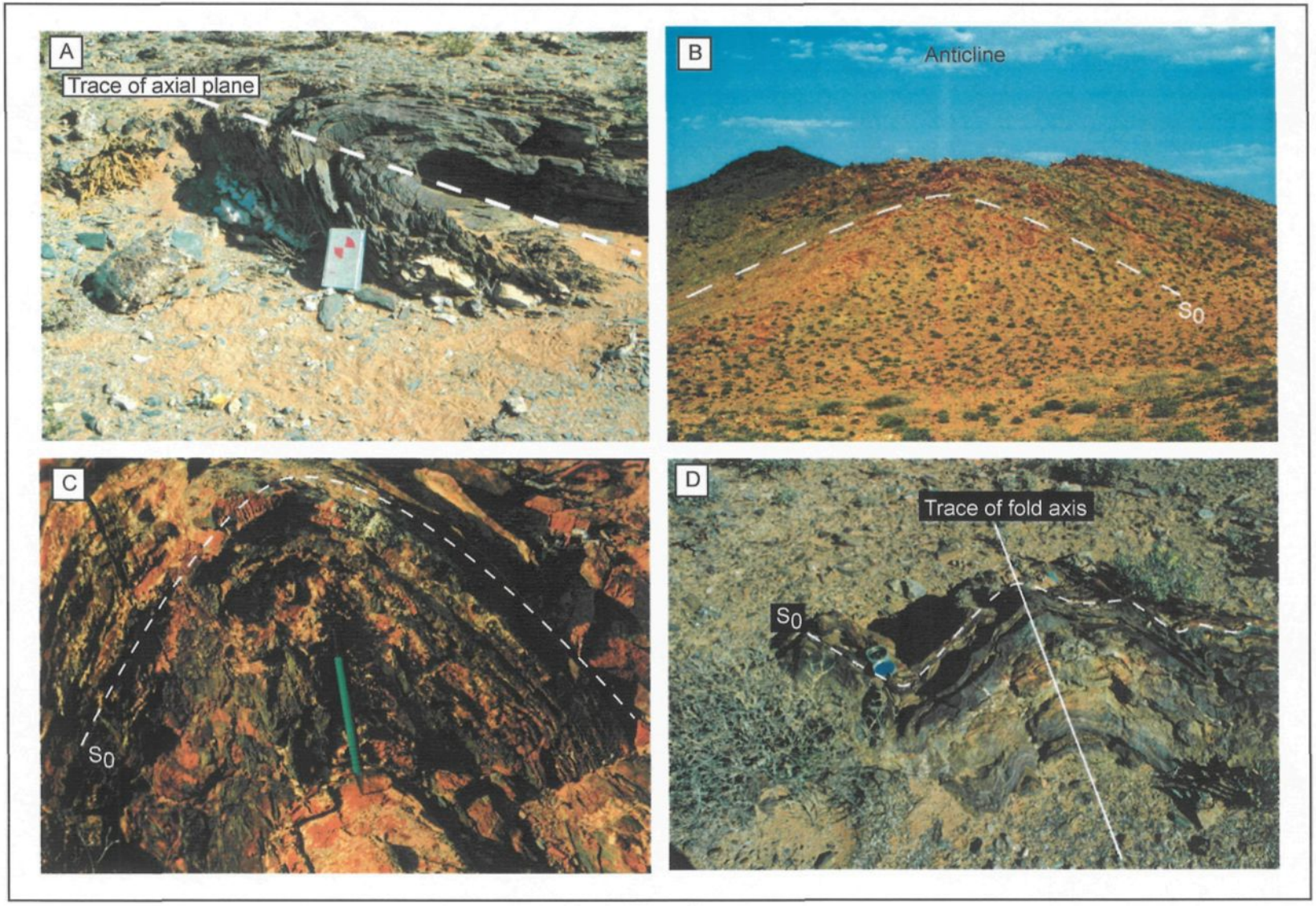
A
Trace of axial plane
B
Anticline
S_0
C
S_0
D
Trace of fold axis
S_0

Plate 1

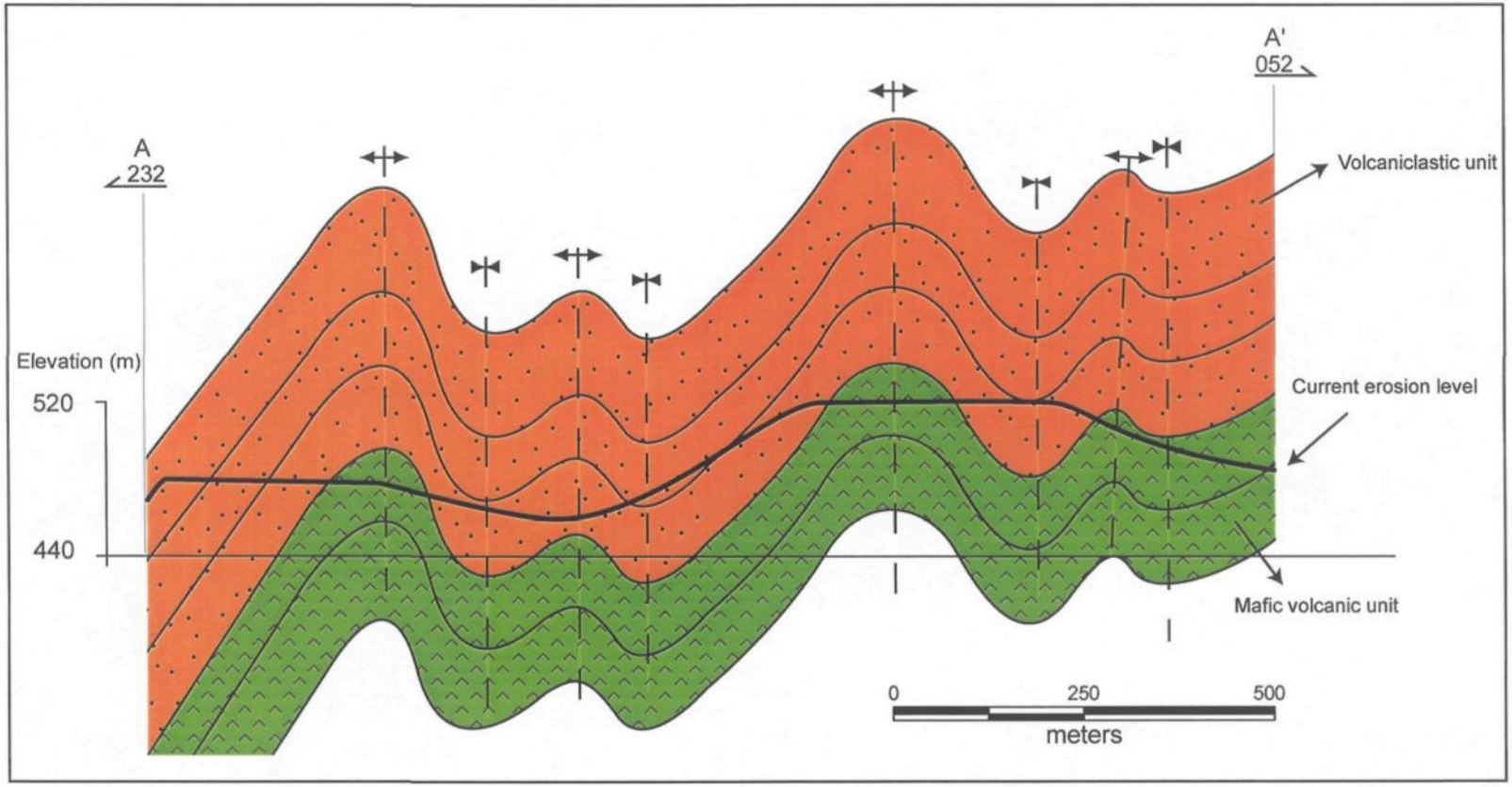

Figure 11: Simplified cross-section along the A-A' line (Map 2, in pocket). No vertical exaggeration.

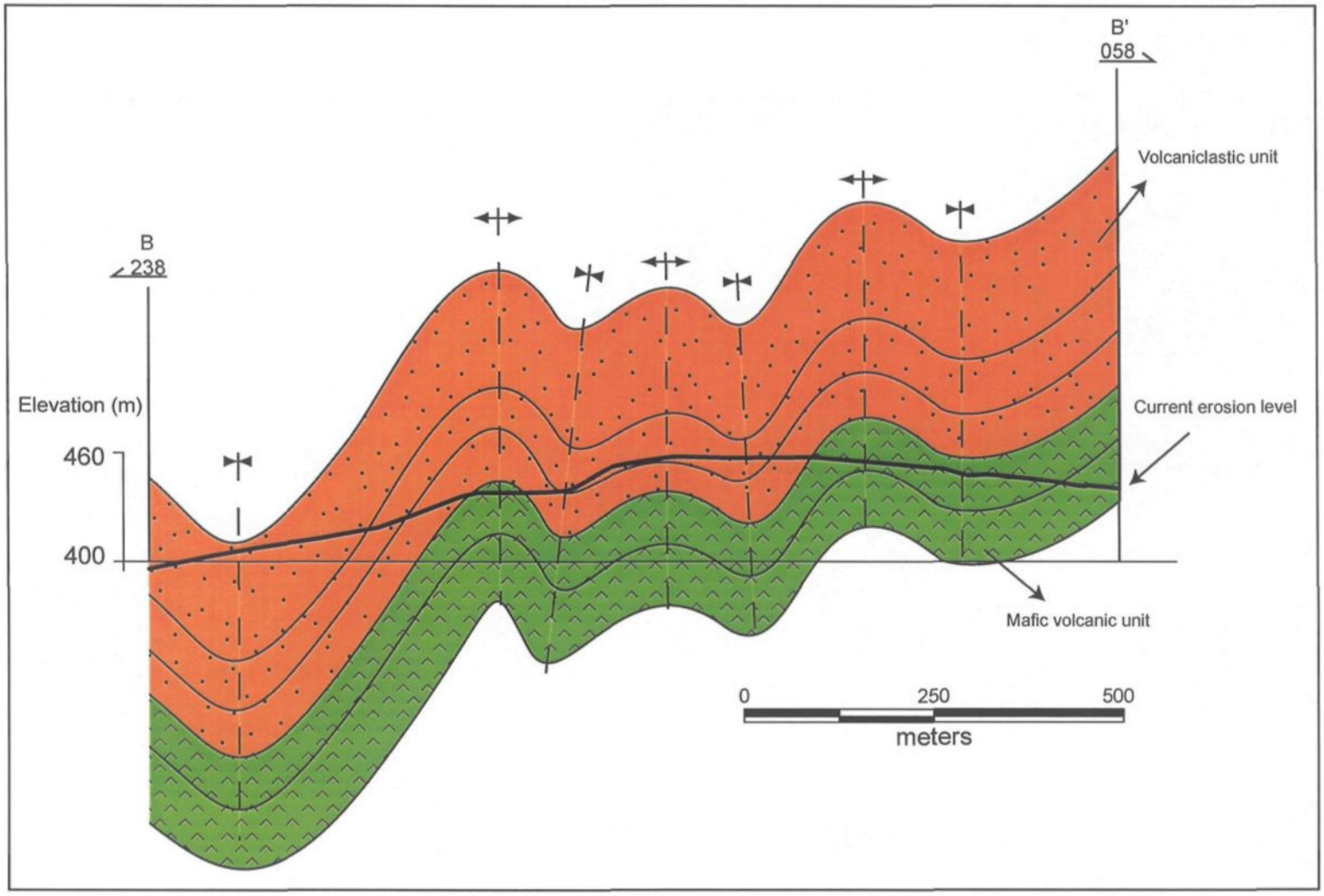

Figure 12: Simplified cross-section along the B-B' line (Map 2, in pocket). No vertical exaggeration.

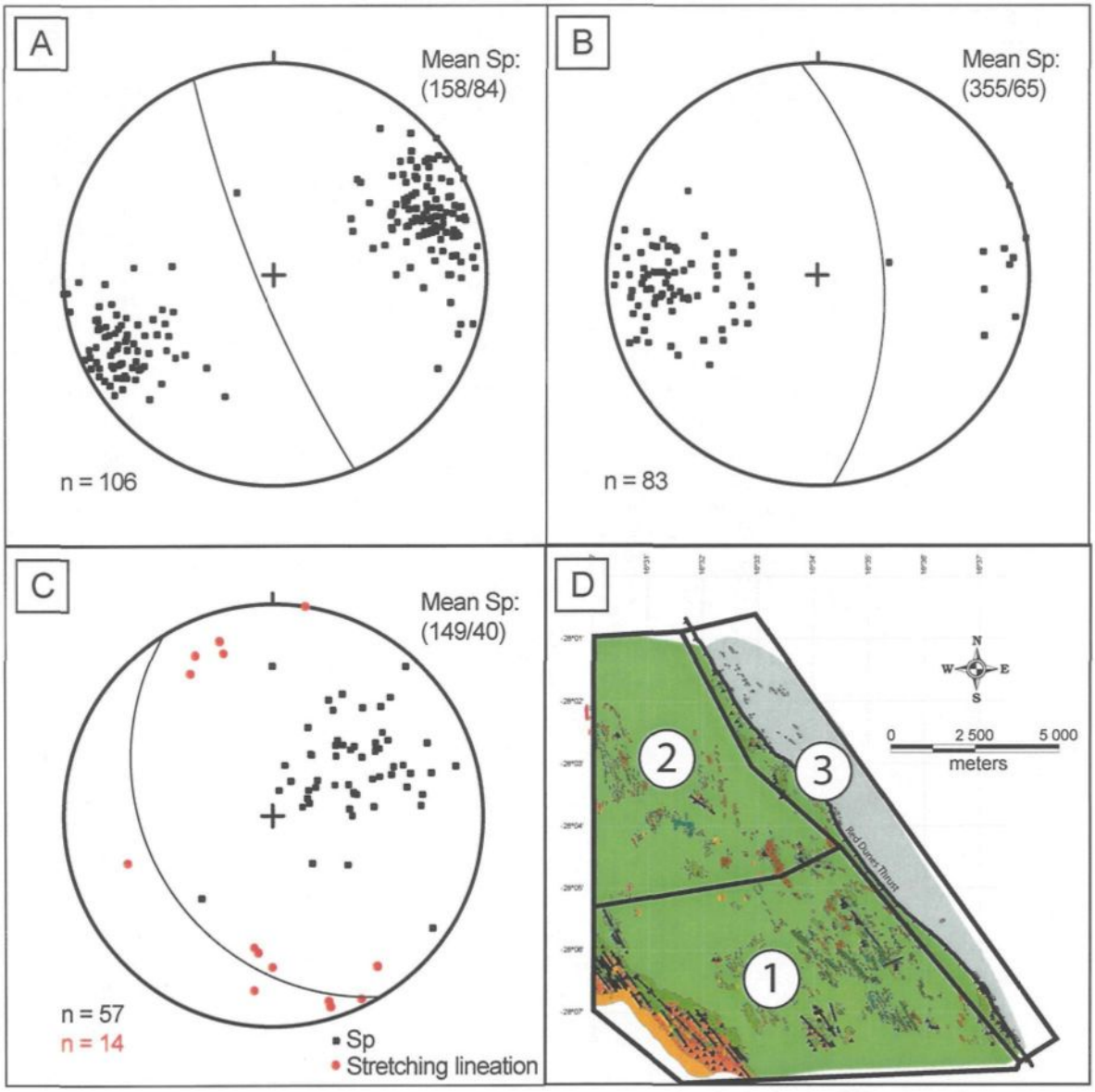

Figure 13: Principal schistosity (Sp) and stretching lineations in the structural domains of the Schakalsberg Mountains. A) structural domain 1; B) structural domain 2; C) structural domain 3; D) location of the structural domains. Projection: Schmidt equal area .

Plate 2 (A): Carbonatized lapilli tuff breccia with relationship between bedding (green pen, 138/73) and the principal schistosity (red pen, 164/83). Fragments in the lapilli tuff breccia are oriented parallel to the schistosity rather than the bedding. Pens, 14 cm.

Plate 2 (B): Photomicrograph of tuff (sample AA-132-2001). Note that the relationship between S_0 and Sp is only visible under the microscope in carbonatized rocks.

Plate 2 (C): Closely-packed pillows in the aphanitic mafic volcanic facies. Notebook, 18 cm.

Plate 2 (D): Longitudinal section of a pillow tube in the aphanitic mafic volcanic facies. Notebook, 18 cm.

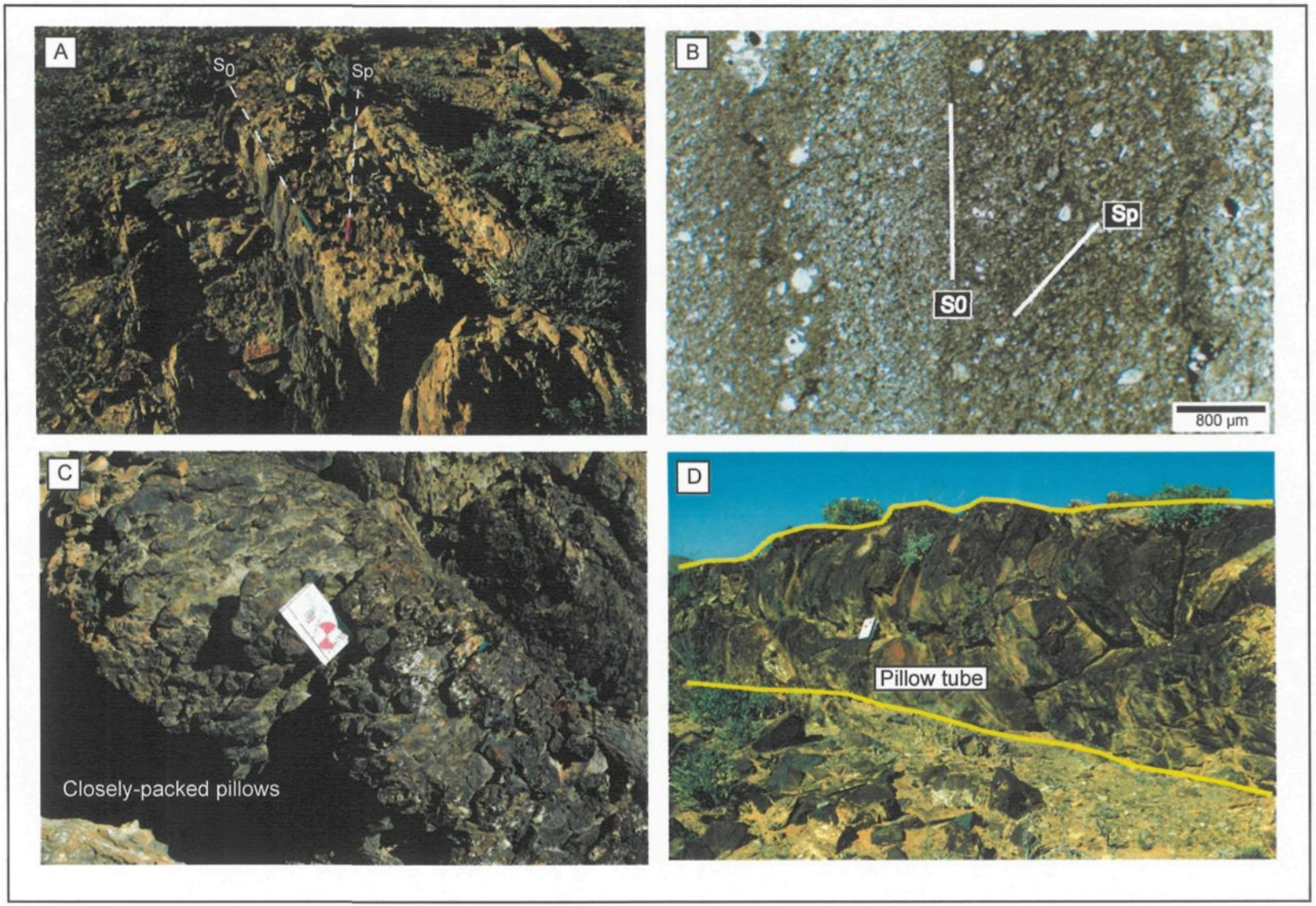

Plate 2

The Red Dunes thrust (149/40) is the principal structural element of the property, separating the volcano-sedimentary rocks in the west and the carbonate rocks in the east (Map 1, in pocket). The schistosity in the vicinity of the thrust has the same trend as the thrust plane. A recumbent fold (Plate 1A) was also observed near the inferred location of the thrust. Stretching lineations on the foliation plane (149/40), combined with the recumbent folding, give a transport direction of south over north (Figure 13, Map 1, in pocket).

3.3 Interpretation

The deformation history and structural elements in the study area display a thrust and fold geometry common to modern and ancient orogenic belts (i.e. Daigneault et al., 2002). The principal schistosity (Sp) cuts the traces of axial planes and indicates two phases of deformation, because an early phase creates a schistosity parallel to the fold axes, whereas the second deformation phase produced a schistosity transacting the folds (c.f. Johnson and Woodcock 1991). The schistosity and folding pattern support a thrusting event that is indicated by, 1) a low-angle fault plane separating two distinct lithofacies, 2) stretching lineations on the foliation plane suggesting south over north movement, 3) folding parallel to the thrust suggesting compression (or shortening), and 4) recumbent folding, commonly associated with thrusting (Yang and Nielsen 1995). Thrusting displaced the volcanic rocks over the carbonates (Figure 14), and stretching lineations are consistent with a sinistral transpressive component (south over north) during the latter stages of shortening. The eastern part of the property west of the thrust is lower in the stratigraphy

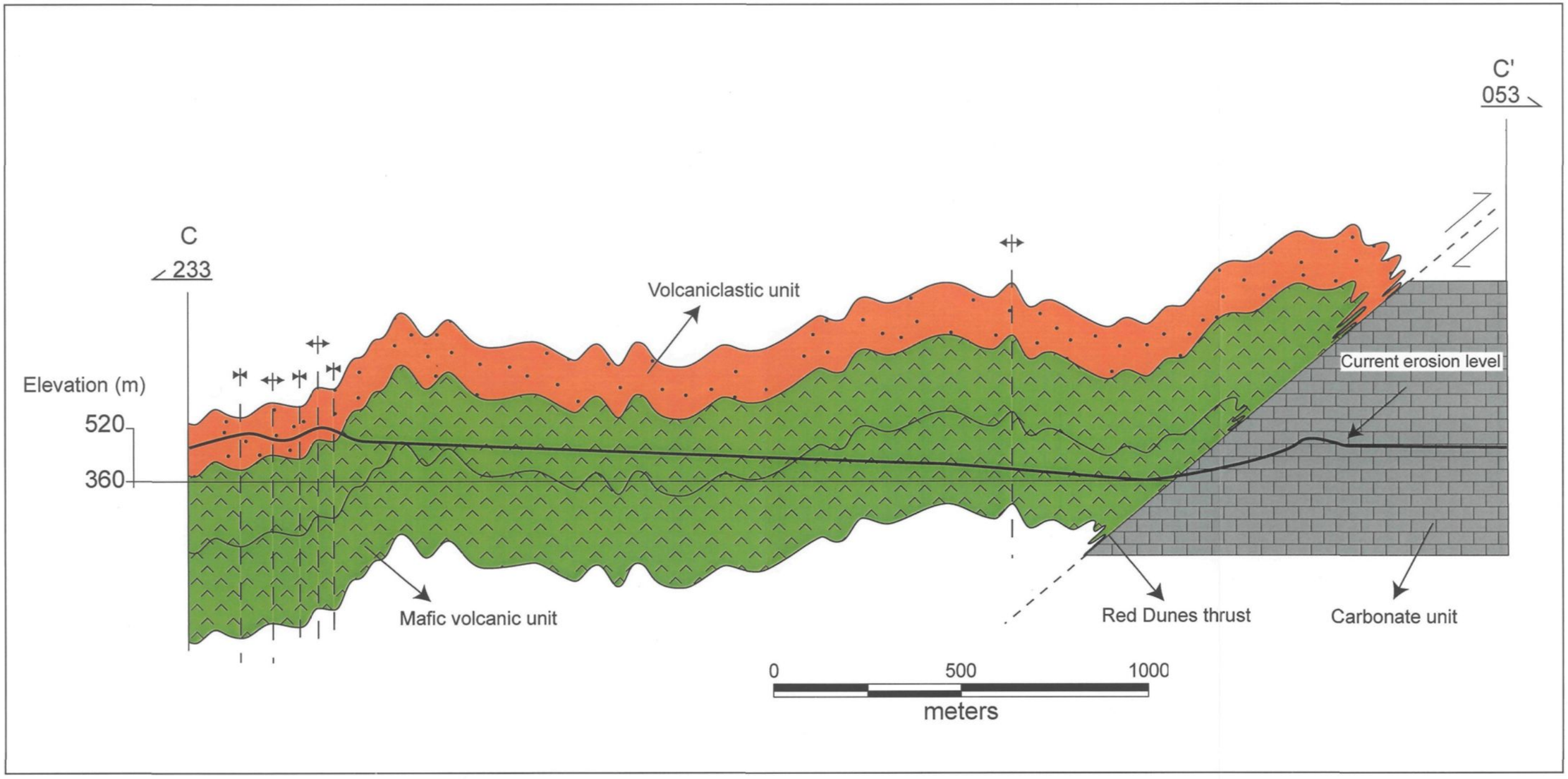

Figure 14: Simplified cross-section along the C-C' line (Map 1, in pocket). No vertical exaggeration.

than the extreme west. Thrusting affected the principal schistosity of the volcanic rocks only in proximity to the thrust, whereas such a signature is absent in the west. The overall structural setting of the Schakalsberg volcano-sedimentary sequence is consistent with sinistral transpression, a phenomenon commonly observed in other Neoproterozoic terranes (e.g. Abdelsalam et al. 1998; Johnson and Kattan 2001).

The different types of folds require additional consideration. The change in the main schistosity within structural domains suggests the presence of other deformation phases. The small folds (Plate 1C) found on the flanks of large open folds cannot be secondary (s,z,m,w) because the stress responsible for the large open folds cannot produce small and tight varieties in the same deformational event. Similarly, small folds with different axial planes (Plate 1D) support this contention; at least one other large-scale phase of deformation is required.

CHAPTER 4

VOLCANIC-VOLCANICLASTIC LITHOFACIES AND STRATIGRAPHY

4.1 Introduction

The volcano-sedimentary stratigraphy of the Schakalsberg Mountains in the Sperrgebiet is based on detailed facies mapping (Maps 1 to 4, in pocket) and structural analyses (Chapter 3). In the field, the various lithofacies and their lateral changes could be traced around the fold hinges and along the flanks for several 100's of metres. A ca. 1.4 km-thick composite stratigraphy (Figure 15), based on numerous detailed sections in the study area, is proposed. The term "lithofacies" represents the salient rock unit, such as a mafic volcanic or volcaniclastic deposit that has been subdivided into specific facies according to phenocryst composition, grain-size and sedimentary structures.

4.2 Volcanic nomenclature and terminology

Ancient rocks commonly pose problems with respect to nomenclature and terminology. A new classification scheme proposed by Mueller and White (2003) is utilized in this thesis (Table 1). The table explains the nomenclature of volcaniclastic rocks that clearly have a volcanic component. Because of this volcanic component, the grain-size terms tuff <2 mm, lapilli 2-64 mm, and breccia >64 mm can be employed and composite

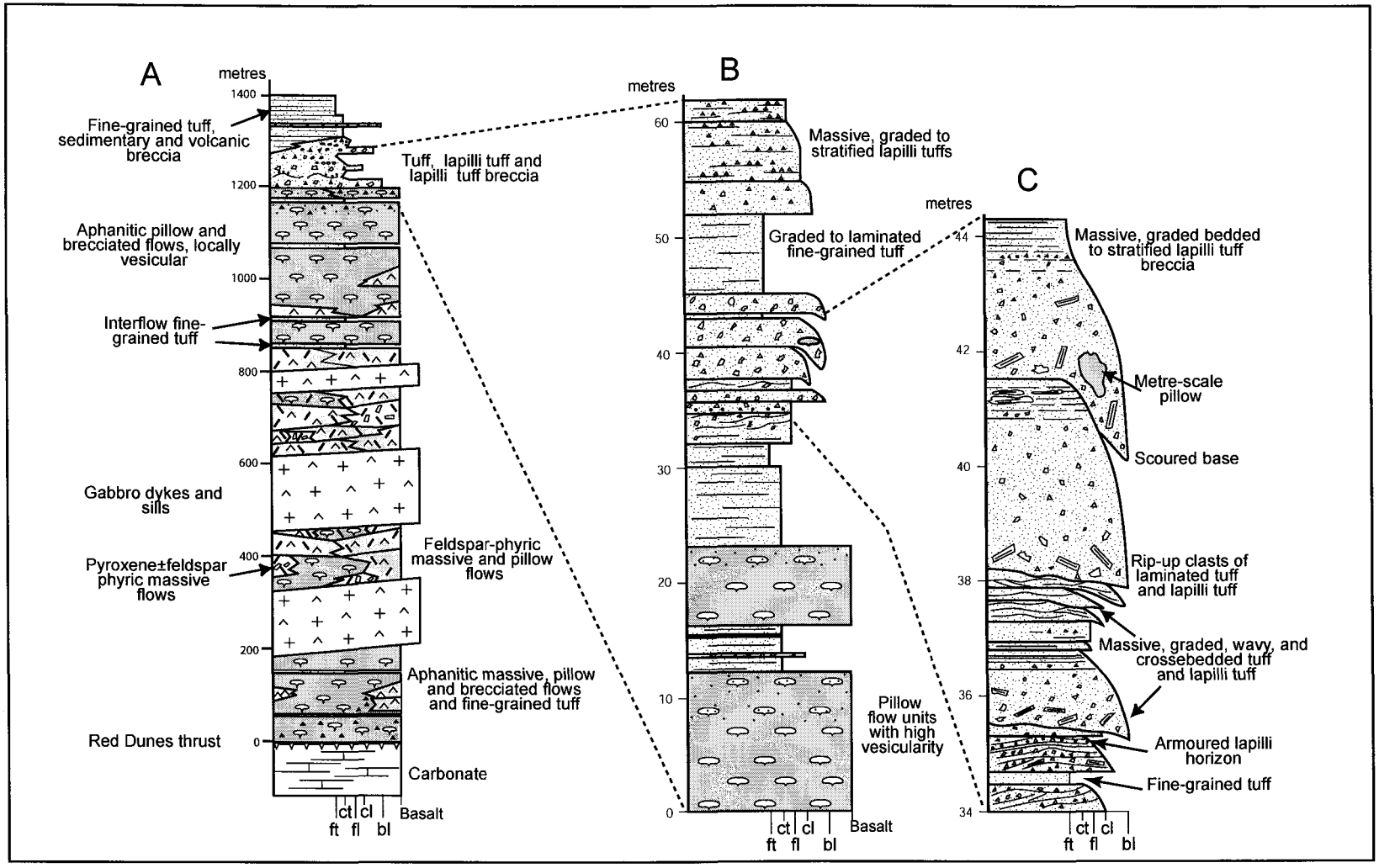

Figure 15: Schakalsberg Mountains stratigraphy and lithological units. A) General stratigraphy with subaqueous basalt flows intruded by low-angle dykes or sills. Top of the sequence features volcaniclastic rocks. B) Volcanic lava flows and pyroclastic deposits of the upper volcaniclastic-dominated segment. C) Detailed section of the volcaniclastic segment (Mueller 2002).

Grain-size	Schmid (1981), Fisher & Schmincke (1984)	Unconsolidated deposit name	Rock name	Complete rock name
finer than 4 phi (<0.0625 mm)	fine ash[1]	mud-grade ash	mud-grade tuff	mudstone-grade tuff
between 4 and 3 phi (0.0625 – 0.125 mm)		very fine ash	very fine tuff[3]	very fine-grained tuff[5]
between 3 and 2 phi (0.125 – 0.25 mm)		fine ash	fine tuff[3]	fine-grained tuff[5]
between 2 and 1 phi (0.25 – 0.5 mm)	coarse ash	medium ash	medium tuff[3]	medium-grained tuff[5]
between 1 and 0 phi (0.5-1 mm)		coarse ash	coarse tuff[3]	coarse-grained tuff[5]
between 0 and – 1 phi (1 – 2 mm)		very coarse ash	very coarse tuff[3]	very coarse-grained tuff[5]
between –1 and – 2 phi (2 – 4 mm)	lapilli[2]	fine lapilli (lapilli bed[4])	fine lapillistone	fine lapillistone
between –2 and – 4 phi (4 – 16 mm)	lapilli	medium lapilli	medium lapillistone	medium lapillistone
between –4 and – 6 phi (16 – 64 mm)		coarse lapilli	coarse lapillistone	coarse lapillistone
coarser than – 6 phi (>64 mm)	blocks and bombs	blocks and bombs	breccia	breccia

Table 1: Grain-size classification for pyroclastic (volcaniclastic) rocks after Mueller and White (2003). Notes: 1) "ash" is an aggregate name; single particles are ash grains, or ash particles. 2) "lapilli" is a plural particle name and singular is "lapillus"; aggregates of lapilli alone form a deposit, e.g. lapilli unit, lapilli bed and a consolidated lapilli unit is lapillistone. 3) Deposits or rocks composed of a mixture of grains within a single major class, such as a lithified aggregate of fine to coarse ash, default to the class name, e.g. "tuff" rather than "fine-medium-coarse tuff". 4) Deposits or rocks composed of a mixture of grain sizes are modified in the same way as are sedimentary rocks using the Wentworth scale, e.g. "lapilli ash" for ash containing >25 % lapilli and ash components (cf. pebbly sand), or "ash-bearing lapilli bed" for bed of lapilli with subordinate ash (cf. sandy [pebble] gravel). "Tuff breccia" is a rock containing >25% blocks or bombs with a >25% lithified ash matrix (cf. sandy conglomerate). 5) The attribute "-grained" represents the full rock name in the tuff grade scheme and is comparable to "fine-grained sandstone".

terms such as lapilli tuff breccia or tuff breccia indicate that >25% of the deposit has that specific grain size. This classification scheme takes into consideration the inherent problems of naming an ancient volcaniclastic rock, and is based on the early work of Fisher (1961, 1966) and integrates that of Schmid (1981), Fisher and Schmincke (1984) and Busby-Spera (1988). The North Amercian school of thought wherein the size of volcanic grains or clasts defines the name irrespective of primary or secondary origin (reworking) stands in sharp contrast with that of the Australian school (e.g. Cas and Wright 1987; McPhie et al. 1993), in which only primary pyroclastic material can be called tuff, lapilli and breccia.

Volcanic flows are simpler to name because they can usually be easily recognized in the field, and consequently termed according to their flow morphology. It is important to note that breccia is a product of an autoclastic fragmentation process rather than a grain-size denomination (see Table 1). The term breccia may also be allocated to a specific portion of the flow such as flow-top breccia. Pillow fragment breccia, pillow breccia and pillow rind breccia are types of autoclastic breccias. Massive flows are structureless and pillowed flows represent a subaqueous flow form, probably the subaqueous counterpart of subaerial pahoehoe tubes. These flow forms of massive, pillowed and breccia can be lateral and vertical equivalents of the same flow (Wells et al. 1979; Dimroth et al. 1979, 1985).

4.3 Mafic volcanic lithofacies

The dark green weathered rocks of the mafic volcanic lithofacies are primary volcanic flows of basaltic composition. The petrographic field divisions, based on phenocryst composition, define the various facies. Geochemistry is used to distinguish these units because the morphological flow forms are comparable. The following mappable units constitute the mafic volcanic lithofacies: 1) aphanitic, 2) microporphyritic, 3) feldspar-phyric, 4) pyroxene±feldspar-phyric, 5) gabbro, and 6) phonolitic volcanic facies. The individual flow forms are described for each facies.

4.3.1 Aphanitic volcanic facies

Description:

The 1-100 m-thick aphanitic facies is composed of 1-10 m-thick massive, 5-60 m-thick pillowed and 2-35 m-thick brecciated flow forms with local 15-20 cm in diameter columnar joints in massive units. Pillow sizes range from 10 cm to several metres (Plates 2C, 2D) and quartz-filled drainage cavities were locally observed (Plate 3A). Flow banding developed at flow margins, and 1-10 mm size quartz-carbonate filled vesicles constitute up to 30% of the rock (visual estimate; Plate 3B). Vesicles are located preferentially at the margins of massive and pillowed units. Pillow breccias up to 35 m-thick contain both poorly- to highly-vesicular irregular to amoeboid pillow fragments (up to 20 cm) in a hyaloclastite matrix that is locally altered to massive carbonate at certain localities (Plate 3C). Millimetre- and submillimetre phenocrysts of predominantly feldspar (Plate 3D) constitute <5% of the rock. Minor phenocrysts of pyroxene and possibly relic olivine were

Plate 3 (A): Quartz drainage cavity in a pillow, indicating the orientation of the palaeosurface (S_0). Pen (14 cm) points to stratigraphic top.

Plate 3 (B): Photomicrograph of sample AA-52-2001 in XPL. Pillow basalt with well-preserved rounded, non-deformed amygdule. Amygdule are composed of carbonate (orange-brown) and actinolite-chlorite-quartz (white).

Plate 3 (C): Pillow breccia with carbonatized matrix and unaltered clasts. Pen, 14 cm.

Plate 3 (D): Photomicrograph of sample AA-33-2001 in XPL. Aphanitic basalt flow with feldspar (Fsp) and opaques (O).

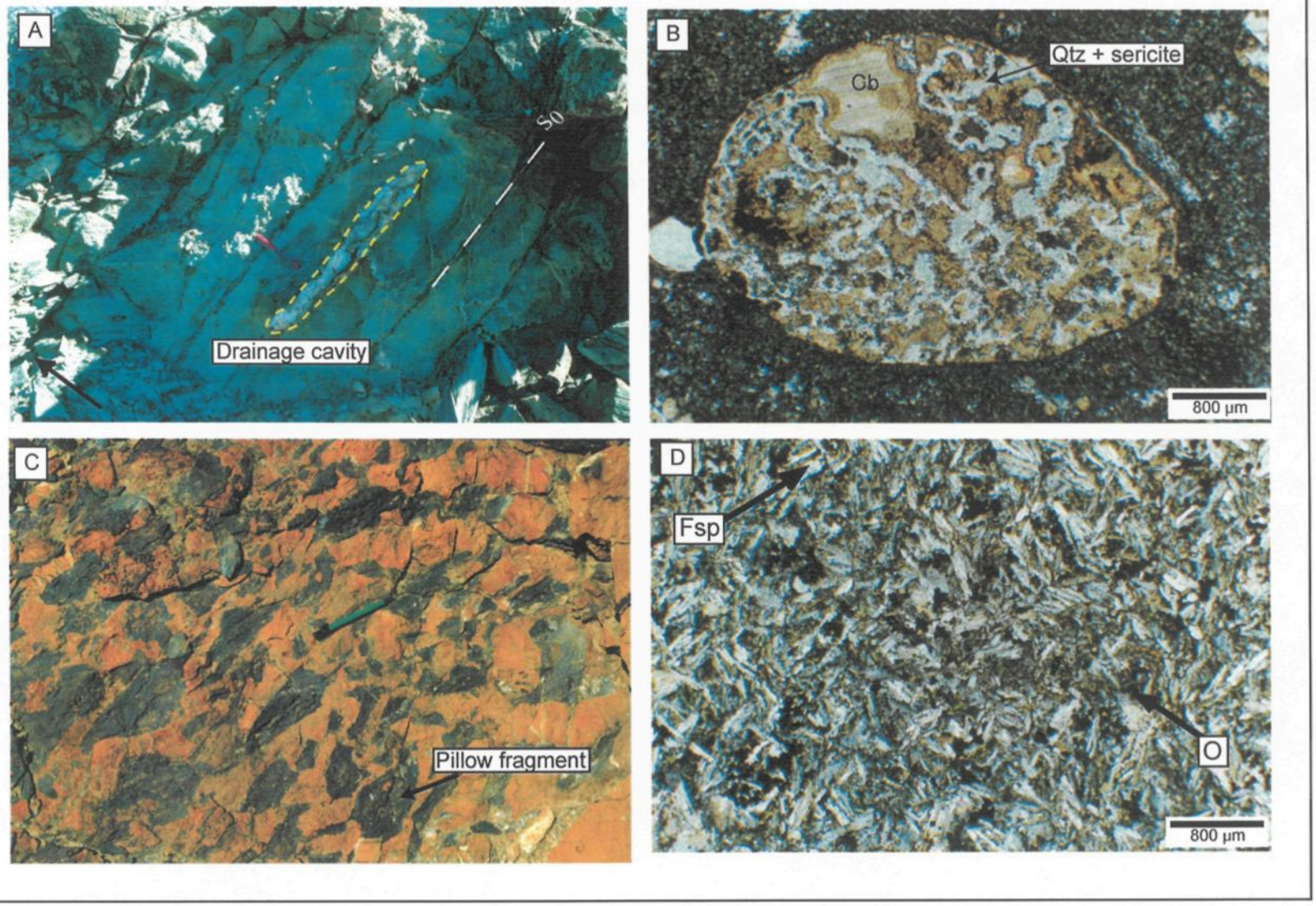
A
S0
Drainage cavity
B
Qtz + sericite
Cb
800 µm
C
Pillow fragment
D
Fsp
O
800 µm

Plate 3

also identified. Magnetite and hematite represent up to 10% of the rock in samples. Contacts of massive flows with tuffs are sharp (Plate 4A) and locally erosive.

Interpretation:

The volcanic rocks are typical of submarine mafic flows and show a flow combination of massive, pillowed, and pillow breccia, commonly found in ancient and modern flow successions (Dimroth et al. 1979, 1985; Staudigel and Schmincke 1984; Fornari 1986). The difference in pillow size either corresponds to a different extrusion volume, or a different position within the flow, whereby larger pillows are closer to the emission centre. The abundance of vesicles indicates that gas characterized the flow and probably facilitated autoclastic fragmentation. Flow banding at the margins of pillows and massive flows formed as a result of an increase in internal shear stress during continued flow. The quartz-filled drainage cavities which indicate paleobedding, are consistent with selective draining of magma in the tube.

Massive flows are considered proximal to the vent with respect to the other two flow forms. Columnar joints indicate rapid cooling perpendicular to the cooling front, which is a common feature in basalts. The pillow breccias are autoclastic products resulting from pillow disintegration due to thermal contraction and granulation during flow. Amoeboid-shaped pillow fragments are consistent with high-temperature fragmentation, possibly related to magma pouring out of pillow tubes on a volcanic slope.

Plate 4 (A): Sharp contact between a tuff unit and a massive flow of the aphanitic mafic volcanic facies. Arrow points to stratigraphic top. Pen, 14 cm.

Plate 4 (B): Feldspar-phyric mafic volcanic facies. Note the positive relief of the feldspar phenocrysts. Pencil, 14 cm

Plate 4 (C): Feldspar-phyric mafic volcanic facies with a trachytic texture, characterized by alignment of feldspars (Fsp). Pen, 10 cm.

Plate 4 (D): Photomicrograph of feldspar-phyric mafic volcanic facies in PPL. Feldspar phenocrysts are replaced by titanite (Ti).

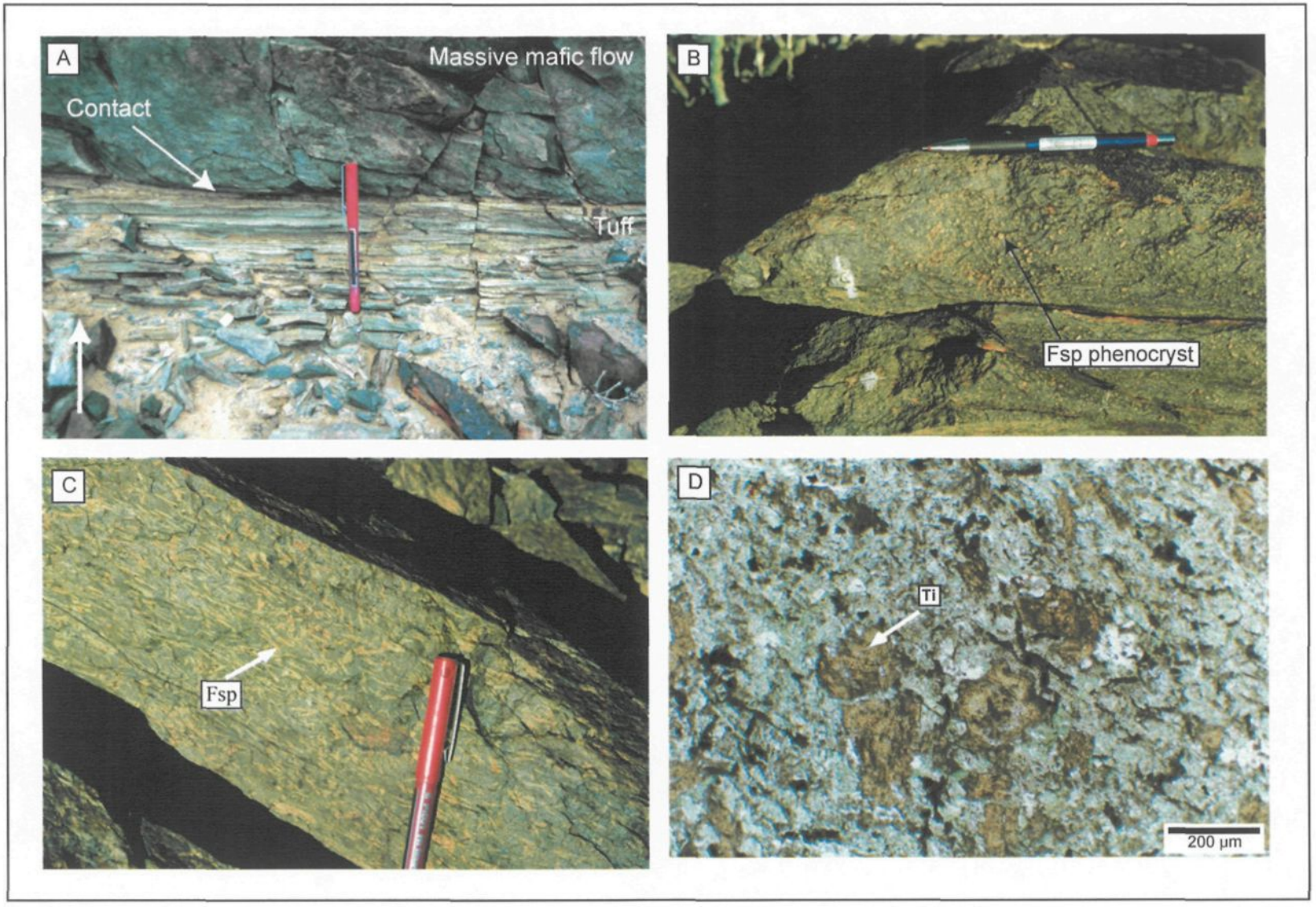
A
Massive mafic flow
Contact
Tuff
B
Fsp phenocryst
C
Fsp
D
Ti
200 µm

Plate 4

4.3.2 Microporphyritic volcanic facies

Description:

The 1-5 m-thick microporphyritic facies is composed of massive and pillowed flow units. A granular-intergranular texture with <5% phenocrysts defines this facies and differentiates it from the aphanitic facies in the field. Plagioclase and pyroxene are up to 2 mm and 0.5-2 mm in size, and rounded quartz-carbonate-filled vesicles were observed.

Interpretation:

Similar to the aphanitic volcanic facies, the microporphyritic volcanic facies is composed of massive and pillowed flows that compare favourably with a submarine setting (Dimroth et al. 1979; Wells et al. 1979; Cousineau and Dimroth 1982). The close association of both flow facies in the field suggests a cogenetic origin.

4.3.3 Feldspar-phyric volcanic facies

Description:

The 10-150 m-thick feldspar-phyric volcanic facies is predominantly composed of massive flows and subordinate pillowed units (<10%). Individual massive flows up to 30 m thick contain prominent flow banding at the margins and are composed of 5-30%, 1-10 mm-size plagioclase and <5%, 1-3 mm pyroxene phenocrysts (Plate 4B). The phenocrysts show a typical flow orientation or trachytic type texture (Plate 4C), generally referred to as porphyritic. Titanite ($CaTiSiO_5$) was locally observed (Plate 4D). Transitions to m-scale pillowed segments of the flow unit are subtle, but pillows are constrained to the flow top. The massive nature of the feldspar-phyric volcanic facies made it difficult to discern

between flows and sills unless contacts were observed. The mineralization includes disseminated magnetite and hematite, which represents up to 5% of the rock.

Interpretation:

The predominance of massive phenocryst-rich flows in the feldspar-phyric volcanic facies is consistent with thick viscous lava flows (Macdonald 1972; Gill 1981; Mueller 1991) probably close to an emission centre. The high viscosity is indicated by the phenocryst content and size (Mcdonald, 1972; Williams and McBirney 1979), and suggests a high-level phenocryst-rich magma chamber associated with volcanic construction. Massive flows are generally considered proximal to the source (Dimroth et al. 1985). In the field, a synvolcanic fault (Map 1, in pocket) is associated with this facies, so that a proximal setting is tenable. The pillowed parts of the flows support a subaqueous setting (Wells et al. 1979).

4.3.4 Pyroxene± feldspar-phyric volcanic facies

Description:

Massive flows are predominant in the pyroxene±feldspar-phyric lithofacies, whereas pillowed flow units are minor (<10%). The units are 1-15 m thick and consist of 1-4 mm plagioclase feldspar (5-10%) and 1-4 mm pyroxene phenocrysts (5-15%). Plagioclase is replaced by actinolite, chlorite and leucoxene, and the pyroxene was replaced by hornblende, chlorite, epidote and leucoxene (Plates 5A, 5B). Mineralized phases include magnetite and hematite, constituting 2% of the lithofacies.

Plate 5 (A): Photomicrograph of sample AA-71-2001 in PPL. Pyroxene±feldspar-phryric mafic volcanic facies. Alteration is represented by chlorite (Chl), actinolite (Act), and epidote (E).

Plate 5 (B): Photomicrograph of sample AA-71-2001 in XPL. Pyroxene±feldspar-phyric mafic volcanic facies. Alteration is represented by chlorite (Chl), actinolite (Act), and epidote (E).

Plate 5 (C): Photomicrograph of sample AA-53-2001 in XPL. Rock consists mainly of K-feldspar (Fsp) and epidote (E).

Plate 5 (D): Graded bedded, unaltered tuff with sedimentary structures (wavy beds). Arrow points to stratigraphic top. Pen, 14 cm.

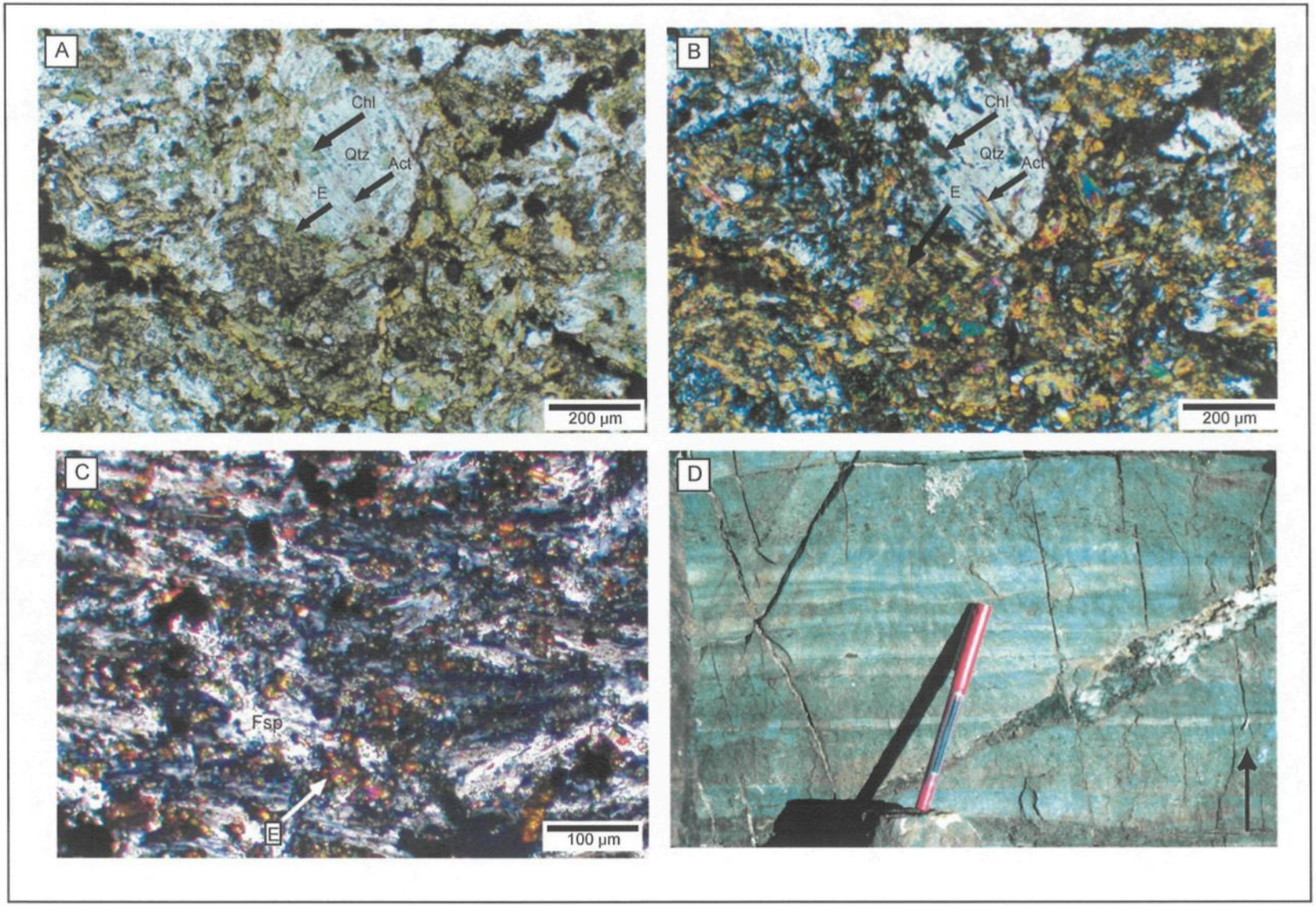

Plate 5

Interpretation:

The pyroxene±feldspar-phyric facies displays the features of submarine volcanism as indicated by the pillowed flow units (Dimroth et al. 1979, 1985). The 10-25% phenocryst content is suggestive of viscous flow from a high-level magma system.

4.3.5 Gabbro volcanic facies

Description:

The 5-40 m-thick gabbro volcanic facies is massive with an intergranular to subophitic texture, and is characterized by a brownish-green weathering colour. Magnetite and hematite locally constitute up to 15% of the rock. A large-scale low-angle intrusive relationship could be inferred from the map pattern (see Maps 1 to 4, in pocket).

Interpretation:

The gabbros are considered coeval with the mafic volcanic sequence, as is suggested by the geochemistry. The massive bodies are interpreted as low-angle dykes or sills.

4.3.6 Phonolitic volcanic facies

Description:

At one location, an aphanitic volcanic rock was observed (AA-53-2001; Maps 1 and 3, in pocket). The unit was massive with columnar joints and in thin-section, the rock is characterized by abundant feldspar (Plate 5C).

Interpretation:

This volcanic rock has a phonolitic geochemical composition (see geochemistry segment). The massive columnar jointed unit could be either effusive or intrusive, but a lack of contacts inhibits interpretation.

4.4 Volcaniclastic lithofacies

The volcaniclastic lithofacies was divided into facies according to a volcanic grain-size scheme that included tuff, lapilli tuff and lapilli tuff breccia. The lithofacies was affected by hydrothermal carbonate alteration, but selected areas exhibit excellent primary features and delicate volcanic textures. The volcaniclastic lithofacies has been described by Mueller (2003), but deposits surrounding the mineralization are part of this thesis. The lapilli tuff breccia facies, not identified by Mueller (2003), is considered in this thesis and is a new but important element due to its spatial relationship with the Mn-mineralization (Figure 16).

4.4.1 Tuff facies

Description:

The tuff facies consists of 0.10-5 m-thick units between pillowed and massive basalt flows (Plate 4A), as thick lapilli tuff beds and as an up to 90 m-thick sequence capping the stratigraphy (Figure 17, section 10; Figure 18). The 0.5-3 cm-thick, fine- to- coarse-grained tuffs are mafic and are composed of lithic volcanic fragments, sideromelane and scoria. Beds contain graded bedding, parallel lamination (Plate 5D) and minor rippled horizons. Contacts with the

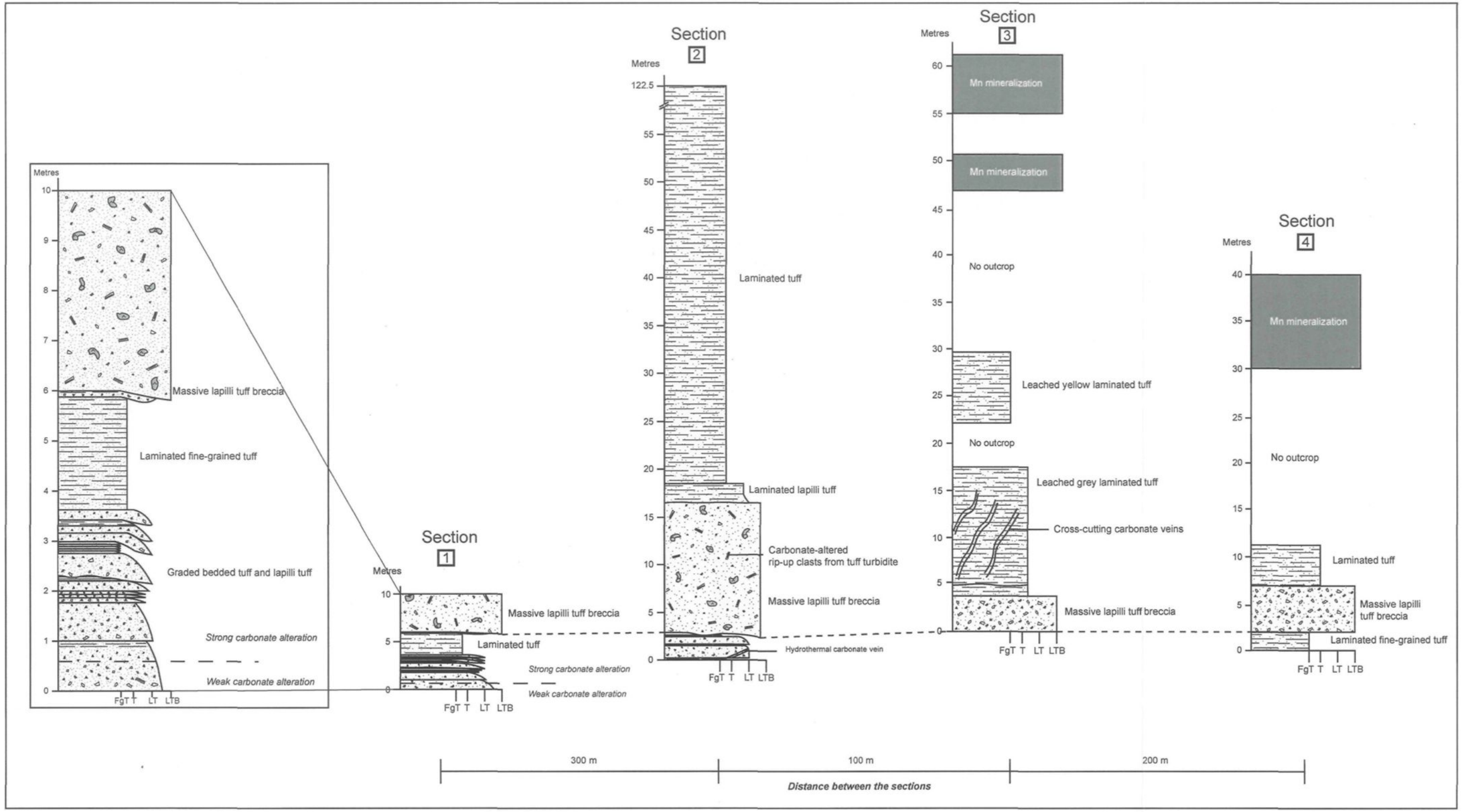

Figure 16: Stratigraphic sections of the Schakalsberg area. Numbers in the squares above the sections represent the location of the sections on Maps 1 and 2 (in pocket). Fgt - fine-grained tuff, T - tuff, LT - lapilli tuff, LTB - lapilli tuff breccia.

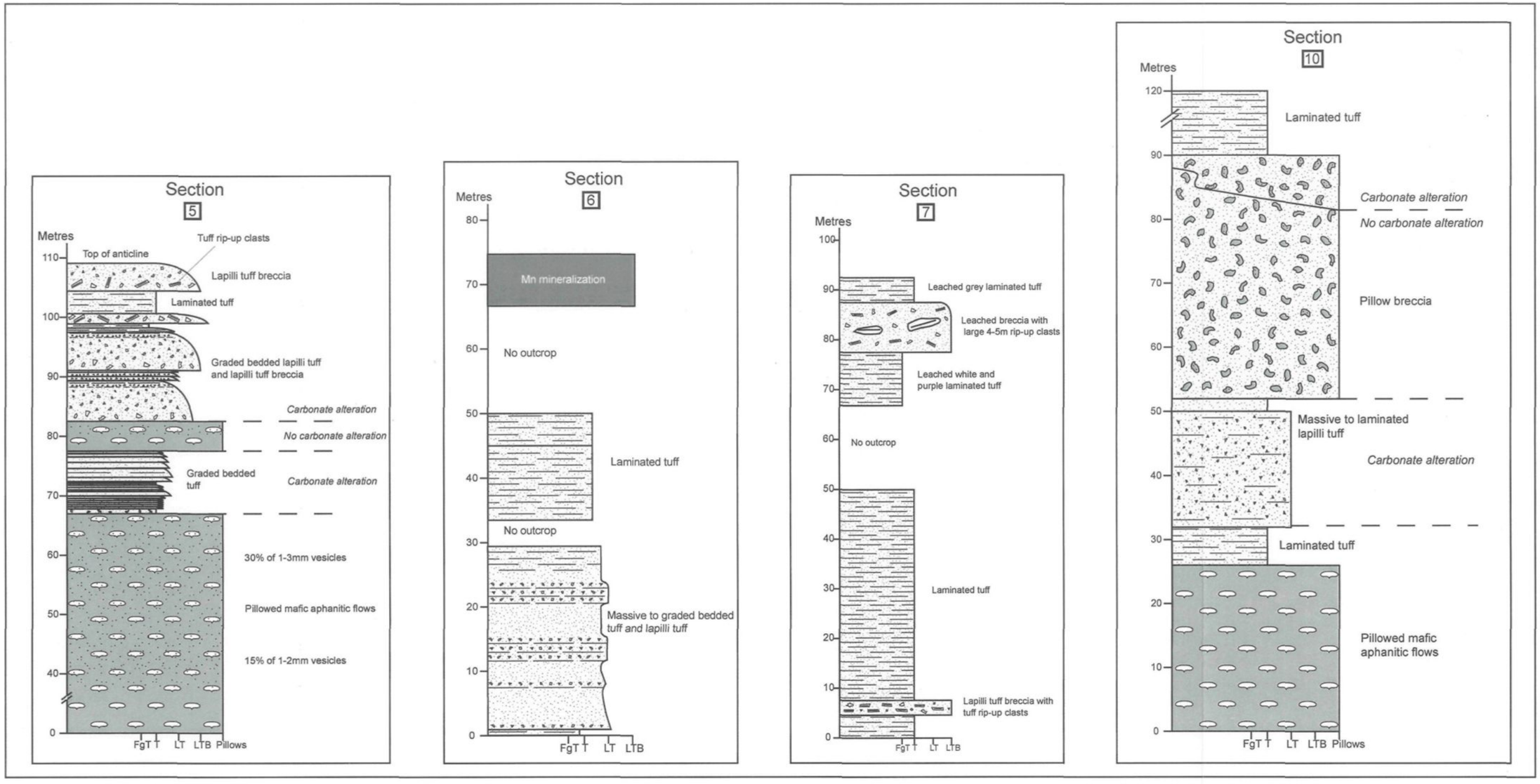

Figure 17: Stratigraphic sections of the Schakalsberg Mountains. Numbers in the squares above the sections represent the location of the sections on Maps 1 and 2 (in pocket). Fgt - fine-grained tuff, T - tuff, LT - lapilli tuff, LTB - lapilli tuff breccia.

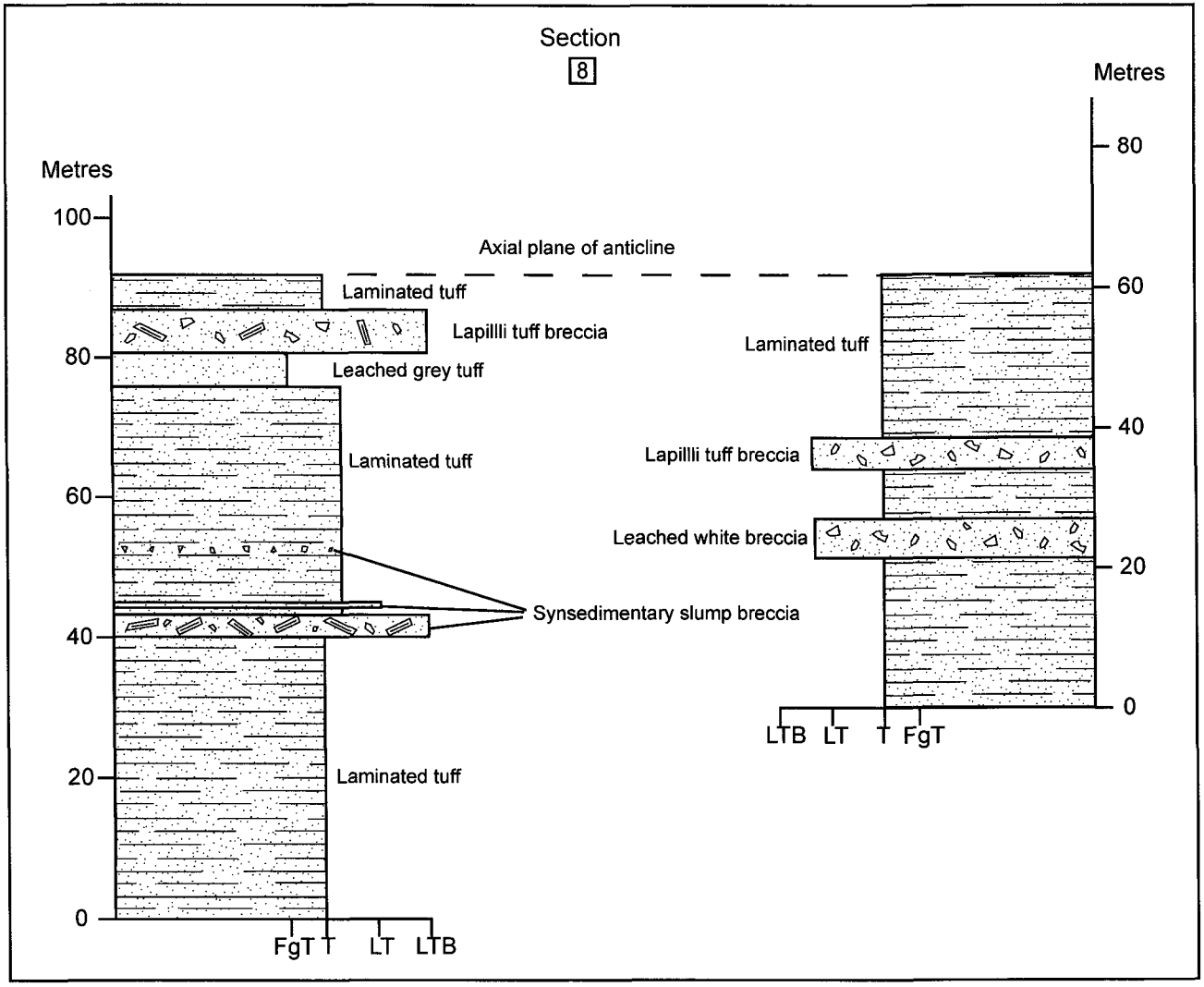

Figure 18: Stratigraphic sections from the Schakalsberg area. Number in upper middle corresponds to the number on Map 2 (in pocket).Fgt - fine-grained tuff, T - tuff, LT - lapilli tuff, LTB - lapilli tuff breccia.

overlying lapilli tuff and primary volcanic flows are sharp and locally erosive (Figure 17), whereas basal contacts are sharp and depositional but non-erosive.

Interpretation:

The tuff facies represents deposition from dilute turbidity currents with Bouma T_{bd} and T_{cd} divisions, and rippled horizons are considered T_c-layers (Lowe 1982, 1988). Suspension deposits, T_d, settled out of the water column. These low-concentration, fine-grained deposits with abundant low-density volcanic shards and scoria and lithic particles congested the water column and could only have settled during volcanic quiescence and an absence of water turbulence (Lowe 1988; Mueller and White 1992). Their association as caps to lapilli tuffs and lapilli tuff breccias suggests that elutriation processes possibly occurred during subaqueous transport.

4.4.2 Lapilli tuff facies

Description:

The 0.20-1.50 m-thick lapilli tuff (Figure 17, section 5, 6 and 10) is composed of planar-bedded to crossbedded structures that display wavy bedforms, but are also massive to poorly graded. They are conformably overlain by thin-bedded graded to laminated tuffs and eroded thick massive lapilli tuff breccias. Stratification is accentuated by grain-size changes. Planar beds locally grade laterally into crossbeds, which inturn change back into planar beds. Synsedimentary deformation and scour surfaces are common. Lithic volcanic fragments and scoria are abundant, whereas liberated crystals and armoured lapilli are minor (Plate 6A).

Interpretation :

The planar-bedded to crossbedded lapilli tuffs with a pronounced stratification and armoured lapilli were interpreted by Mueller (2003) to have resulted directly from subaqueous eruptions. These types of deposits, the results of small volume, shallow-water eruptions, are referred to as (sub)aqueous eruption-fed density current deposits (White 1996, 2000; Mueller et al. 2000). Planar and wavy beds with cross stratification and scouring suggest bedload transport but also unsteady, turbulent density currents with low- to high-particle concentrations (White 1996; Mueller et al. 2000). Massive to graded beds reflect high concentration density (turbidity) flows with rapid en-masse fallout (Lowe 1982), but if the lapilli tuffs are only massive and matrix-supported, a laminar debris flow process is inferred. Grading reflects a decrease in transport-settling velocity.

4.4.3 Lapilli tuff breccia facies

Description:

The newly identified 3-13 m-thick lapilli tuff breccia facies represents property scale marker horizons that may or may not be related to mineralized sections (Figure 16). The massive to graded beds are both framework- and matrix-supported. Breccia size clasts are generally in a lapilli grade matrix. The deposits are compositionally heterolithic containing primary volcanic clasts, rip-up clasts of tuff, and more importantly, carbonate altered rip-up clasts in which bedding is still discernable (Plate 6B). The bases of the deposits are sharp and erosional as well as non-erosive.

Plate 6 (A): Photomicrograph of an armoured lapillus in PPL. The lapillus is a scoria fragment surrounded by consolidated volcanic ash.

Plate 6 (B): Lapilli tuff breccia with volcanic and sedimentary clasts. Note that bedding is visible in the sedimentary clasts which are now altered to carbonates.

Plate 6 (C): Landscape view of the southern part of the Schakalsberg Mountains. The orange colour represents the carbonatized volcaniclastic lithofacies whereas the green color corresponds to the unaltered mafic volcanic lithofacies. Field of view is 1 km.

Plate 6 (D): Intensely carbonatized tuff. Note that despite the alteration, primary textures are readily observed. Arrow indicates the stratigraphic top. Pen, 14 cm.

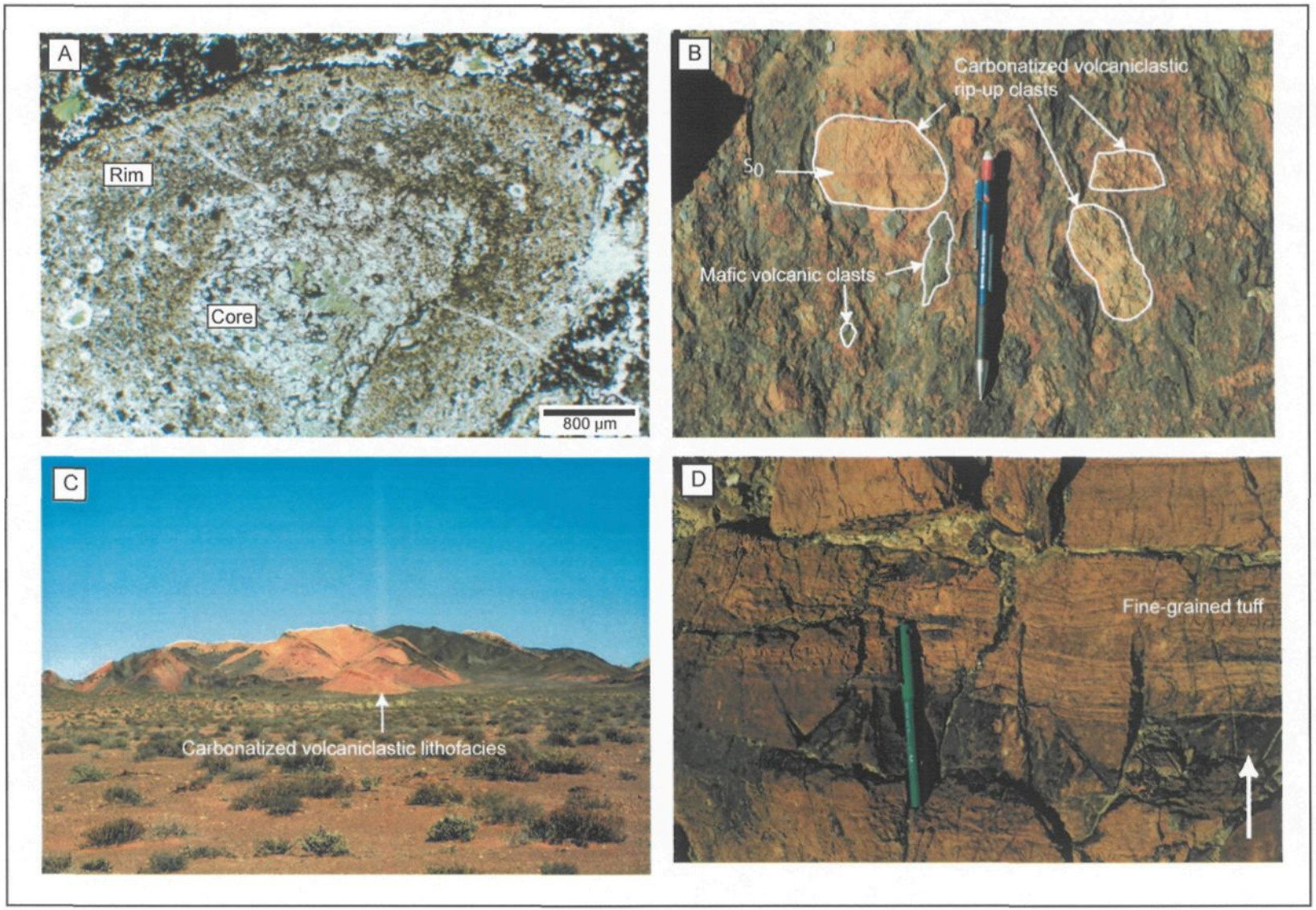
A
Rim
Core
800 µm
B
Carbonatized volcaniclastic rip-up clasts
S0
Mafic volcanic clasts
C
Carbonatized volcaniclastic lithofacies
D
Fine-grained tuff

Plate 6

Interpretation:

The massive, matrix-supported lapilli tuff breccia is consistent with deposition from subaqueous debris flows, whereas the graded counterparts reflect high-concentration turbidity current deposition (Lowe 1982). Transport in the debris flows was under laminar flow conditions, but erosive basal contacts at certain localities indicate that turbulence within the flow was locally operative. The deposits are reworked volcaniclastic material transported downslope via sediment gravity flows, as indicated by the hydrothermally altered rip-up clasts of tuff and numerous other clast types.

4.4.4 Sedimentary breccia facies

Description:

The 2-10 m-thick sedimentary breccia lithofacies is restricted to the upper part of the stratigraphy (Figure 15) and is only interstratified with the 90 m-thick tuff sequence. The fragments are generally angular tuff rip-up clasts which are up to 4-5 m in diameter (Figure 17, section 7). This lithofacies is matrix-supported and disorganized, and shows no grading.

Interpretation:

The matrix-supported sedimentary breccia lithofacies is interpreted as a subaqueous debris flow deposit (Lowe 1982) that may have been triggered by seismic activity. The large out-sized 4-5 m blocks reflect slope failure, which is a common phenomenon on volcanic edifices.

4.5 Carbonate lithofacies

Description:

Located to the east of the Red Dunes thrust (Map 1, in pocket), blue-grey weathered carbonates over 100 m were mapped. The carbonates rocks consisting of 100% fine-grained carbonate (<0.1 mm) are not interstratified with the volcanic sequence.

Interpretation:

The carbonates are interpreted as being primary in origin and could be the lateral equivalent of the Schakalsberg Mountains section (Map 1, in pocket).

4.6 Stratigraphy

The general stratigraphy (Figure 15) of the Schakalsberg Mountains stems from Mueller (2003). The ca. 1.4 km-thick succession represents a shoaling upward sequence strikingly similar to that described by Staudigel and Schmincke (1984) for the Canary Islands. The lower part of the studied stratigraphy is dominated by massive to pillowed basalts that display a low degree of vesicularity, and are intruded by thick gabbro sills. In contrast, the upper part of the stratigraphy is composed of abundant volcaniclastic units with a low to moderate degree of vesicularity. Autoclastic and pyroclastic fragmentation processes increased up-section, and can be an indirect measure of shoaling. The phenocryst-rich lavas are prominent at the base of the sequence whereas aphanitic facies predominate the summital part of the succession. Recent mapping by Kumba Resources teams (2002-2003) and Mueller (2003) has shown that the final stage of volcanic edifice construction was not purely volcanic. The continued shoaling of the edifice could be

documented in the adjacent concession to the southeast, where a 40 m-thick oolite sequence and 5 m-thick stromatolite unit were observed. In addition, hydrothermal Fe-rich fluids partially replaced the stromatolites, so that even though the final stage of edifice construction reflects local emergence, hydrothermal activity was still prominent. The physical volcanology, volcaniclastic lithofacies, stratigraphy and setting of such a volcanic sequence is suggestive of a seamount (Corcoran 2000; Schmidt and Schmincke 2000).

CHAPTER 5

CARBONATIZATION

5.1 Introduction

A principal characteristic of the Schakalsberg Mountains is a pervasive carbonatization, affecting both the volcaniclastic units and mafic flows over tens of kilometres. In order to understand the mineralization, the alteration process must be considered. Carbonate alteration due to hydrothermal fluids is a prevalent characteristic of mineralized environments, and especially base metal deposits. Moreover, the Fe-Mg element ratio in carbonates is an important tool in targeting economic deposits (Franklin 1990; Lafrance 2003). This section considers carbonatization, its effects on the protolith, the mechanisms involved, and the relation to mineralization in the study area.

5.2 Characteristics

Carbonatization is a hydrothermal process by which rock-forming minerals are replaced by carbonates. This can occur in various environments and the chemical reactions are different. Carbonate is a mineral characterized by a $(CO_3)^{2-}$ ion (Foucault and Raoult 1995), and has more than 60 mineral species (Deer et al. 1992). Carbonates are common, and mainly present in sedimentary rocks, as ancient organisms and chemical precipitates, but also as alteration minerals. In order to produce alteration carbonates, a change in the

environment or in the conditions of the host rock is required. Because the CO_3^{2-} ion is an essential component of carbonates, a source of carbon and oxygen is required for their formation. At the magmatic level, the two main volatile phases are CO_2 and H_2O (Wilson 1989). In addition to sea water, volcanoes with magmatic reservoirs also contain CO_2. These two sources are the prime candidates for providing CO_2 required to form carbonates. Alteration is achieved by the hydrothermal circulation derived from a magmatic source, and/or from the interaction of the rock with sea water. The magma chamber is the heat source that drives the circulation of hydrothermal fluids.

Carbonatization, like most types of alteration, is a replacement process. While circulating through the rock, hydrothermal fluids rich in CO_2 mainly dissolve silicate mineral phases (Wilson 1989). The dissolved mineral phases release ions or molecules which are able to react, resulting in a new mineral phase, carbonate. The silica part of the dissolved mineral is commonly transported at the rock-water interface, or is precipitated at the subsurface. Precipitation of silica in porous volcano-sedimentary units commonly forms "cap rock", a salient feature of massive sulfides.

Precipitation of carbonates or silicate ions in new mineral species also depends on the fluid's saturation state and the conditions during circulation. For example, a temperature or pressure change will cause some mineral species to precipitate. Some mineral phases only form under certain pressure (P) and temperature (T) conditions (Deer et al. 1992). The main factor ruling the dissolution and replacement rates of carbonates is the partial pressure of CO_2 (P_{CO2}) in the circulating fluid (Wilson 1989). The greater the P_{CO2}, the easier it will be for the fluid to dissolve the silicates and the more prominent the

carbonatization. With the evolution of the hydrothermal system, other fluids can interact and the carbonate can be destroyed by the superposition of another type of alteration (e.g. chlorite; Thompson and Thompson 1996). According to rock composition, the resulting carbonate composition varies (Figure 19).

Cations present in the carbonatization process are Fe^{2+}, Ca^{2+} and Mg^{2+}, and are dependent on host rock and dissolved mineral phases. Even if one element is more abundant, for example more Ca with respect to Fe, calcite will not necessarily be formed. This is because Fe is easier to dissolve, the resultant carbonate will be siderite.

Figure 19 illustrates the most abundant carbonate phases, but other carbonates, such as rhodocrosite ($MnCO_3$) may form if P_{CO2} is very high and if the system is rich in manganese. Moreover, there is a wide variety of carbonates with compositions varying from rhodocrosite to siderite and from rhodocrosite to calcite (Deer et al. 1992).

5.3 Protoliths and mechanism

The rocks in the Schakalsberg study area are mafic volcanic and mafic volcaniclastic rocks. Mafic volcanic rocks are the most common protolith in which carbonatization occurs. Carbonatization can occur before or after metamorphism (Melling et al. 1990), with the most abundant carbonate species being calcite and dolomite (Davies et al. 1990). Ankerite, siderite and magnesite can also be present in the system and depend on the initial composition of the rock and the fluid. For example, basalt can be altered and be composed of up to 80% ankerite-quartz (Penczak and Mason 1999), whereby

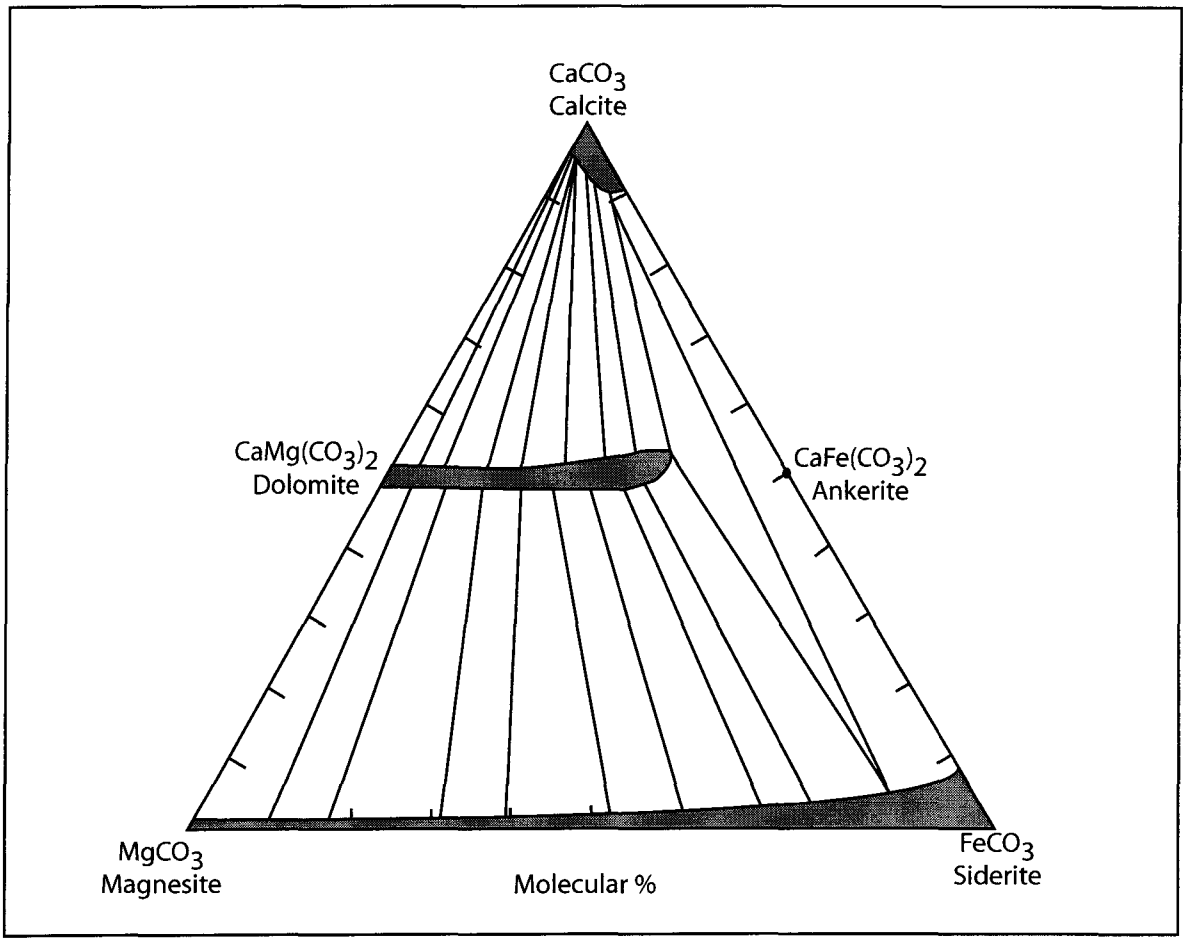

Figure 19: Carbonates of the calcite group (modified from Deer et al. 1967). Shaded areas represent the compositional fields of the most common phases.

replacement of silicate phases occur in the phenocrysts and in the matrix (Melling et al. 1990). Replacement in phenocrysts takes place along cleavage planes and grain boundaries.

The following reactions at greenschist or amphibolite metamorphic facies occur in the carbonatization of basalt.

According to Thomson (1987):

3 Actinolite $[Ca_2(Mg, Fe^{2+})_5[Si_8O_{22}](OH, F)_2]$ + 2 Zoïsite $[Ca_2Al_3Si_3O_{12}(OH)]$ + 10 CO_2 + 8 $H_2O \Rightarrow$ 3 Chlorite $[(Mg, Fe^{2+}, Fe^{3+}, Mn, Al)_{12}[(Si, Al)_8O_{20}](OH)_{16}]$ + 10 Calcite ($CaCO_3$) + 21 Quartz (SiO_2)

Biotite $[K(Mg, Fe)_3(AlSi_3O_{10})(OH)_2]$ + Chlorite $[(Mg, Fe^{2+}, Fe^{3+}, Mn, Al)_{12}[(Si, Al)_8O_{20}](OH)_{16}]$ + 8Calcite ($CaCO_3$)+ $CO_2 \Rightarrow$ Muscovite $[KAl_2(AlSi_3O_{10})(OH)_2]$ + 8Dolomite $[(CaMg(CO_3)_2]$ + 3Quartz (SiO_2)+ $4H_2O$

Other reactions including the same components have also been determined by Hynes (1980). Kerrich and Fyfe (1981) took into consideration free cations in the fluid, therefore resulting in the reaction:

3 aluminous Chlorite $[(Mg_2Al_3)(AlSi_3O_{10})(OH)_8]$ + 6 Epidote $[Ca_2(Al, Fe)Al_2O(SiO_4)(Si_2O_7)(OH)]$ + 6 SiO_2 + 24 CO_2 + 10 $K^+ \Rightarrow$ 10 Muscovite $[KAl_2(AlSi_3O_{10})(OH)_2]$ + 12 Fe-Dolomite $[Ca(Mg, Fe^{2+})(CO_3)_2]$ + 10 H^+

In the case of siderite as an alteration product, the reactions can be the following (Veizer et al. 1989):

Actinolite [$Ca_2(Mg, Fe)_5Si_8O_{22}(OH)_2$] + Epidote [$Ca_2(Al, Fe)Al_2O(SiO_4)(Si_2O_7)(OH)$] + Fluid ($CO_2$, H_2O) $\Rightarrow$ Chlorite [$(Mg, Fe^{2+}, Fe^{3+}, Mn, Al)_{12}[(Si, Al)_8O_{20}](OH)_{16}$] + Calcite ($CaCO_3$) + Chert ($SiO_2$)

Chlorite [$(Mg, Fe^{2+}, Fe^{3+}, Mn, Al)_{12}[(Si, Al)_8O_{20}](OH)_{16}$] + Calcite ($CaCO_3$) + Fluid ($K^+$, CO_2) $\Rightarrow$ Sericite [$KAl_2(AlSi_3O_{10})(OH)_2$] + Fe-Dolomite [$Ca(Mg, Fe^{2+})(CO_3)_2$] + Chert ($SiO_2$) + Fluid ($H_2O$, H^+)

Magnetite (Fe_3O_4) + CO_2 $\Rightarrow$ Siderite ($FeCO_3$)

Carbonatization not only produces carbonates, but also chlorite and quartz (chert). In addition, one carbonate phase can be replaced by another carbonate phase, as shown by the following reaction (Franklin et al. 1975):

$CaMg(CO_3)_2 + 2Fe^{2+} \Rightarrow 2FeCO_3 + Ca^{2+} + Mg^{2+}$

The carbonatization process can also impact the degree of metamorphism of the rock. The presence of fluids can inhibit the growth of some mineral phases, which is particularly true with low-grade metamorphic minerals (prehnite and pumpellyite) because

the partial pressure of CO_2 is high (Greenough and Papezik 1985). Evidently, carbonatization and metamorphism must be differentiated.

5.4 Fluid movement in volcanic systems

Carbonatization requires hydrothermal circulation, which is a common characteristic in volcanic environments. The key fluid component is highly variable in such a setting, but because hydrothermal activity is linked to mineralization, it has been extensively studied (Franklin et al. 1975; Leleu 1978; Kerrich and Fyfe 1981; Drummond and Ohmoto 1985; Greenough and Papezik 1985; Dubé and Hubert 1991; Sketchley and Sinclair 1991; Larocque and Hodgson 1993; Schandl and Wicks 1993; Penczak and Mason 1999). All of these studies showed that there was a direct link between hydrothermal carbonate alteration and massive sulfide mineralization.

Carbonates provide information concerning the composition of hydrothermal fluids. Isotopic and geochemical studies are employed to differentiate between metamorphic, marine, meteoritic or magmatic waters. In many cases, the fluid is a mixture from different sources (e.g. Veizer et al. 1989). Furthermore, carbon analysis elucidates the source of CO_2, be it organic, magmatic or derived from host rocks. Although the fluids and their composition differ between sites, CO_2 and H_2O are essential in the carbonatization process. In certain cases, the fluid will be composed of 2 different phases, an aqueous fluid rich in CO_2 and a critical carbon dioxide fluid with a high concentration of H_2O (Guthrie Jr et al. 2001). In addition, different conditions of P, T and oxygen fugacity will influence reactions

and lead to the transport of elements generally considered immobile (Ti, Y, Zr; Hynes 1980).

Fluid circulation occurs via synvolcanic fracture systems in submarine volcanic edifices on the ocean floor. Sea water interacts with volcanic rock and magmatic hydrothermal fluids. Apart from synvolcanic faults, porous volcaniclastic beds are rich in hydrothermal fluids and are commonly highly altered in comparison with adjacent lava flows. The circulation of fluids can begin during and may continue until the termination of volcanic activity. Later intrusions, faults, and fractures create favourable conditions for the carbonatization process and show the complexity of hydrothermal processes.

Epithermal mineralization is another type of hydrothermal circulation system that is linked to subaerial volcanic systems. Fluids circulate through conduits and fractures and then interact with the host rock. The fluid composition is generally magmatic water combined with meteoritic water, this phenomena taking place above sea level.

5.5 Carbonatization and mineralization

Numerous mineral deposits are related to carbonatization (e.g.VMS and lode gold). In addition to the role of CO_2, this section discusses the relation between carbonatization and the mineralizing systems.

5.5.1 Lode gold deposits

Carbonate alteration is common in Archean lode gold deposits (Kerrich and Fyfe 1981), and is associated with structurally-controlled mineralized veins that have

pervasively altered host rocks. Carbonates have a negative solubility coefficient regarding the temperature (the higher the temperature, the less soluble they are), and special conditions (boiling) are required in order to precipitate carbonates in a cooling solution (Kerrich and Fyfe 1981). This feature explains why mineralization and carbonatization are not necessarily contemporaneous (Drummond and Ohmoto 1985).

Two types of carbonate alteration, a regional and a local phase, are commonly observed (Figures 20 and 21). The regional carbonatization pervasively alters the protolith and generally occurs before the mineralizing event (Veizer et al. 1989; Melling et al. 1990), whereas local carbonatization is directly linked to mineralization, generally concentrated in quartz-carbonate veins. The composition of local and regional carbonates can vary depending on the fluid's composition and on the nature of the host rock. The most common carbonate phases associated with mineralization are calcite, dolomite and ankerite (Melling et al. 1990; Penczak and Mason 1999). Archean lode gold deposits often show a zoned alteration pattern. Figure 20 shows an example of zonation in the case of a gold bearing vein.

Isotopic studies can also help differentiate between regional and local carbonates (Figure 22). The carbonates in the regional alteration will tend to have a more marine C signature whereas the carbonates in the conduit (local alteration) will tend to have a magmatic C signature, with the fluids affecting the conduit being derived from the magma.

The composition of local and regional carbonates can change, depending on the conditions under which they form. Sketchley and Sinclair (1991) gave a proximal assemblage of dolomite-ankerite and a distal assemblage of calcite-siderite-ankerite,

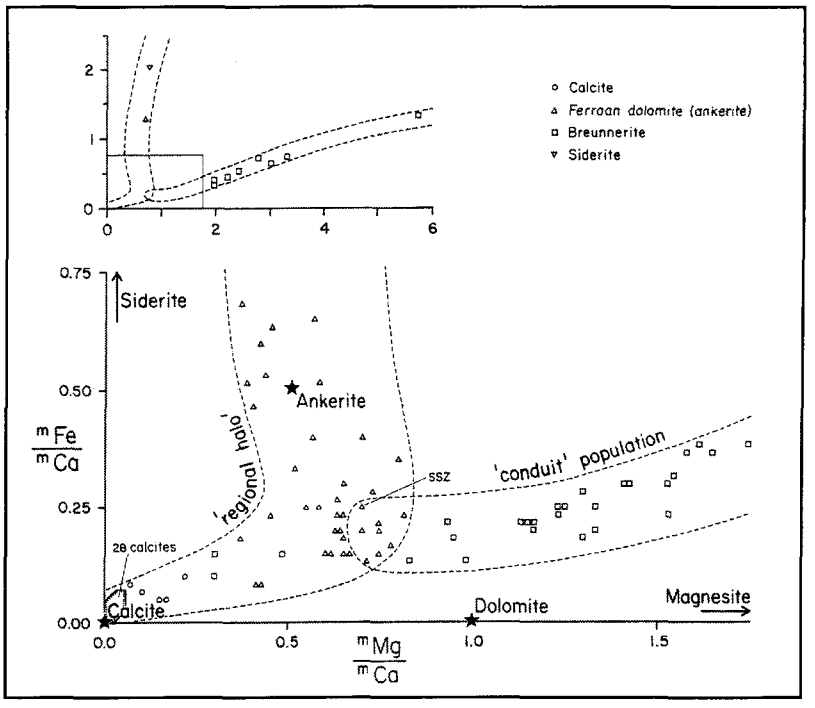

Figure 20: Mineralogy and geochemistry of selected carbonates, in addition to a regional and conduit discrimination in the case of a gold vein (Veizer et al. 1989).

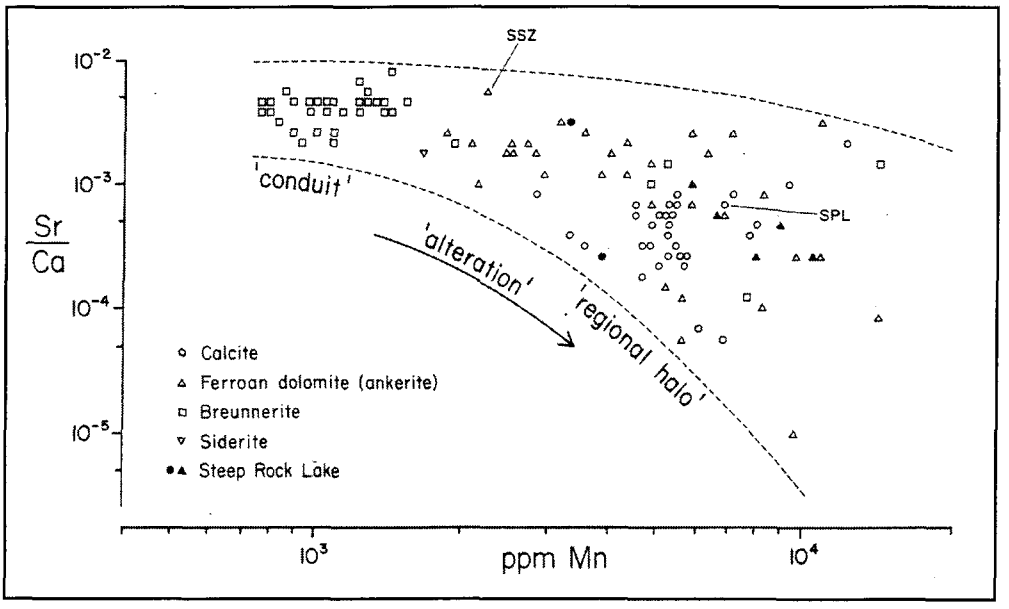

Figure 21: Sr/Ca vs Mn diagram of selected carbonates, in addition to a regional and local (conduit) division (Veizer et al. 1989).

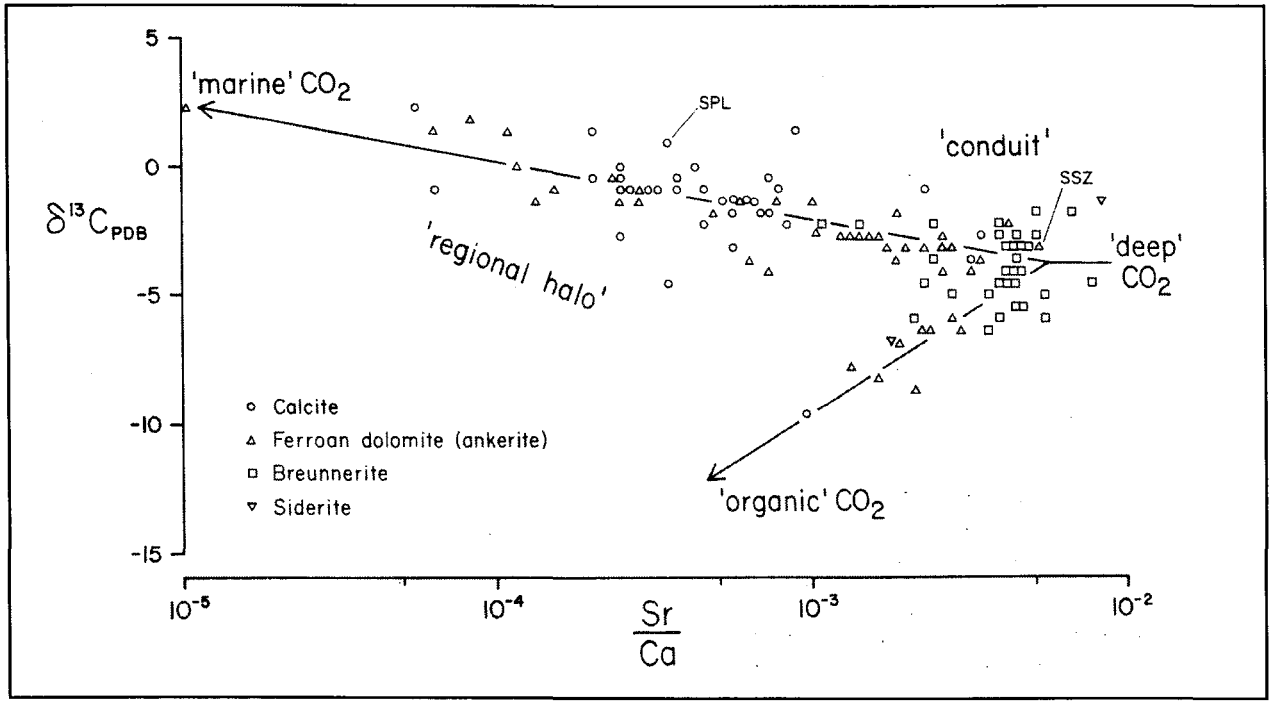

Figure 22: Isotopic diagram for selected hydrothermal carbonates (Veizer et al. 1989). The local (conduit) carbonates have an isotopic composition close to "deep" CO_2 (magmatic), whereas regional carbonates are a mixture of magmatic and marine CO_2.

whereas Veizer et al. (1989) gave a ferroan dolomite-breunnerite assemblage for the proximal phase and a calcite-siderite-ankerite assemblage for the distal phase. In most cases, the proximal phases are dolomite and ankerite, the distal phases are calcite and siderite.

According to Veizer et al. (1989), fluids that have circulated through mineralized conduits are more representative of a magmatic source, whereas fluids that created the regional alteration are the results of a mixing of fluids (magmatic, oceanic, metamorphic and meteoritic). This is consistent with the observations of many authors (e.g. Sketchley and Sinclair 1991; Penczak and Mason 1999). The regional alteration is late and is mainly caused by the interaction of sea water with volcanic rocks.

5.5.2 Volcanogenic massive sulfides

Volcanogenic massive sulfides (VMS), specifically the Mattabi-type (Franklin 1993), feature pervasive carbonate alteration with a semi-conformable zone (Figure 23). In VMS deposits, calcite, dolomite, ankerite, siderite and magnesite are the most common carbonates. The regional carbonatization is an early feature (Franklin et al. 1975; Larocque and Hodgson 1993). Being in a volcanic system, the volcanic rocks interacted with hydrothermal fluids during and after the formation of the edifice. This process creates the regional carbonatization. Subsequently, a mineralizing system ensues, creating the mineralization-related carbonatization. For the Mattabi-type deposit, the main regional alteration mineral is dolomite whereas siderite occurs at the local scale. The phenomenon

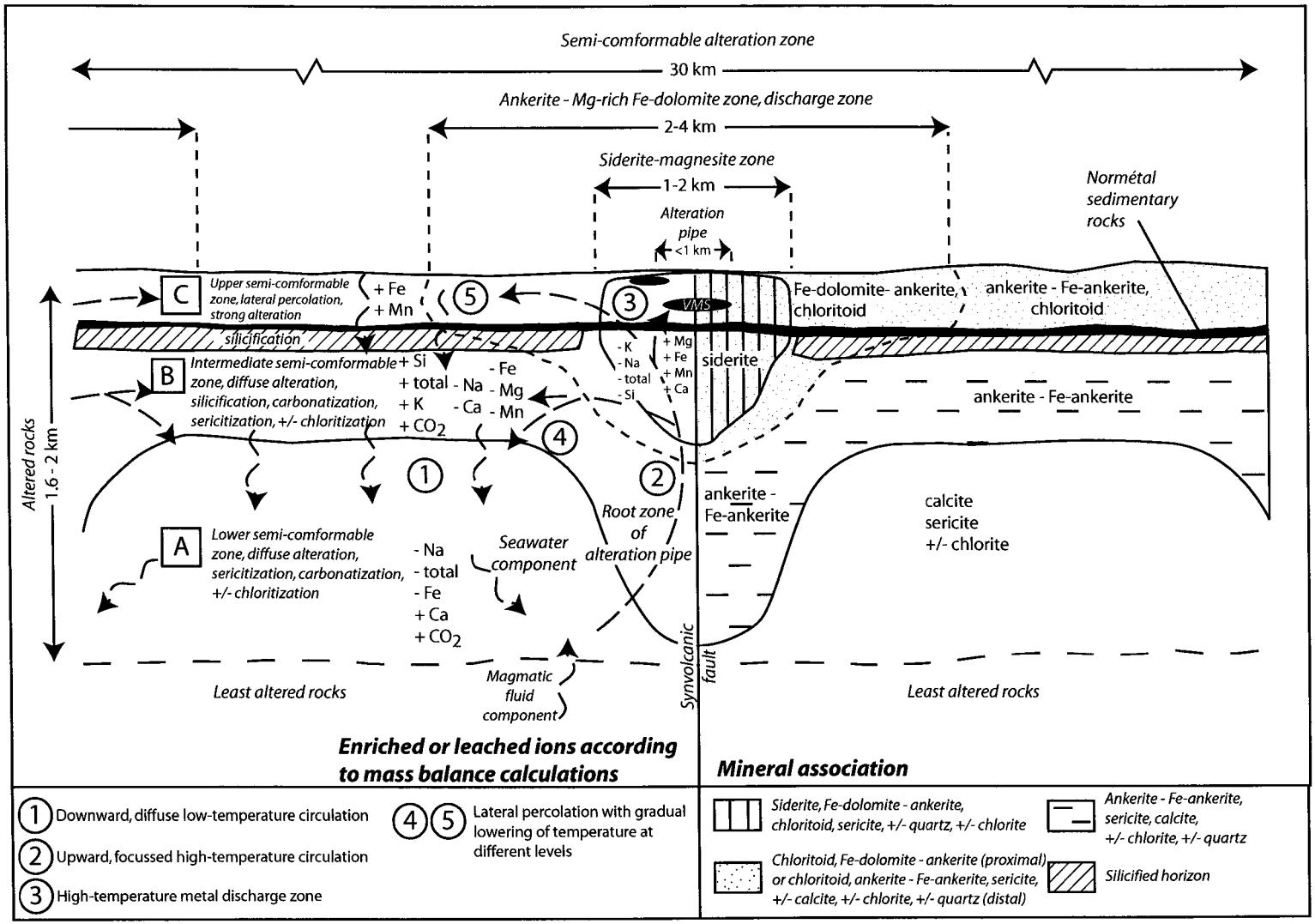

Figure 23: Alteration geometry of a Mattabi-type VMS deposit (Lafrance 2003). Note the difference in composition for local carbonates (siderite and Fe-dolomite) and regional carbonates (calcite and dolomite).

can by explained by the replacement of dolomite by siderite as iron-rich mineralizing fluids circulated through the rock (Franklin et al. 1975).

The regional alteration can be either absent or discrete. For example, Mobrun (now Bouchard-Hebert) deposit has ferroan dolomite that is restricted to the mineralized zone and its surrounding host rock (Larocque and Hodgson 1993), but also occurs at a regional scale. If VMS deposits form at the same time as the submarine volcanic edifice is evolving, it is then possible that the alteration occurs before and during mineralization.

The 120 million tonne Kidd Creek deposit is also an example of a Mattabi-type VMS deposit (Schandl and Wicks 1993) where a pervasive regional carbonatization affects the volcanic rocks. Locally, two generations of carbonates have been observed, a first generation of magnesite and dolomite, and a second generation of ankerite and ferroan dolomite. The first generation is believed to be linked to the mineralization whereas the second could be the result of a post-mineralization event (Schandl and Wicks 1993).

5.5.3 CO_2 and mineralization

The source of the metals responsible for mineralization can be magmatic or can be derived from the leaching of rocks during hydrothermal circulation. Reactions and the dissolution-transportation-precipitation process of metals in a carbonate system are complex. The CO_2-bearing hydrothermal solutions contain numerous other fluid phases, including H_2O, CH_4, H_2S, F, and Cl. The rock mineral phases can also react with these compounds (i.e. H_2S and gold). The metals combine with CO_2 to precipitate carbonate and bicarbonate complexes. In the case of lead (Pb), CO_2 combines to form complex ions

$Pb[HCO_3]x^2$-x et $Pb(CO_3)y^2$-2y (Leleu 1978). After CO_2 and metal ion transportation, a phase of mineral precipitation occurs during a change of the system's conditions. For metals and carbonate to precipitate contemporaneously, the precipitation domains of each phase must overlap (Figure 24). This depends on pressure, temperature, partial pressure of the fluid components, concentration of elements in the fluid, and pH (Leleu 1978).

5.6 Schakalsberg carbonate alteration

The striking characteristic of the Schakalsberg rocks is their pervasive carbonate alteration which gives them an orange colour (Plate 6C). The rocks resemble massive carbonate with an iron component that, when weathered, turns orange (oxidation of the iron). The carbonate alteration mainly affects the volcaniclastic lithofacies (90%), with some alteration in the volcanic facies (10%; Plates 6D and 7A). The degree of alteration varies between 100% (complete replacement of the initial minerals) for fine grained tuffs to about 50% in lapilli tuff breccias, where only the matrix is replaced (Plate 7B). Locally the rocks appear to be affected by many phases of carbonatization and some beds are of different colours (e.g. grey and white; Plate 7C, 7D and 8A), as are some carbonatized clasts in the lapilli tuff breccias. This was easier to observe in dry river beds, where the rock is best exposed. The change in colour could be the result of varying carbonate composition, but when the rocks are weathered, the orange coloration is consistent. It is thus more likely that the colour change could be due to a variation in grain size.

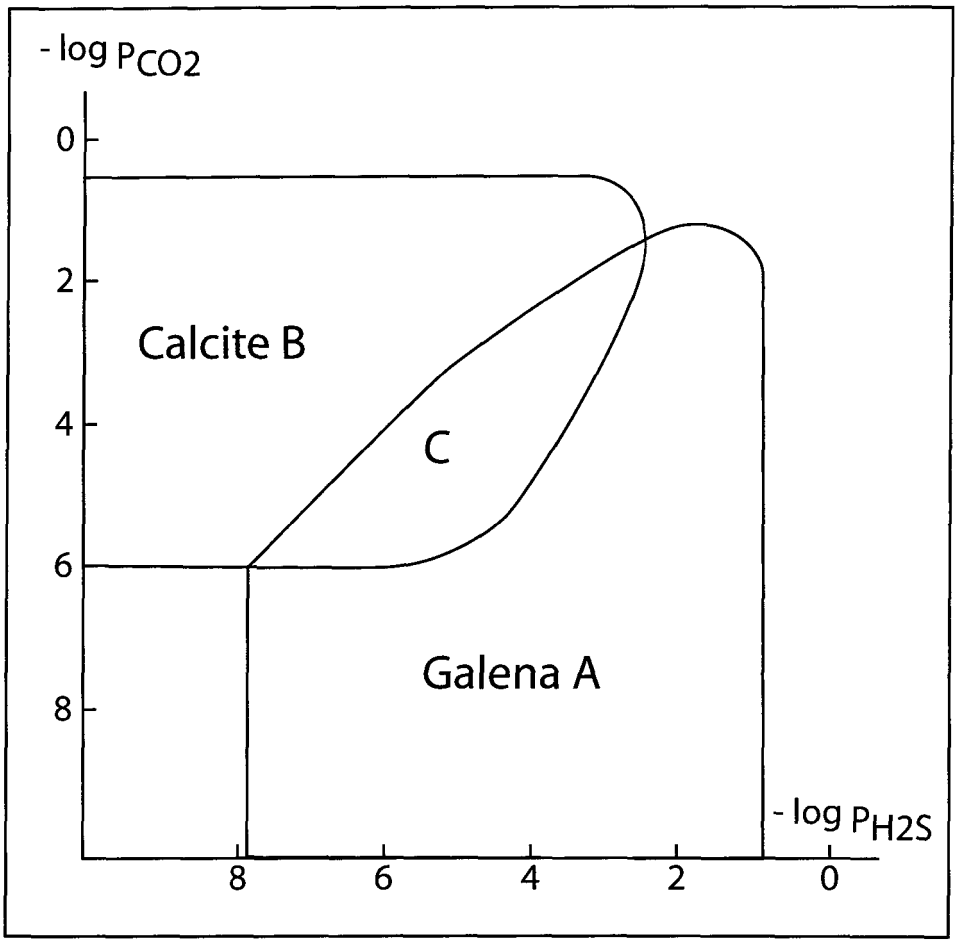

Figure 24: Precipitation fields of calcite and galena with respect to CO_2 and H_2S partial pressures (Leleu 1978).

Plate 7 (A): Intensely carbonatized lapilli tuff. The fragments, still visible and in positive relief, are locally unaltered. Arrow points to stratigraphic top. Pen, 10 cm.

Plate 7 (B): Carbonatized lapilli tuff breccia. The matrix is highly altered whereas the fragments are mostly unaltered (green). Arrow points to stratigraphic top. Pen, 14 cm.

Plate 7 (C): Carbonatized tuff. Despite the difference in alteration colour, the entire rock is altered. Arrow points to stratigraphic top. Pen, 14 cm.

Plate 7 (D): Carbonatized tuff. Note grey alteration colour. Arrow points to stratigraphic top. Pen, 14 cm.

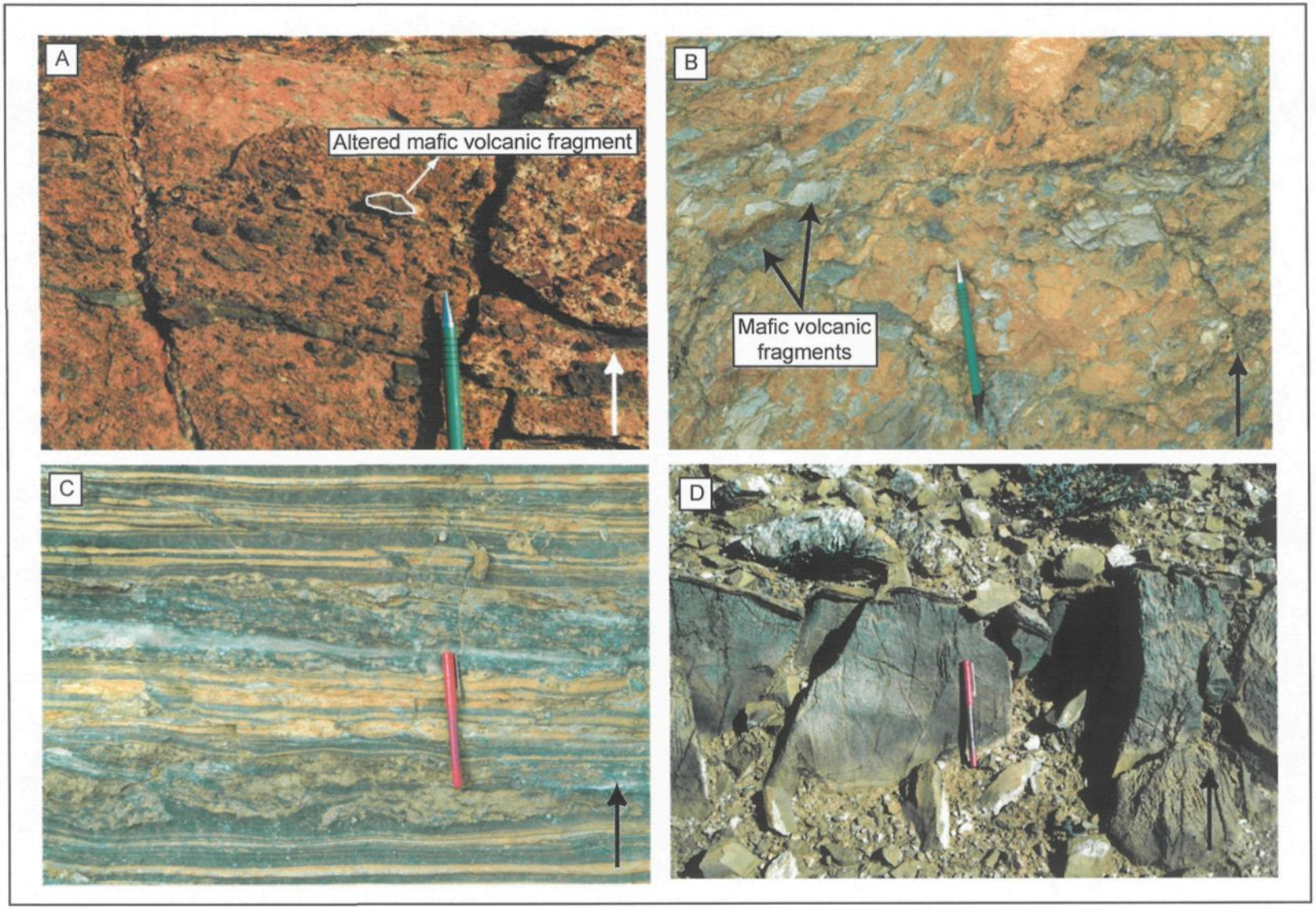
A
Altered mafic volcanic fragment
B
Mafic volcanic fragments
C
D

Plate 7

Plate 8 (A): Carbonatized tuff with different coloured carbonates. Arrow points to stratigraphic top Pen, 14 cm.

Plate 8 (B): Photomicrograph of sample AA-31-2001 in XPL showing oxidation of the carbonates.

Plate 8 (C): Thin horizon of massive hematite mineralization (black) conformable with the bedding. Arrow points to stratigraphic top. Notebook, 18 cm.

Plate 8 (D): Photomicrograph of sample AA-41-2001 in RL. Euhedral magnetite (light brown) is selectively replaced by hematite (light grey). Note minute needles of hematite (white arrow). The hyaloclastite shows preferential precipitation of oxides via hydrothermal fluids.

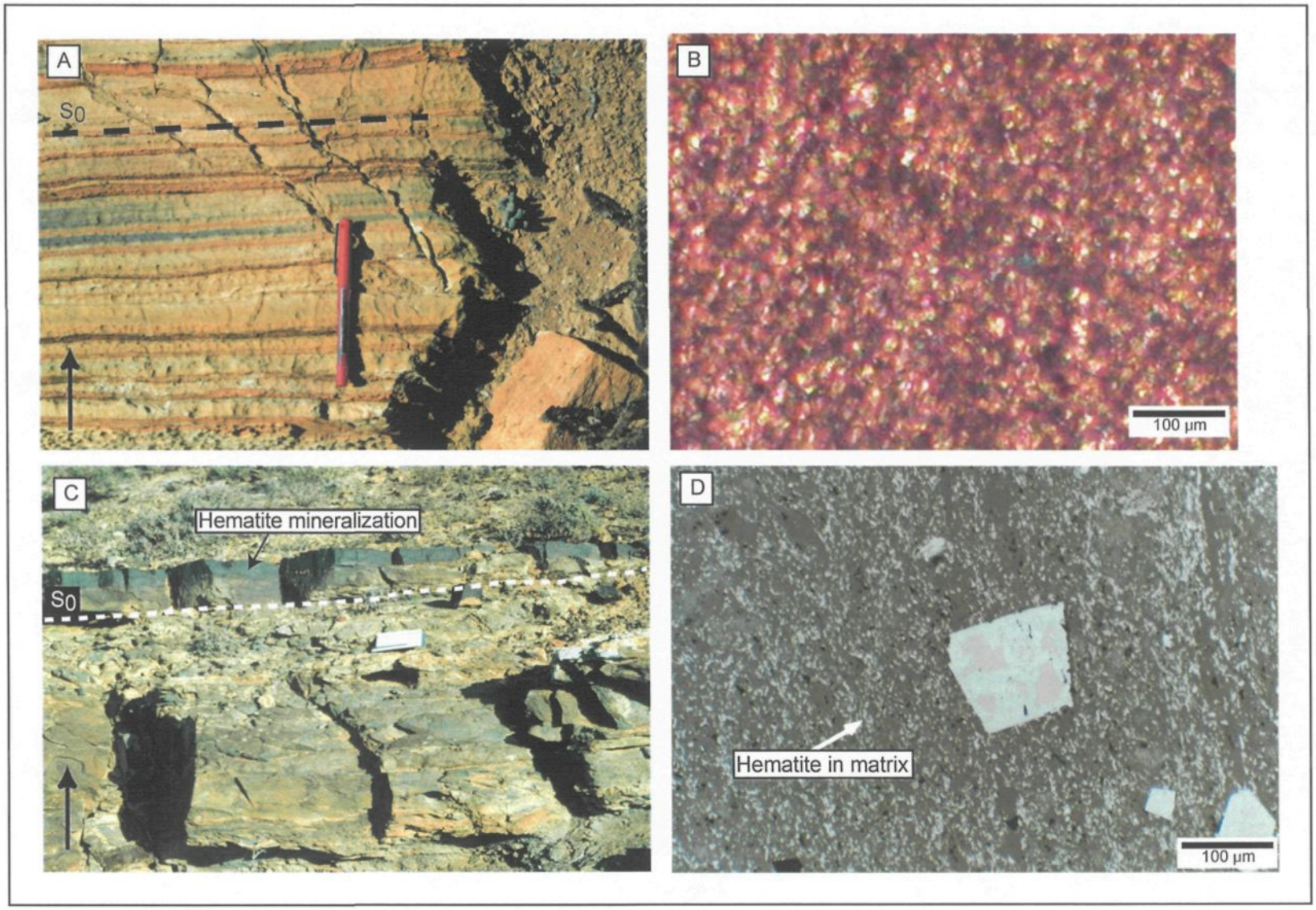
A
S0
B
100 µm
C
Hematite mineralization
S0
D
Hematite in matrix
100 µm

Plate 8

Petrography of carbonatized samples shows a massive carbonate replacement of volcaniclastic and volcanic rocks. In some samples, bedding was observed on the megascopic scale, but was completely obliterated in thin section. The carbonates are mainly xenomorphic, sub-rounded, and vary from a few μm to 2 mm. The orange colour is mainly due to oxidation on and around the carbonate grains (Plate 8B). No microscopic difference was observed between the different colours of carbonate alteration. In volcaniclastic rocks, the carbonate replacement is up to 100%, whereas it is up to 25% in volcanic rocks.

In order to investigate carbonate composition, the samples were analyzed using microprobe techniques. A total of 84 analyses were conducted, and the main characteristics of the carbonates are presented in Table 2. The data from microprobe analyses are provided in Appendix 2. Some analyses have a very high total due to the fact that samples were coated with C before being probed, thus interfering with the C already present in the carbonates. Also C, being a light element, is more difficult to accurately read using the microprobe.

Three types of carbonates were identified, 1) calcite ($CaCO_3$), 2) dolomite [$CaMg(CO_3)_2$)] and 3) Fe-dolomite [$Ca(Mg, Fe)(CO_3)_2$]. Most of the dolomites contain Fe, but the division between dolomite and Fe-dolomite was set at >3% $FeCO_3$. All samples contain calcite, which is readily identified using the energy dispersive spectrometer (EDS) on the microprobe. Although the carbonates were first believed to be siderite ($FeCO_3$) or ankerite [$Ca(Fe,Mg,Mn)(CO_3)_2$] based on the orange colour, iron is not a major phase, but is sufficient enough to create the orange colour when weathered.

Mineral	Samples	Analyses	Weathering colour
Calcite ($CaCO_3$)	7	25	Orange to grey, sometimes white
Dolomite [$CaMg(CO_3)_2$]	6	31	Orange to grey
Fe-Dolomite [$Ca(Mg,Fe)(CO_3)_2$]	5	28	Orange to grey

Table 2: Characteristics of the alteration carbonates. The samples column represents the amount of samples where the mineral of the first column was the predominant carbonate. The analyses column represents the number of microprobe analyses conducted on each carbonate phase. The weathering colour was determined in the field. The study was conducted on 18 samples, and 84 different crystals were analyzed. Note that weathering colour has no relation to the composition of the mineral.

Component	Range (%)
SiO_2	0.10 - 2.24
TiO_2	0.00 - 0.04
Al_2O_3	0.38 - 8.74
V_2O_3	0.00 - 0.15
Cr_2O_3	0.00 - 0.09
MgO	0.04 - 0.89
CaO	0.11 - 0.77
MnO	2.48 - 3.06
MnO_2	66.92 - 82.53
Fe_2O_3	0.00 - 4.66
NiO	0.00 - 0.79
Na_2O	0.21 - 2.00
K_2O	1.64 - 5.19
H_2O	4.04 - 4.42
Total	87.62 - 95.78

Table 3: Compositional range of the Mn-oxyhydroxide mineralization (manjiroite), based on 30 microprobe analyses. The low total is due to the H_2O component of the mineral.

The composition of the alteration carbonates can be a tool for targeting a mineral deposit. The alteration carbonates analyzed in this study have been spatially analyzed in order to determine a zonation. Carbonate composition shows a trend in the amount of metal (Mg and Fe) contained, creating a (i) distal zone composed of calcite ($CaCO_3$), (ii) medial zone composed of calcite-dolomite, and (iii) a proximal zone composed of calcite-Fe-dolomite (Figure 25; Map 5, in pocket). The metal content increases from the northwest to the southeast, indicating an evolution from distal to proximal assemblages towards the southeast (and outside the property), where phases such as ankerite and siderite could be present. This resembles a distal facies of the carbonate alteration pattern found in VMS deposits of the Mattabi-type, as described in the Abitibi (e.g. Lafrance 2003).

Silicification of the volcaniclastic rocks was observed in the western part of the property (Map 1, in pocket). This alteration completely replaces the volcaniclastic rocks with xenomorphic silica varying from a few μm up to 0.5 mm. This silicification could be an early feature, as observed in numerous VMS deposits, or could be the result of the carbonatization process, which can also produce silica (Thomson 1987, Veizer et al. 1989).

The carbonatization in the Schakalsberg Mountains must have occurred during volcanic activity to allow for circulation of the hydrothermal fluids. The source of the CO_2 may have been the marine carbonates located on the eastern side of the Red Dunes thrust (Map 1, in pocket), which are inferred to be the lateral equivalents of the volcanic edifice. Sea water interacted with the carbonates, gained some ions, and passed through the volcanic hydrothermal system via fractures and more porous layers. As a result elements were leached and calcite, dolomite and Fe-dolomite were precipitated in the units. The fact

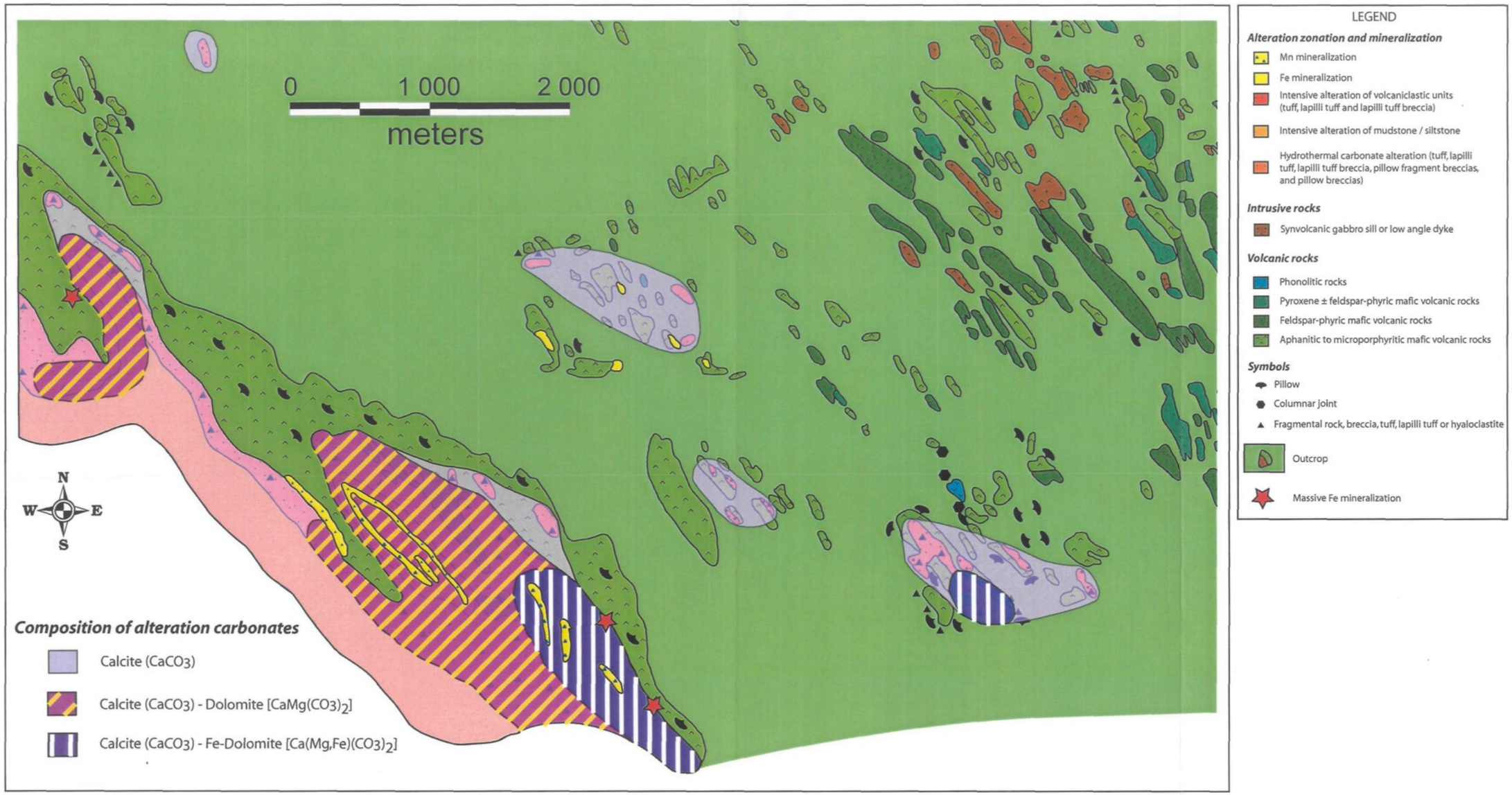

Figure 25: Zoning in the composition of alteration carbonates in the southwestern part of the property. See Map 5 (in pocket) for the entire property. The zoning pattern suggests a metal (Mg, Fe) increase in the carbonates towards the south.

that the volcaniclastic rocks are more affected by the alteration than their volcanic counterparts is a result of their higher relative porosity. The hydrothermal fluids took the path of least resistance. This hydrothermal system must have been extensive, as the pervasive carbonatization can be observed for tens of kilometres around the study area.

CHAPTER 6

MINERALIZATION

6.1 Introduction

Two principal types of mineralization were identified in the study area: 1) Fe-mineralization and 2) Mn-mineralization (see Maps 1 to 4, in pocket).

6.2 Fe-mineralization

Description:

Fe mineralization characterizes the study area as 2 forms, 1) magnetite ($Fe^{2+}Fe_2^{3+}O_4$) and 2) hematite (α-Fe_2O_3). The magnetite mineralization is represented by disseminated (up to 5% of the rock) euhedral grains varying from 0.1 mm to 3 mm. This mineralization was observed in the non-altered volcaniclastic and volcanic lithofacies located in the southwestern part of the property. The hematite mineralization is dessiminated (up to 10% of the rock) and massive to dessiminated (up to 50% of the rock; Plate 8C). In the field, the massive mineralization is contained in thin (5-20 cm, traceable for up to 10 m), sometimes slightly magnetic, dark green to black beds, in volcanic rocks near the contact with the volcaniclastic rocks (Figure 25; Map 5, in pocket). The dessiminated hematite was not identified in the field. Petrographic studies revealed that the hematite is preserved as disseminated idiomorphic hematite needles (few μm to 0.1 mm) in

the matrix (although sometimes counting for up to 50% of the rock) (Plate 8D) and replacement of euhedral magnetite crystals along cleavage planes (Plate 9A). Replacement varies from 1% to 100% of the magnetite crystals, the latter producing magnetite ghosts. Approximately 100 microprobe analyses were conducted on samples from the different types of Fe mineralization. In addition to hematite and magnetite, other minor iron phases include ilmenite, goethite and various Fe-Si-Al oxides, hydroxides and oxyhydroxides (Appendix 2).

Interpretation:

From the observations, it is clear that the magnetite mineralization occurred before the hematite mineralization. The growth of euhedral magnetite crystals is a common feature of submarine volcanic edifices and can be related to modern, low-temperature seafloor alteration (Wooldridge et al. 1990; Booij et al. 1995; Bogdanov et al. 1999; Pichler et al. 1999). The hematite is a replacement mineral that formed when the seafloor conditions were more oxidizing than during formation of the magnetite mineralization (Deer et al. 1992). The Fe mineralization resulted from circulation of hydrothermal fluids rich in Fe that gradually replaced the minerals present in the initial rock. Other oxides (e.g. Si, Al) transported by the mineralizing fluids were leached from the rocks and were incorporated during deposition. The source of Fe is inferred to be the volcanic edifice, and mainly the mafic volcanic flows. The fact that the Fe mineralization is preserved in volcanic rocks and in non-carbonatized volcaniclastic rocks suggests that it occurred following the carbonatization phase. The carbonatization affected the most permeable units, thus making

Plate 9 (A): Photomicrograph of sample AA-90-2001 in RL. Euhedral (cubic) magnetite (Mag) is selectively replaced by hematite (Hem) along cleavage plane (111).

Plate 9 (B): Landscape view of manganese mineralization found in the hinges of synclines (black stretch of rock in the middle of picture). Extent of the mineralization on the photo is approximately 400 m.

Plate 9 (C): Alteration near the manganese mineralization. The surrounding volcaniclastic rocks are altered to whitish mud (leaching). Height of the man on the picture is approximately 1.80 m.

Plate 9 (D): Close-up of black manganese mineralization (Man). White fragments are quartz and/or carbonate. Diameter of coin is approximately 3 cm.

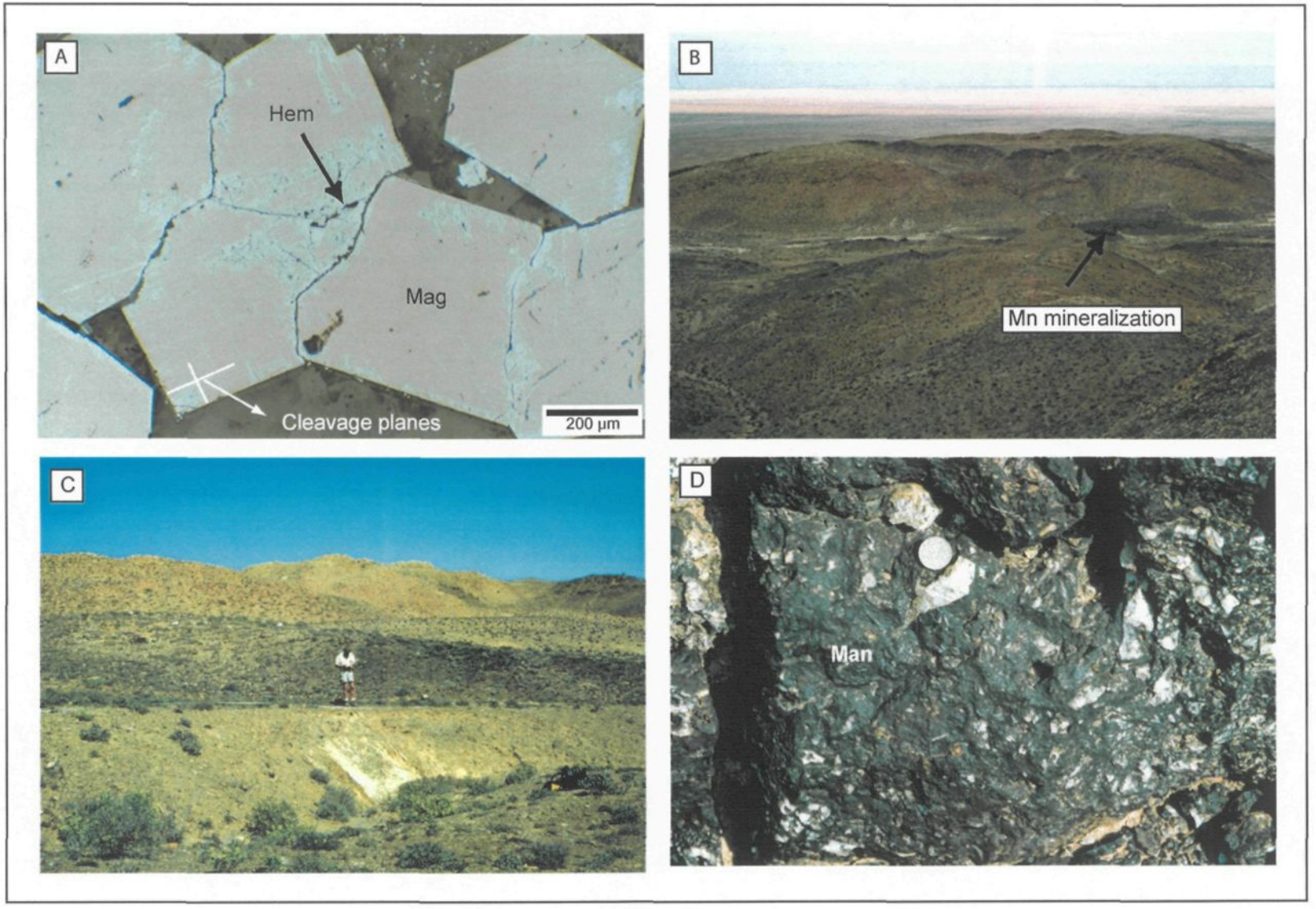

Plate 9

them impermeable. The iron-bearing fluids then passed through the most permeable units available including unaltered volcaniclastic rocks and mafic volcanic rocks.

6.3 Mn mineralization

Description:

The 0.5-4 m-thick Mn-oxyhydroxide mineralization, exposed in the southwest, formed in topographic lows (valleys) and can be traced for more than 1 km (Plate 9B). The limit of the mineralization is distinct, characterized by a 2 m-thick white-grey leached tuff altered to clay (Plate 9C) at the contact with volcaniclastic rocks. The mineralization is dull grey to dark blue and is associated with a massive to brecciated texture (Plate 9D), where the fragments ,quartz and/or carbonates, are up to 10 cm in size. The mineralization varies from massive Mn-oxyhydroxide to quartz-Mn-oxyhydroxide-carbonate breccia. Depending on location, the content of Mn oxyhydroxide varies from 100% to approximately 10% of the rock. The Mn is superficial, with the deeper material having a higher carbonate+quartz / Mn ratio (Plate 10A). Petrographically, the Mn mineralization is massive (no grains) and displays a distinct zonation, resembling a cavity-fill pattern (Plate 10B), representing episodic growth. The Mn oxyhydroxide grew from the surrounding material, originating at grain rims and slowly filling cavities. Microprobe analyses conducted on more than 30 Mn-oxyhydroxide points coupled with X-Ray diffraction, identified the manganese-oxyhydroxide as manjiroite $[(Na,K)(Mn^{4+}, Mn^{2+})_8O_{16}\cdot n(H_2O)]$. Table 3 provides the compositional range for this mineral.

Plate 10 (A): Lower part of black manganese mineralization. The percentage of manganese (black) diminishes with depth. Photo was taken 2 meters below the top of the mineralization. Notebook, 18 cm.

Plate 10 (B): Photomicrograph of sample AA-9-2001 in RL. Note the association of manjiroite (Man) and quartz (Qtz). Zoning in the mineralization represents episodic growth.

Plate 10 (C): Photomicrograph of sample AA-13-2001 in RL showing the growth pattern of the Mn mineralization (Man) and its association with quartz (Qtz).

Plate 10 (D): Leached volcaniclastic rock. Rock is now composed of white clays. Hammer, 30 cm.

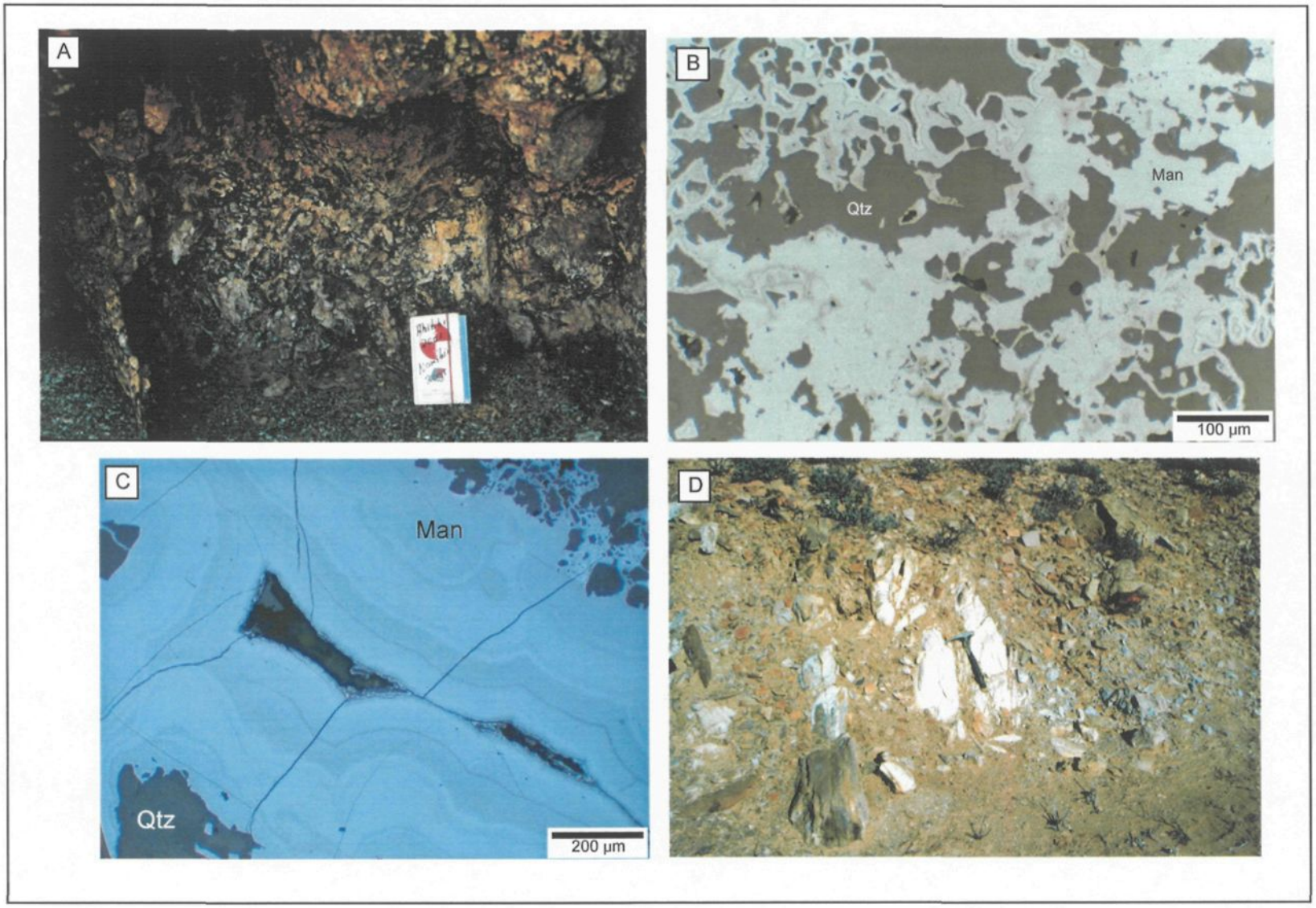

Plate 10

Interpretation:

The Mn-mineralization is inferred to be a supergene deposit and its growth pattern indicates that it formed gradually (Plate 10C). The best hypothesis is that manganese nodules or crusts, commonly found in submarine settings with volcanic activity (e.g Ridout et al. 1984; Koski 1988; Lazur et al. 1992; Kuhn et al. 1996) must have been present at some point on the seafloor and that these nodules were then dissolved and the Mn was remobilized. This is most likely to have occurred during or following folding because the mineralization is found in topographic lows or syncline hinges. Leaching and alteration of the surrounding volcaniclastic rocks (Plate 10D; Table 4) is explained by the circulation of the mineralizing fluids that leached the rocks en route to the deposition site.

	AA-182-2001	AA-196-2001
SiO2	60.58	66.46
TiO2	1.34	1.05
Al2O3	13.5	14.84
Fe2O3	11.78	2.21
MnO	0.13	
MgO	2.83	1.3
CaO	0.54	0.12
Na2O	1.06	1
K2O	3.99	4.75
P2O5	0.22	0.11
LOI	4.79	8.62
TOTAL	100.76	100.45

Table 4: Geochemical composition of the leached volcaniclastic units near the Mn-oxyhydroxide mineralization.

CHAPTER 7

DISCUSSION AND CONCLUSIONS

7.1 Introduction

The Schakalsberg area, initially surveyed by Frimmel et al. (1996a,b), is a volcanic-dominated succession that has never been documented in detail. This study was initially conducted to unravel the geology, but (1) a detailed volcanic-volcaniclastic facies analysis study, (2) a geochemical study of the volcanic rocks, (3) a survey of the carbonate hydrothermal alteration pattern and associated mineralization, and (4) a structural analysis, showed that more focus could be placed on the evolution of an ancient seamount.

7.2 Stratigraphy: lithofacies and geochemistry

The lithological assemblage in the Schakalsberg Mountains is a typical volcano-sedimentary sequence. The initial 1200 m is dominated by effusive volcanic lava flows whereas volcaniclastic deposits constitute the upper 200 m. The distribution of flows is: i) 540 m (45%) aphanitic, ii) 60 m (5%) microporphyritic, iii) 240 m (20%) feldspar-phyric, iv) 60 m (5%) pyroxene±feldspar-phyric, and v) 300 m (25%) comagmatic gabbro sill intrusions. Interflow tuffs are minor (<1%). The flows are interstratified throughout the sequence, with the initial 600 m-thick basal sequence containing porphyriticc flows and the upper 600 m containing aphanitic to microporphyritic flows. Massive to minor pillowed

flows dominate the base, whereas pillowed flows and pillow breccias prevail in the upper part of the sequence. The flow morphology from massive to pillowed to pillow breccia, is characteristic of modern and ancient subaqueous flow successions (Dimroth et al. 1979, 1985; Staudigel and Schmincke 1984; Fornari 1986). As for the pillow size, the change corresponds either to different extrusion volumes, or a different position within the flow, larger pillows being located closer to the emission centre. The phenocryst content can be explained by a high-level phenocryst-rich magma chamber associated with volcanic construction (Mcdonald 1972; Williams and McBirney 1979).

The upper volcaniclastic part of the stratigraphy is composed of 150 m (75%) tuffs, 20 m (10%) lapilli tuffs, and 20 m (10%) lapilli tuff breccias, with 10 m (5%) interstratified aphanitic flows. Tuffs are graded and massive beds, lapilli tuffs are massive and graded beds with local crossbedding, and the lapilli tuff breccias are massive. The tuffs are interpreted as dilute turbidity current deposits (Lowe 1982, 1988). The lapilli tuff units are considered subaqueous eruption-fed density currents deposits (White 1996, 2000; Mueller 2003). The lapilli tuff breccia units represent subaqueous debris flows and high-concentration turbidity current deposits (Lowe 1982). The 90 m-thick tuff unit at the top of the stratigraphy suggests deposition along the flanks of this submarine volcanic edifice.

Geochemical analyses indicate that the flows represent oceanic basalts. The lower part of the stratigraphy is dominated by tholeiitic basalts, whereas the upper part is dominated by transitional to alkali-type basalts (Figures 5 and 7). The two suites are representative of two different sources, probably from a heterogeneous mantle, given the significant difference in HFSE and LREE abundances and trace element characteristics

(Mueller et al. 2001; Figure 6). The tectonic discrimination diagrams of Wood (1980) and Meschede (1986) (Figure 7) support the inference of an oceanic setting.

The occurrence of pillowed flows and graded tuff turbidite beds, as well as the geochemical composition of the rocks, are consistent with a submarine depositional setting. The stratigraphy shows a change from flow-dominated, effusive volcanism in the lower part to a volcaniclastic-dominated, explosive volcanism in the upper part. This corresponds to a shoaling sequence of a submarine volcanic edifice (Dickinson 1998; Eddy et al. 1998; Schmidt and Schmincke 2000; Trua et al. 2002). Although only 1400 m of the stratigraphy is exposed, the extent of the sequence could have been greater. The lower part of the stratigraphy is unexposed because of the Red Dunes thrust, whereas the upper part of the sequence is exposed south of the study area (Mueller 2003).

7.3 Carbonatization

Carbonatization of the volcaniclastic units is an early seafloor alteration that occurred while volcanic activity was still driving hydrothermal fluids through the rocks. The carbonatization can be observed for tens of kilometres around the property, making this an extensive hydrothermal system.

Carbonate composition is zoned on the property, similar to Mattabi-type VMS deposits (Veizer et al. 1989; Penczak and Mason 1999; Lafrance 2003). Although the composition of the alteration carbonates does not include ankerite or siderite, there is a distinct zoning in the metal content of the carbonates (Fe and Mg) towards the southwest of the alteration halo (Figure 25; Map 5, in pocket). The higher metal content is also

consistent with the occurrence of massive Fe mineralization (Figure 25; Map 5, in pocket). It is highly probable that the zoning extends beyond the limits of the property (south?) and possible ankerite and siderite would locate a proximal VMS alteration assemblage.

The Schakalsberg carbonatization with its considerable extent possibly acted as a cap rock, trapping other fluids in the system and causing them concentrate mineralization. However, the width of the system could have lead to fluid dispersal, creating disseminated, non-economic mineralization. The carbonatization process often produces chert (SiO_2), which results from dissolution of a silicate phase by carbonated fluids. The silica is then transported elsewhere in the hydrothermal system. Minor silicifed horizons observed on the property (Map 1, in pocket) could have also acted as cap rocks, facilitating concentrated mineralization.

Mattabi-type VMS deposits also have a chlorite alteration zone that is mainly restricted to the deposit margins, in the local alteration facies. This alteration zone was not observed on the property, possibly because the volcanic rocks were metamorphosed to greenschist facies (containing chlorite), or because the study area is located in the regional (distal) alteration halo of a deposit, where the chlorite facies is absent.

7.4 Mineralization

Although no economic mineralization was found on the property, many of the elements required to form a VMS deposit are preserved, including a cap rock (?), hydrothermal fluids, and volcanic activity. Notwithstanding, other conditions such as concentration of mineralized phases, specific P-T conditions, and proper oxidizing or

reducing conditions are needed in order to create a deposit. The magnetite is typical of a low temperature (<200°C) seafloor alteration type of mineralization, whereas the hematite resulted from remobilization of iron from the magnetite under oxidizing conditions (Butler 1992; Alt 1995; Alt and Bach 2001). In order to form a VMS-type deposit, the conditions must be reducing and high temperature. Precipitation occurs when oxidized hydrothermal fluids enter a zone of reducing conditions. The study area could represent the distal facies, where such conditions were not met. With respect to the Mn mineralization, nodules are common features in submarine volcanic regions (Ridout et al. 1984; Koski 1988; Lazur et al. 1992; Kuhn et al. 1996). The mineralization in the study area is consistent with dissolution-transportation-redeposition (supergene) of the Mn, which occurred after deformation (Quaternary?). The Mn mineralization is not linked to the iron and carbonate alteration.

7.5 Geological setting: an ancient seamount

The stratigraphy of the Schakalsberg Mountains is typical of volcanic edifices built by early effusive and later explosive volcanism. Pillows in flow units and graded bedding in the volcaniclastic rocks indicate that the deposits formed underwater, which is typical of seamounts and ocean islands (Dickinson 1998; Eddy et al. 1998; Schmidt and Schmincke 2000; Trua et al. 2002). A seamount is a volcanic edifice with an elevation on the seafloor of more than 1000 m (Schmidt and Schmincke 2000), whereas ocean islands represent emerged seamounts (Schmidt and Schmincke 2000). Figure 26 illustrates the stages of seamount evolution. The early stage is represented by lava flows on

the sea floor, and a paucity of volcaniclastic facies. The latter characteristic is a result of high pressure preventing explosive volcanism. The volcanic edifice grows with a mainly effusive component and minor pyroclastic events. As the seamount approaches the water surface the volcaniclastic/volcanic ratio increases. Eventually, the seamount breaches the surface and forms an ocean island, such as the Canary Islands or the Azores.

On a passive margin, seamounts are created by volcanic activity generated from a mantle plume or hotspot. As the tectonic plate moves over the hotspot, a chain of seamounts develops (e.g. Hawaiian Islands). After termination of volcanic activity, the island is eventually eroded to below the water surface. Volcanic activity can also cease before the island emerges and in shallow tropical water, coral reefs develop, creating atolls (Schmidt and Schmincke 2000). With the movements of plate tectonics, the atoll is then dragged deeper under water and is then called a guyot (Schmidt and Schmincke 2000). Figure 27 illustrates the steps involved in the evolution of a seamount. The volcano-sedimentary sequence of the Schakalsberg Mountains is believed to represent the upper part of a seamount, ocean island, atoll or guyot (depending on what is overlying the exposed sequence), where explosive volcanic activity is predominant. The exposed part of the edifice is believed to have been completely submerged in water based on the presence of pervasive hydrothermal alteration of volcaniclastic units.

7.6 Conclusions

1- The Schakalsberg Mountains represent an ancient seamount with an extensive hydrothermal carbonate alteration zone. Figure 28 illustrates a schematic reconstruction of

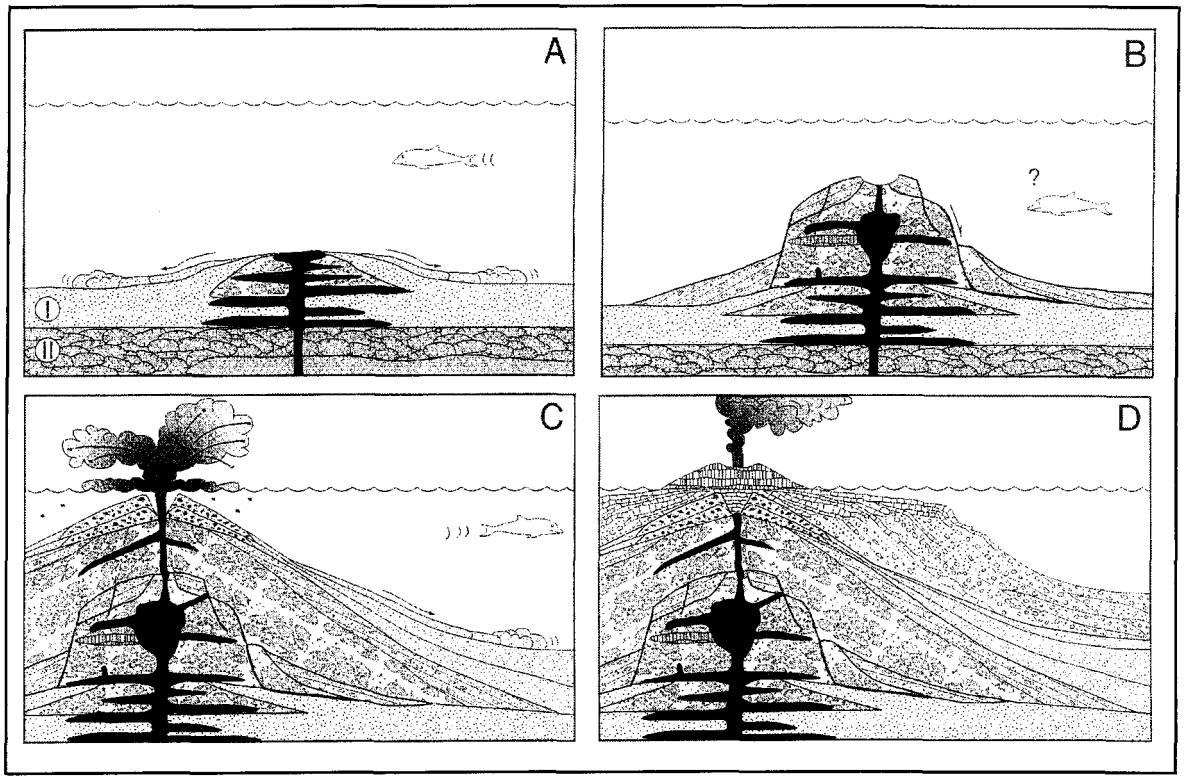

Figure 26: Growth stages of a seamount based on La Palma seamount, Canary Islands. (A) deep water stage, mainly characterized by intrusion of flows under the seafloor. (B) Deep water stage characterized by an equal amount of intrusive and extrusive flows, with minor volcaniclastites. (C) Final subaqueous stage (shallow water) with Surtseyan-type eruptions and predominant volcaniclastic component. (D) Ocean island stage with subaerial flows and pyroclastic deposits (Schmidt and Schmincke 2000).

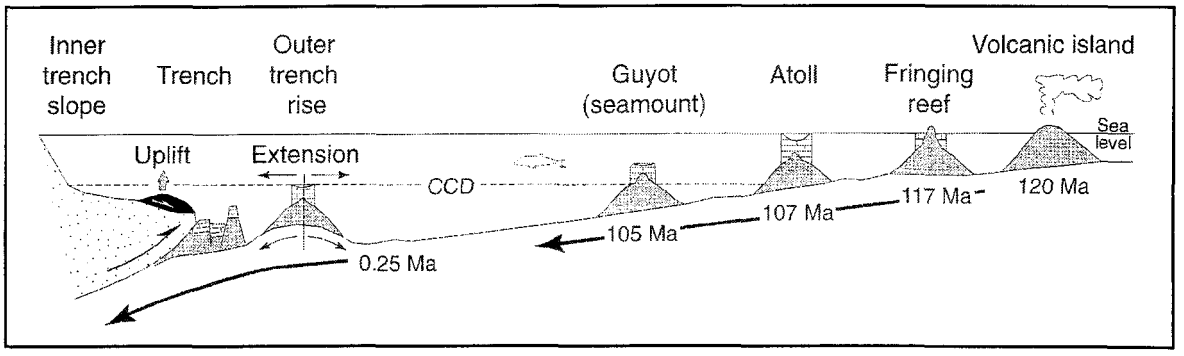

Figure 27: Evolution of a volcanic island to guyot (example of the Daiichi Kashima seamount, Japan) (Schmidt and Schmincke 2000).

the Schakalsberg seamount, with a carbonate platform in the vicinity. The seamount developed on the passive margin of the Adamastor Sea as a result of mantle plume activity. The sequence exposed on property EPL 2757 represents a 1.4 km thick ocean island/seamount succession with concentration of volcaniclastic lithofacies in the upper part of the stratigraphy, consistent with shoaling. The volcanic part of the sequence consists of aphanitic, microporphyritic, feldspar-phyric and pyroxene±feldspar-phyric mafic volcanic rocks, and gabbro sills and dykes. These facies represent the early stages of seamount evolution. The upper part of the stratigraphy, consisting of tuffs, lapilli tuffs, lapilli tuff breccias, and pillow breccias, is consistent with a more shallow water (0-200 m) seamount setting.

2- The volcano-sedimentary sequence has been folded and thrusted over marine carbonates (probably lateral equivalents of the volcano-sedimentary sequence) during a sinistral transpression event that was part of the global closing of the Adamastor sea.

3- The majority of the volcaniclastic rocks were affected by a pervasive hydrothermal carbonatization (calcite, dolomite and Fe-dolomite) that extends for 10's of kilometres outside the property. Three assemblages are preserved and include calcite (distal), calcite-dolomite (medial), and calcite-Fe-dolomite (proximal). The composition of the carbonate indicates an increase in metal content (Mg, Fe) towards the southeast. The carbonates correspond to seafloor alteration where CO_2 rich hydrothermal fluids circulated through the volcanic system (Figure 29). The source of CO_2 was marine carbonates that were forming

concommitent with growth of the edifice (lateral equivalents). Euhedral magnetite mineralization was identified in unaltered volcaniclastic rocks and volcanic rocks. This is the result of low-temperature seafloor alteration. Later in the history of the Schakalsberg seamount, the conditions were oxidizing and hematite mineralization replaced the magnetite. The source for the Fe is inferred to be the mafic volcanic flows. Supergene manganese oxyhydroxide mineralization (massive to brecciated) exposed in hinges of synclines formed after deformation and is not related to the carbonatization or the Fe-mineralization. The source of the Mn is believed to be Mn nodules.

4- The Schakalsberg seamount presents many characteristics of Mattabi-type VMS environments: 1) a volcano-sedimentary submarine sequence, 2) hydrothermal carbonate alteration, and 3) zoning in the carbonate composition and hydrothermal mineralization (Fe). This indicates that conditions needed for the formation of a VMS deposit in the Schakalsberg seamount were favourable.

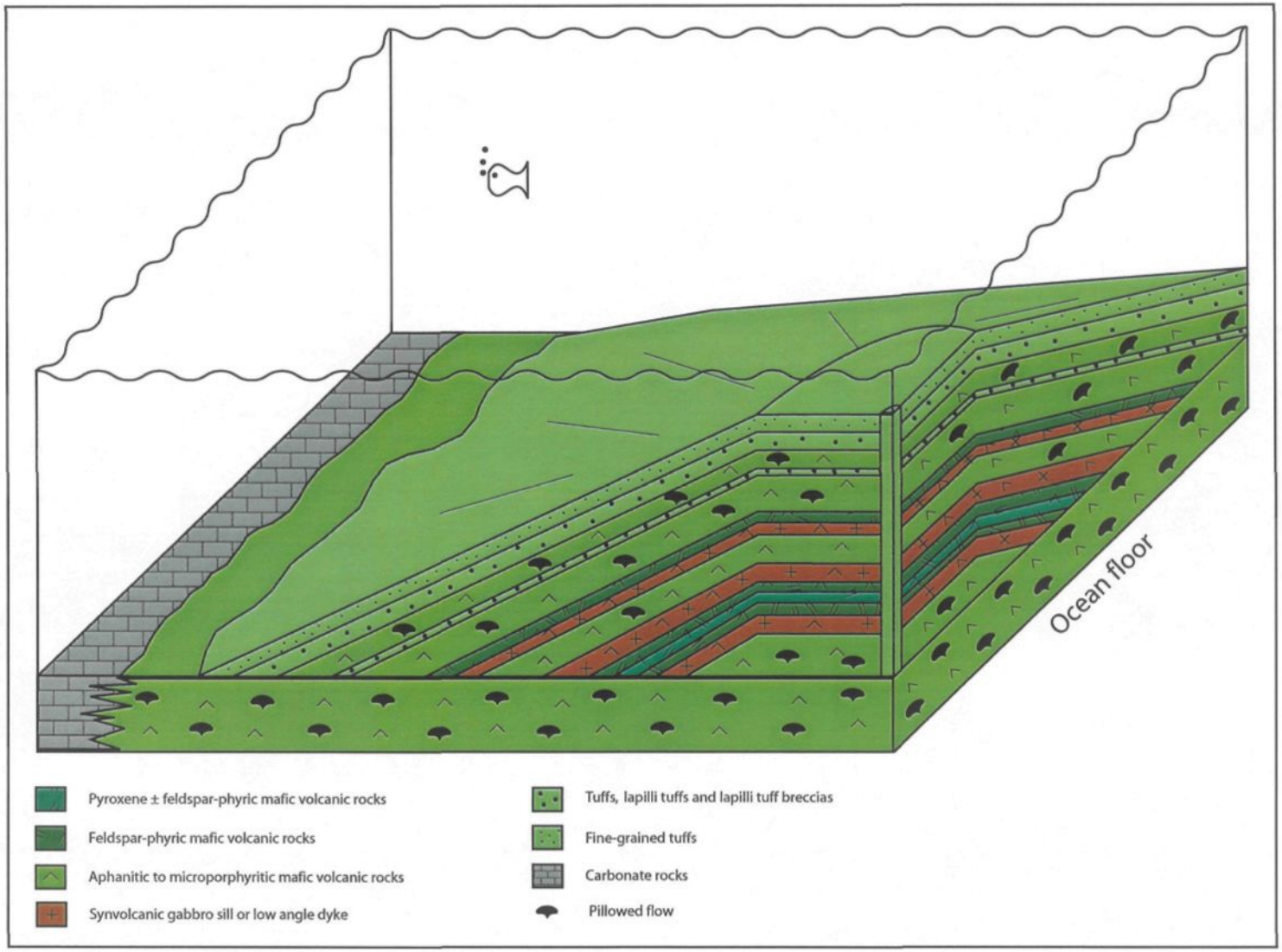

Figure 28: 3D model of the shallow-water (200-300 m) stage of the Schakalsberg seamount using simplified geology and stratigraphy of the area. Diagram not to scale.

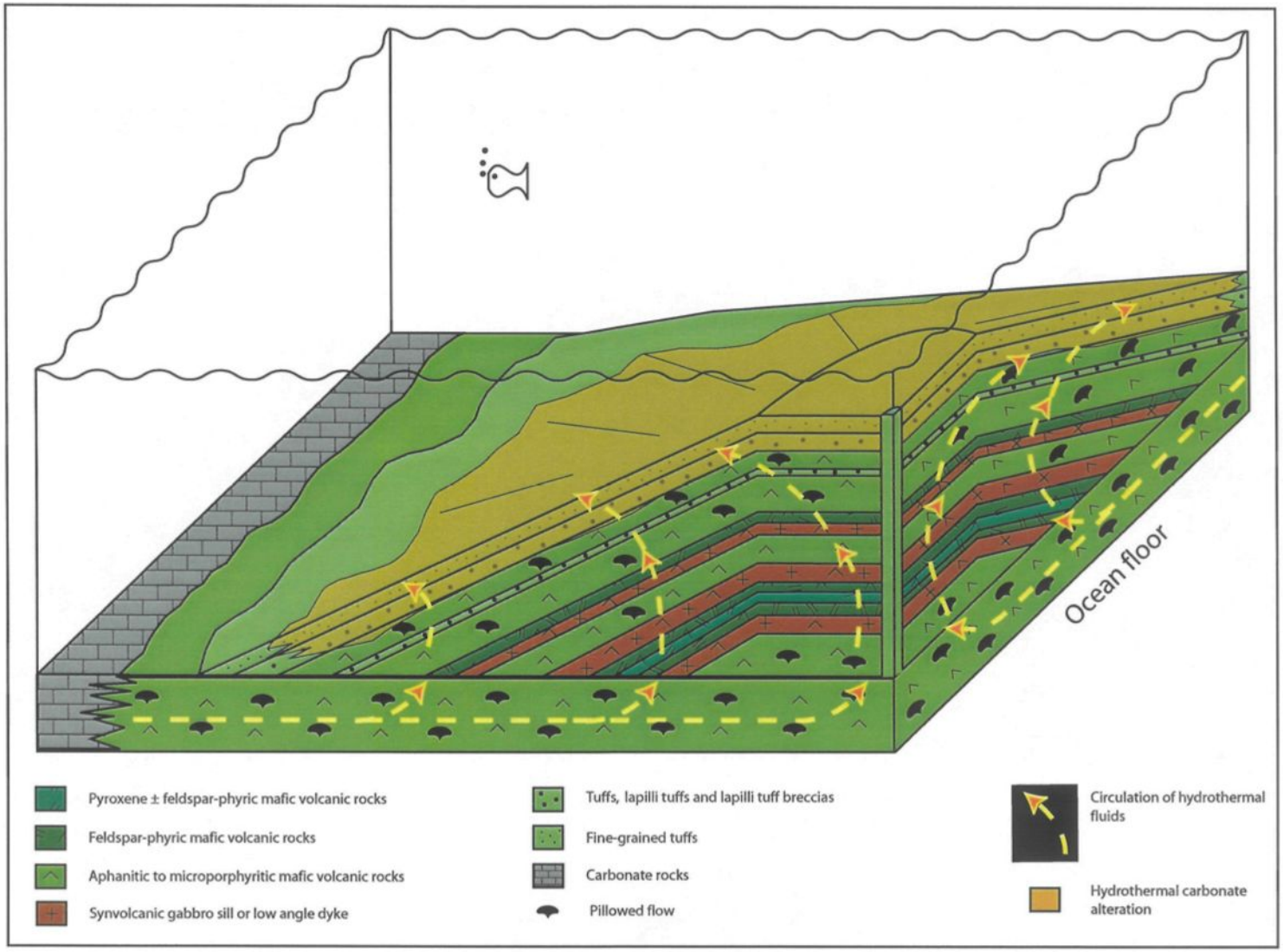

Figure 29: 3D alteration model of the shallow-water (200-300 m) stage of the Schakalsberg seamount using simplified geology and stratigraphy of the area. Diagram not to scale.

REFERENCES

Abdelsalam, M.G., Stern, R.J., Copeland, P., Elfaki, E.M., Elhur, B., and Ibrahim, F.M. 1998. The Neoproterozoic Keraf Suture in NE Sudan: sinistral transpression along the Eastern Margin of West Gondwana. The Journal of Geology, **106**: 133-147.

Alt, J.C. 1995. Subseafloor processes in mid-ocean ridge hydrothermal systems. *In* Humphris, S.E., Zierenberg, R., Mullineaux, L., and Thomson, R. (editors) Seafloor hydrothermal systems: physical, chemical, biological and geological interactions within hydrothermal systems. American Geophysical Union Monography, **91**: 85-114.

Alt, J.C., and Bach, W. 2001. Data report: low-grade hydrothermal alteration of uplifted lower oceanic crust, Hole 735B: mineralogy and isotope chemistry. In Natland, J.H., Dick, H.J.B., Miller, D.J., and Von Herzen, R.P. (editors), Proceedings of the Ocean Drilling Program, scientific results, **176**: 1-24.

Bogdanov, Y.A., Gorshkov, A.I., and Bogdanova, O.Y. 1999. Low-temperature iron and manganese mineral phases of an active hydrothermal mound; TAG hydrothermal field, Mid-Atlantic Ridge. Exploration and Mining Geology, **8**: 355-364.

Booij, E., Staudigel, H., and Gallahan, W.E. 1995. Dating of low-temperature seafloor alteration in the Troodos Ophiolite, Cyprus. Terra Abstracts, **7**: 210-211.

Busby-Spera, C.J., 1988. Evolution of a Middle Jurassic back-arc basin, Cedros Island, Baja California: Evidence from a marine volcaniclastic apron: Geological Society of America Bulletin, **100**: 218-233.

Butler, R.F. 1992. Paleomagnetism: magnetic domains to geologic terranes. Blackwell Scientific Publications, 238 p.

BVSP, 1981. Basaltic Volcanism on the Terrestrial Planets. Pergamon, New York, NY, 1286 p.

Cas, R.A.F., and Wright, J.V., 1987. Volcanic Successions, Modern and Ancient. Allen and Unwin, London. 528 p.

Chaffey, D. J., Cliff, R.A., and Wilson, B. M. 1989. Characterization of the St. Helena magma source. *In* Saunders AD, Norry MJ (editors), Magmatism in the Ocean Basins. Geological Society London, Spec Pub **42**: 257-276.

Chartrand, F., and Cattalani, S. 1990. Massive sulphide deposits in northwestern Quebec. *In* The northwestern Quebec polymetallic belt; a summary of 60 years of mining exploration; Proceedings of the Rouyn-Noranda 1990 symposium, Canadian Institute of Mining and Metallurgy Special Volume, **43**: 77-91.

Clague, D.A., and Dalrymple, G.B. 1987. The Hawaiian-Emperor volcanic chain, Part I: Geologic evolution. *In* Volcanism in Hawaii, *edited by* R.W. Decker, T.L. Wright, and P.H. Stauffer. Geological Survey Professional Paper, U.S. **1350**: 5-54.

Corcoran, P.L. 2000. Recognizing distinct portions of seamounts using volcanic facies analysis; examples from the Archean Slave province, NWT, Canada. Precambrian Research, **101**: 237-261.

Cousineau, P., and Dimroth, E., 1982. Interpretation of the relations between massive, pillowed and brecciated facies in an Archean submarine andesite volcano-Amulet Andesite, Rouyn-Noranda, Canada. Journal of Volcanology and Geothermal Research, **13**: 83-102.

Daigneault, R., Mueller, W.U., and Chown, E.H., 2002. Oblique Archean subduction: accretion and exhumation of an oceanic arc during dextral transpression, Southern Volcanic Zone, Abitibi Greenstone Belt, Canada. Precambrian Research, **115**: 261-290.

Davies, G.R., Norry, M.J., Gerlach, D.C., and Cliff, R.A. 1989. A combined chemical and Pb-Sr-Nd isotope study of the Azores and Cape Verde hot-spots: the geodynamic implications. *In* Saunders AD, Norry MJ (editorss), Magmatism in the Ocean Basins. Geological Society London, Special Publication **42**: 231-255.

Davies, J.F., Whitehead, R.E., Huang, J., and Nawaratne, S. 1990. A comparison of progressive hydrothermal carbonate alteration in Archean metabasalts and metaperidotites. Mineralium Deposita, **25**: 65-72.

Deer, W.A., Howie, R.A., and Zussman, J. 1967. Rock-Forming minerals. Longmans, Green and co ltd, London, v. 5 non-silicates, 5th print, p. 227-301.

Deer, W.A., Howie, R.A., and Zussman, J. 1992. An introduction to rock-forming minerals, 2nd edition. Pearson Education Limited, Harlow, England. 695 p.

Dickinson, W.R. 1998. Geomorphology and geodynamics of the Cook-Austral island-seamount chain in the South Pacific Ocean: implications for hotspots and plumes. International geology Review, **40**: 1039-1075.

Dimroth, E., Cousineau, P., Leduc, M., Sanschagrin, Y., and Provost, G., 1979. Flow mechanisms of Archean subaqueous basalt and rhyolite flows. *In* Current Research, Part A, Geological Survey of Canada, Paper **82-1A**: pp. 29-36.

Dimroth, E., Imreh, L., Cousineau, P., Leduc, M., and Sanschagrin, Y. 1985. Paleogeographic analysis of mafic submarine flows and its use in the exploration for

massive sulphide deposits. *In* Evolution of Archean Supracrustal Sequences. *Edited by* L.D. Ayres, P.C. Thurston, K.D. Card and W. Weber. Geological Association of Canada Special Paper, **28**: 203-222.

Drummond, S.E., and Ohmoto, H. 1985. Chemical evolution and mineral deposition in boiling hydrothermal systems. Economic Geology, **80**: 126-147

Dubé, L., and Hubert, C. 1991. The Telbel orebody of the Agnico-Eagle gold mine of the Abitibi greenstone belt, Joutel, Québec: a stratabound, gold-bearing massive siderite deposit with carbonatization related to mineralization. GAC-MAC joint annual meeting, program with abstracts, **16**: 31.

Eddy, C.A., Dilek, Y., Hurts, S., and Moores, E.M. 1998. Seamount formation and associated caldera complex and hydrothermal mineralization in ancient oceanic crust, Troodos Ophiolite (Cyprus). Tectonophysics, **292**: 189-210.

Fisher, R.V. 1961. Proposed classification of volcaniclastic sediments and rocks. Geological Society of America Bulletin, **72**: 1409-1414.

Fisher, R.V. and Schmincke, H.-U., 1984. Pyroclastic Rocks. Springer, Heidelberg: 427 p.

Fornari, D.J. 1986. Submarine lava tubes and channels. Bulletin of Volcanology, **48**: 291-298.

Foucault, A., and Raoult, J.-F. 1995. Dictionnaire de géologie, 4th edition. Paris Masson, France. 324 p.

Franklin, J.M. 1990. Volcanic-associated massive sulphide deposits. *In* Gold and base-metal mineralization in the Abitibi subprovince, Canada, with emphasis on the Quebec

segment. *Edited by* S.E. Ho, F. Roberts and D.I. Groves. Short course notes, The University of Western Australia, Publication No. **24**: 211-241.

Franklin, J.M. 1993. Volcanic-associated massive sulphide deposits. *In* Mineral Deposit Modeling. *Edited by* R.V. Kirkham, W.D. Sinclair, R.I. Thorpe and J.M. Duke. Geological Association of Canada Special Paper, **40**: 315-334.

Franklin, J.M., Kasarda, J., and Poulsen, K.H. 1975. Petrology and chemistry of the alteration zone of the Mattabi massive sulphide deposit. Economic Geology, **40**: 63-79.

Franklin, J.M., Sangster, D.M., and Lydon, J.W. 1981. Volcanic-associated massive sulphide deposits. Economic Geology: Seventy-fifth anniversary volume; 1905-1980, pp. 485-627.

Frimmel, H.E., and Frank, W. 1998. Neoproterozoic tectono-thermal evolution of the Gariep Belt and its basement, Namibia and South Africa. Precambrian Research, **90**: 1-28.

Frimmel, H.E., Hartnady, C.J.H., and Koller, F. 1996a. Geochemistry and tectonic setting of magmatic units in the Pan-African Gariep Belt, Namibia. Chemical Geology, **130**: 101-121.

Frimmel, H.E., Klötzli, U.S., and Siegfried, P.R. 1996b. New Pb-Pb single zircon age constraints on the timing of Neoproterozoic glaciation and continental break-up in Namibia. The journal of Geology, **104**: 459-469.

Frimmel, H.E., Fölling, P.G., and Eriksson, P. 2002. Neoproterozoic tectonic and climatic evolution recorded in the Gariep Belt, Namibia and South Africa. Basin Research, **14**: 55-67.

Galley, A.G. 1993. Characteristics of semi-conformable alteration zones associated with volcanogenic massive sulphides districts. Journal of Geochemical Exploration, **48**: 175-199.

Gibson, H.L., and Watkinson, D.H. 1990. Volcanogenic massive sulphide deposits of the Noranda cauldron and shield volcano, Quebec. *In* The northwestern Quebec polymetallic belt; a summary of 60 years of mining exploration; Proceedings of the Rouyn-Noranda 1990 symposium, Canadian Institute of Mining and Metallurgy Special Volume, **43**: 119-132.

Gill, J. 1981. Orogenic andesites and plate tectonics. Springer, Heidelberg: 390 p.

Greenough, J.D., and Papezik, V.S. 1985. Chloritization and carbonatization of Cambrian volcanic rocks in eastern Newfoudland and southern New-Brunswick, Canada. Chemical Geology, **53**: 53-70.

Guthrie Jr, G.D., Carey, J.W., Bergfeld, D., Byler, D., Chipera, S., Ziock, H.-J., and Lackner, K. 2001. Geochemical aspects of the carbonation of magnesium silicates in aqueous medium. Zeca document (www.zeca.org).

Hynes, A. 1980. Carbonatization and mobility of Ti, Y, and Zr in Ascot Formation metabaslats, SE Quebec. Contributions to Mineralogy and Petrology, **75**: 79-87.

Johnson, P.R., and Kattan, F. 2001. Oblique sinistral transpression in the Arabian shield: the timing and kinematics of a Neoproterozoic suture zone. Precambrian Research, **107**: 117-138.

Johnson, T.J., and Woodcock, N.H. 1991. Detecting cleavage-transected folds using cleavage-bedding intersections. Journal of Structural Geology, **13**: 919-925.

Kerrich, R., and Fyfe, W.S. 1981. The gold-carbonate association: source of CO_2, and CO_2 fixation reactions in Archean lode deposits. Chemical Geology, **33**: 265-294.

Kerrich R., and Wyman D. A. 1996. The trace element systematics of igneous rocks in mineral exploration: an overview. *In* Wyman, DA (editor) Trace element geochemistry of volcanic rocks: Application for massive sulphide exploration. GAC Short Course **12**: 1-50.

Koski, R.A. 1988. Ferromanganese deposits from the Gulf of Alaska seamount province: mineralogy, chemistry and origin. Canadian Journal of earth Sciences, **25**: 116-133.

Kuhn, T., Halbach, P., and Maggiulli, M. 1996. Formation of ferromanganese microcrusts in relation to glacial/interglacial stages in Pleistocene sediments from Ampere Seamount (subtropical NE Atlantic). Chemical Geology, **130**: 217-232.

Lafrance, B. 2003. Reconstruction d'un environnement de sulfures massifs volcanogènes déformé: exemple Archéen de Normétal, Abitibi. PhD thesis, Université du Québec à Chicoutimi, Chicoutimi, Qc, Canada, 362 p.

Larocque, A.C.L., and Hodgson, C.J. 1993. Carbonate-rich footwall alteration at the Mobrun mine, a possive Mattabi-type VMS deposit in the Noranda Camp. Exploration and Mining Geology, **2**: 165-169.

Lazur, Y.M., Varenstov, I.M., Kropachev, V.V., and Melamedov, S.V. 1992. Dispersed native elements in the oceanic Mn-Fe oxyhydroxide crusts: indicators of genesis and accumulation history (Krylov Seamount, eastern Atlantic). 29th International Geological Congress, Abstracts, **29**: 214.

Leleu, M.G. 1978. L'association sulfures-carbonates: application au cas de la galène en milieu hydrothermal. Chemical Geology, **22**: 43-70.

Lowe, D.R. 1982. Sediment gravity flows: II. Depositional models with special reference to the deposits of high-density turbidity currents. Journal of Sedimentary Petrology, **52**: 279-297.

Lowe, D.R. 1988. Suspended-load fallout rate as an independent variable in the analysis of current structures. Sedimentology, **35**: 765-776.

Lydon, J.W. 1984. Ore deposit models - 8. Volcanogenic massive sulphide deposits Part 1: A descriptive model. Geoscience Canada, **11**: 195-202.

Macdonald, G.A., 1972. Volcanoes. Prentice-Hall, Engelwood Cliffs, New Jersey: 510 p.

McPhie, J., Doyle, M., and Allen, R. 1993. Volcanic Textures: a Guide to the Interpretation of Textures in Volcanic Rocks. CODES Key Centre, Univ. Tasmania, Hobart: 198 p.

Melling, D.R., Watkinson, D.H., Fox, P.E., and Cameron, R.S. 1990. Carbonatization and propylitic alteration of fragmental basaltic rocks, Quesnel River gold deposit, Central British Columbia. Mineralium Deposita, **25 [Suppl]**: S115-S124.

Meschede, M. 1986. A method of discriminating between different types of mid-ocean ridge basalts and continental tholeiites with the Nb-Zr-Y diagram. Chemical Geology, **56**: 207-218.

Miall, A.D. 1978. Fluvial sedimentology. Canadian Society of Petroleum Geologists, Clagary, Alberta, Canada. 859 p.

Morton, R.L., and Franklin, J.M. 1987. Two-fold classification of Archean volcanic-associated massive sulfide deposits. Economic Geology, **82**: 1057-1063.

Mueller, W.U. 1991. Volcanism and related slope to shallow marine volcaniclastic sedimentation: an Archean example, Chibougamau, Quebec, Canada. Precambrian Research, **49:** 1-22.

Mueller, W.U., 2003. A subaqueous eruption model for shallow-water, small volume eruptions: evidence from two Precambrian examples. AGU-Monograph, Chapman conference on 'Explosive subaqueous volcanism'. *Edited by* J. White, D. Clague, and J. Smellie. AGU-Monograph, **(in press)**.

Mueller, W.U., and White, J.D.L. 1992. Felsic fire fountaining beneath Archean seas - pyroclastic deposits of the 2730 Ma Hunter Mine Group, Quebec, Canada. Journal of Volcanology and Geothermal Research, **54**: 117-134.

Mueller, W.U., and White, J.D.L., 2003. Terminology of volcaniclastic and volcanic rocks. *In* Developments in Precambrian Geology 12: The Precambrian Earth: tempos and events. *Edited by* P. Eriksson, W. Altermann, D. Nelson, W.U. Mueller, and O. Catuneanu., Elsevier **(in press)**.

Mueller, W.U., Garde, A., and Stendal, H., 2000. Shallow-water, eruption-fed, mafic pyroclastic deposits along a Paleoproterozoic coastline: Kangerluluk volcano-sedimentary sequence, southeast Greenland. Precambrian Research, **101**: 163-192.

Mueller, W.U., Aubin, A,, and Cororan, P.L. 2001. Economic potential of the Schakalsberg Mountains, EPL 2757, Sperrgebiet, Namibia. Kumba Resources internal report, 21 p.

Mueller, W.U., Dostal, J., and Stendal, H. 2002. Inferred Paleoproterozoic arc rifting along a consuming plate margin: insights from the stratigraphy, volcanology and geochemistry of the Kangerluluk sequence, southeast Greenland. International Journal of Earth Sciences (former Geologische Rundschau), **91**: 209-230.

Penczak, R.S., and Mason, R. 1999. Characteristics and origin of Archean premetamorphic hydrothermal alteration at the Campbell gold mine, northwestern Ontario, Canada. Economic geology, **94**: 507-528.

Pichler, T., Ridley, W.A., and Nelson, E. 1999. Low-temperature alteration of dredged volcanics from the southern Chile Ridge; additional information about early stages of seafloor weathering. Marine Geology, **159**: 155-177.

Pik, R., Deniel, C., Coulon, C., Yirgu, G., Hofmann, C., and Ayalew, D. 1998. The northwestern Ethiopian Plateau flood basalts: Classification and spatial distribution of magma types. Journal of Volcanology and Geothermal Research **81** : 91-111.

Reading, H.G., and Levell, B.K. 1996. Controls on the sedimentary rock record. *In* Sedimentary environments: processes, facies and stratigraphy. Edited by H.G. Reading, 3rd edition, Blackwell Science, U.K. 688 p.

Ridout, P.S., Carpenter, M.S.N., and Morris, R.J. Analysis of a metalliferous encrustation from a seamount in the Gulf of Guinea. Chemical Geology, **42**: 219-225.

Schandl, E.S., and Wicks, F.J. 1993. Carbonate and associated alteration of ultramafic and rhyolitic rocks at the Hemingway Property, Kidd Creek volcanic Complex, Timmins, Ontario. Economic Geology, **88**: 1615-1635.

Schmid, R., 1981. Descriptive nomenclature and classification of pyroclastic deposits and fragments: Recommendations of the IUGS Subcommission on the Systematics of Igneous Rocks. Geology, **9**: 41-43.

Schmidt, R., and Schmincke, H.-U. 2000. Seamounts and island building. *In* Encyclopedia of volcanoes. *Edited by* H. sigurdsson, B. Houghton, S.R. McNutt, H. Rymer and J. Stix. Academic Press, San Diego, CA, United States., 383-402.

Sketchley, D.A., and Sinclair, A.J. 1991. Carbonate alteration in basalt, Total Erickson gold mine, Cassiar, northern British Columbia, Canada. Economic Geology, **86**: 570-587.

Staudigel, H., and Schmincke, H.-U. 1984. The Pliocene seamount series of La Palma/Canary Islands. Journal of Geophysical Research, **89**: 11195-11215.

Sun S. S., and McDonough, W. F. 1989. Chemical and isotopic systematics of ocean basalts: implications for mantle composition and processes. *In* Saunders AD, Norry MJ (editors), Magmatism in the Ocean Basins. Geological Socociety London, Special Publication **42**, 313-345.

Thompson, A.J.B., and Thompson, J.F.H. (editors). 1996. Atlas of alteration: a field and petrographic guide to hydrothermal alteration minerals. Geological Association of Canada, Mineral deposit Division, Saint John's, Newfoundland, Canada. 119 p.

Thomson, M.L. 1987. Progressive carbonatization of an epidote amphibolite assemblage within the Crixas gold deposit, central Brazil. Geological Society of America, Annual Meeting, Abstracts with programs, Phoenix: 868.

Trua, T., Serri, G., Marani, M., Renzuli, A., and Gamberi, F. 2002. Volcanological and petrological evolution of Marsili Seamount (southern Tyrrhenian Sea). Journal of Volcanology and Geothermal Research, **114**: 441-464.

Veizer, J., Hoefs, J., Ridler, R.H., Jensen, L.S., and Lowe, D.R. 1989. Geochemistry of Precambrian carbonates: I, Archean hydrothermal systems. Geochimica et Cosmochimica Acta, **53**: 845-857.

Wells, G., Bryan, W.B., and Pearce, T.H., 1979. Comparative morphology of ancient and modern pillow lavas. Journal of Geology, **87**: 427-440.

White, J.D.L. 1996. Pre-emergent construction of a lacustrine basaltic volcano, Pahvant Butte, Utah (USA). Bulletin of Volcanology, **58**: 249-262.

White, J.D.L. 2000. Subaqueous eruption-fed density currents and their deposits. Precambrian Research, **101**: 87-109.

Williams, H., and McBirney, A.R. 1979. Volcanology. Freeman, Cooper and Co., San Fransisco: 397 p.

Wilson, M. 1989. Igneous petrogenesis. Chapman & Hall, London. 466 p.

Winchester, J.A., and Floyd, P.A. 1977. Geochemical discrimination of different magma series and their differentiation products using immobile elements. Chemical Geology, **20**: 325-343.

Wood, D.A.1980. The application of a Th-Hf-Ta diagram to problems of tectonomagmatic classification and to establish the nature of crustal contamination of basaltic lavas of the British Tertiary volcanic province. Earth and Planetary science Letters, **50**: 11-30.

Wooldridge, A.L., Haggerty, S.E., and Rona, P.A. 1990. Magnetic properties and opaque mineralogy of rocks from selected seafloor hydrothermal sites at oceanic ridges. Journal of Geophysical Research, B, Solid Earth and Planets, **95**: 12351-12374.

Yang, Q., and Nielsen, K.C. 1995. Rotation of fold-hinge lines associated with simple shear during southerly directed thrusting, Ouachita Mountains, southeastern Oklahoma. Journal of Structural Geology, **17**: 803-817.

Yardley, B.W.D. 1989. An introduction to metamorphic petrology. Longman Earth Sciences series, London. 248 p.

Zhao, J.-X., McCulloch, M.T., and Korsch, R.J. 1994. Characterisation of a plume-related ~ 800 magmatic event and its implications for basin formation in central-southern Austrtalia. Earth and Planetary Science Letters, **121**: 349-367.

APPENDIX 1

List of samples from EPL 2757 and their position

Sample #			Rock description	Stop #	South Co.	East Co.
AA	1	2001	VOLCANIC MAFIC MAGNETIC AMYGDULAR	2,1	28,12411667	16,54161667
AA	2	2001	BRECCIA FRAGMENT	2,2	28,12395000	16,54075000
AA	3	2001	BRECCIA FRAGMENT	2,6	28,12233333	16,53885000
AA	4	2001	LAPILLI TUFF	3,5	28,12195000	16,53866667
AA	5	2001	LAPILLI TUFF	3.10	28,11960000	16,53330000
AA	6	2001	VOLCANIC MAFIC AMYGDULAR	3,12	28,12038333	16,53306667
AA	7	2001	VOLCANIC MAFIC MAGNETIC	4.1	28,12091667	16,54063333
AA	8	2001	LAPILLI TUFF	4.6	28,12033333	16,53050000
AA	9	2001	MANGANESE - CARBONATES	4.7	28,12091667	16,52940000
AA	10	2001	MANGANESE - CARBONATES	4.17	28,11711667	16,52436667
AA	11	2001	CARBONATES	4.17	28,11711667	16,52436667
AA	12	2001	MANGANESE - CARBONATES	4.27	28,12325000	16,53045000
AA	13	2001	MANGANESE - CARBONATES	5.4	28,12781667	16,53976667
AA	14	2001	MANGANESE - CARBONATES	5.7	28,12606667	16,53950000
AA	15	2001	MANGANESE - CARBONATES	5.9	28,12618333	16,53838333
AA	16	2001	ANKERITE	5.10	28,12618333	16,53838333
AA	17	2001	CARBONATE BRECCIA	5.11	28,12551667	16,53775000
AA	18	2001	VOLCANIC MAFIC	5.13	28,12450000	16,53578333
AA	19	2001	MANGANESE - CARBONATES	5.17	28,12515000	16,52921667
AA	20	2001	CARBONATES	5.20	28,12496667	16,52600000
AA	21	2001	MANGANESE - CARBONATES	5.24	28,12333333	16,53140000
AA	22	2001	BANDED IRON FORMATION	6.3	28,12715000	16,53748333
AA	23	2001	VESICULAR FRAGMENT	6.3	28,12715000	16,53748333
AA	24	2001	MINERALIZATION	6.4	28,12320000	16,53353333
AA	25	2001	MINERALIZATION	6.12	28,12043333	16,52405000
AA	26	2001	MINERALIZATION	6.13	28,11963333	16,52366667
AA	27	2001	VOLCANIC MAFIC MINERALIZED	6.14	28,12080000	16,52300000
AA	28	2001	FINE MINERALIZATION	6.15	28,12008333	16,52310000
AA	29	2001	VOLCANIC MAFIC MINERALIZED?	6.21	28,10916667	16,51333333
AA	30	2001	CARBONATES	7.16	28,11660000	16,51986667
AA	31	2001	FINE MATERIAL - BEDDED	7.18	28,11510000	16,51645000
AA	32	2001	VOLCANIC MAFIC MINERALIZED?	7.25	28,11745000	16,52125000
AA	33	2001	VOLCANIC MAFIC MAGNETIC	8.1	28,10865000	16,51241667
AA	34	2001	HEMATIZED MUDSTONE	8.6	28,10971667	16,50951667
AA	35	2001	MAFIC HYALOCLASTITE LITHOFACIES CARBONATED	9.1	28,10436667	16,50940000
AA	36	2001	MAFIC HYALOCLASTITE LITHOFACIES CARBONATED	9.8	28,10430000	16,50525000
AA	37	2001	MAFIC HYALOCLASTITE LITHOFACIES CARBONATED FOLDED	9.8	28,10430000	16,50525000
AA	38	2001	MINERALIZATION	9.8	28,10430000	16,50525000
AA	39	2001	CARBONATES BRECCIA	9.10	28,10705000	16,50558333

Sample #			Rock description	Stop #	South Co.	East Co.
AA	40	2001	QUARTZ-GOETHITE VEIN	9.13	28,10730000	16,50228333
AA	41	2001	MAFIC HYALOCLASTITE LITHOFACIES NON-CARBONATED MINERALIZED	9.16	28,10468333	16,50176667
AA	42	2001	GABBRO	9.25	28,10205000	16,50916667
AA	43	2001	MAFIC HYALOCLASTITE LITHOFACIES NON-CARBONATED	10.9	28,12470000	16,57036667
AA	44	2001	PILLOW BRECCIA	10.11	28,12501667	16,57075000
AA	45	2001	BANDED IRON FORMATION	10.11	28,12501667	16,57075000
AA	46	2001	PILLOW FRAGMENT	10.11	28,12501667	16,57075000
AA	47	2001	PILLOW FRAGMENT	10.11	28,12501667	16,57075000
AA	48	2001	MINERALIZATION	10.13	28,12558333	16,57091667
AA	49	2001	MAFIC HYALOCLASTITE LITHOFACIES CARBONATED	10.13	28,12558333	16,57091667
AA	50	2001	PILLOW BRECCIA	10.15	28,12596667	16,56931667
AA	51	2001	PILLOW AMYGDULAR	10.22	28,12003333	16,56481667
AA	52	2001	PILLOW AMYGDULAR	10.22	28,12003333	16,56481667
AA	53	2001	COLUMNAR JOINTS IN VOLCANIC MAFIC	10.28	28,11755000	16,56733333
AA	54	2001	VOLCANIC MAFIC NON-MAGNETIC AMYGDULAR	11.1	28,11433333	16,57336667
AA	55	2001	VOLCANIC MAFIC FELDSPAR-PHYRIC MAGNETIC	11.4	28,11598333	16,57376667
AA	56	2001	VOLCANIC MAFIC MINERALIZED	11.15	28,11803333	16,56958333
AA	57	2001	VOLCANIC MAFIC FELDSPAR-PHYRIC NON-MAGNETIC	11.34	28,10286667	16,58975000
AA	58	2001	VOLCANIC MAFIC FELDSPAR-PHYRIC PILLOWED NON-MAGNETIC	11.36	28,10426667	16,59061667
AA	59	2001	VOLCANIC MAFIC MASSIVE MAGNETIC	11.39	28,10498333	16,59050000
AA	60	2001	FLOW BANDING VOLCANIC MAFIC	11.40	28,10673333	16,59103333
AA	61	2001	VOLCANIC MAFIC MASSIVE MAGNETIC	11.43	28,10640000	16,59001667
AA	62	2001	VOLCANIC MAFIC FELDSPAR-PHYRIC PILLOWED NON-MAGNETIC	11.54	28,10281667	16,58796667
AA	63	2001	MAFIC SCHIST CARBONATED	12.20	28,11765000	16,55155000
AA	64	2001	VOLCANIC MAFIC APHANITIC CARBONATED NON-MAGNETIC	12.24	28,12086667	16,55041667
AA	65	2001	MINERALIZATION IN CARBONATED MAFIC SCHIST	12.34	28,10770000	16,53821667
AA	66	2001	MINERALIZATION IN MAFIC HYALOCLASTITE LITHOFACIES CARBONATED	12.45	28,10943333	16,54365000
AA	67	2001	VOLCANIC MAFIC APHANITIC PILLOWED MAGNETIC	12.56	28,11031667	16,55218333
AA	68	2001	VOLCANIC MAFIC FELDSPAR-PHYRIC NON-MAGNETIC	13.6	28,10131667	16,58653333
AA	69	2001	VOLCANIC MAFIC FELDSPAR-PHYRIC NON-MAGNETIC	13.7	28,10135000	16,58678333
AA	70	2001	VOLCANIC MAFIC HORNBLENDE-FELDSPAR-PHYRIC NON-MAGNETIC	13.11	28,09703333	16,58483333
AA	71	2001	VOLCANIC MAFIC HORNBLENDE-FELDSPAR-PHYRIC NON-MAGNETIC	13.16	28,10346667	16,58693333
AA	72	2001	VOLCANIC MAFIC FELDSPAR-PHYRIC NON-MAGNETIC	14.1	28,11175000	16,58836667
AA	73	2001	VOLCANIC MAFIC FELDSPAR-PHYRIC PILLOWED NON-MAGNETIC	14.21	28,11323333	16,58381667
AA	74	2001	VOLCANIC MAFIC FELDSPAR-PHYRIC NON-MAGNETIC	14.34	28,11423333	16,58350000
AA	75	2001	VOLCANIC MAFIC MICROPORPHYRIC	14.60	28,12193333	16,59433333
AA	76	2001	GABBRO NON-MAGNETIC	14.68	28,11711667	16,59711667
AA	77	2001	VOLCANIC MAFIC FELDSPAR-PHYRIC NON-MAGNETIC	15.5	28,10801667	16,58415000
AA	78	2001	VOLCANIC MAFIC FELDSPAR-PHYRIC NON-MAGNETIC	15.21	28,10073333	16,57435000

Sample #			Rock description	Stop #	South Co.	East Co.
AA	79	2001	GABBRO WITH PYRITE	15.24	28,09818333	16,57485000
AA	80	2001	VOLCANIC MAFIC	15.56	28,10691667	16,57833333
AA	81	2001	VOLCANIC MAFIC APHANITIC NON-MAGNETIC	15.57	28,11315000	16,61801667
AA	82	2001	HYALOCLATITES CARBONATED?	15.57	28,11315000	16,61801667
AA	83	2001	MAFIC SCHIST CARBONATED	15.57	28,11315000	16,61801667
AA	84	2001	VOLCANIC MAFIC FELDSPAR-PHYRIC NON-MAGNETIC	15.58	28,09920000	16,59841667
AA	85	2001	VOLCANIC MAFIC FELDSPAR-PHYRIC MAGNETIC	16.1	28,11195000	16,56615000
AA	86	2001	VOLCANIC MAFIC HORNBLENDE-FELDSPAR-PHYRIC PILLOWED NON-MAGNETIC	17.7	28,09575000	16,56683333
AA	87	2001	VOLCANIC MAFIC APHANITIC MINERALIZED PILLOWED NON-MAGNETIC CARBONATED	18.7	28,10745000	16,55611667
AA	88	2001	VOLCANIC MAFIC APHANITIC MINERALIZED SCHIST MAGNETIC	18.8	28,10596667	16,55643333
AA	89	2001	GABBRO NON-MAGNETIC	18.13	28,09425000	16,55565000
AA	90	2001	MINERALIZATION	18.34	28,10693333	16,54583333
AA	91	2001	VESICULAR PILLOW BRECCIA	18.42	28,10161667	16,53763333
AA	92	2001	VOLCANIC MAFIC FELDSPAR-PHYRIC MASSIVE	18.44	28,10306667	16,58983333
AA	93	2001	VOLCANIC MAFIC VESICULAR PILLOWED MAGNETIC CARBONATED	AM-2	28,10383333	16,50800000
AA	94	2001	VOLCANIC MAFIC CARBONATED	AM-3	28,10400000	16,50783333
AA	95	2001	LAPILLI TUFF CARBONATED	AM-3	28,10400000	16,50783333
AA	96	2001	CARBONATED TUFF BROWN	AM-4	28,10416667	16,50750000
AA	97	2001	CARBONATED TUFF GREY	AM-4	28,10416667	16,50750000
AA	98	2001	CARBONATED TUFF GREY	AM-5	28,10466667	16,50733333
AA	99	2001	CARBONATE VEIN	AM-5	28,10466667	16,50733333
AA	100	2001	CARBONATED TUFF RED AND GREY	AM-5	28,10466667	16,50733333
AA	101	2001	CARBONATED TUFF RED AND GREEN	AM-5	28,10466667	16,50733333
AA	102	2001	CARBONATED TUFF RED	AM-5	28,10466667	16,50733333
AA	103	2001	ZEBRA TUFF CARBONATED	AM-6	28,10450000	16,50683333
AA	104	2001	CARBONATE VEIN	AM-8	28,10516667	16,50533333
AA	105	2001	DARK BROWN CARBONATED VOLCANIC MAFIC	AM-9	28,10516667	16,50516667
AA	106	2001	CARBONATE VEIN	AM-11	28,10516667	16,50500000
AA	107	2001	VOLCANIC MAFIC CARBONATED	AM-12	28,10550000	16,50466667
AA	108	2001	BLACK DYKE	AM-12	28,10550000	16,50466667
AA	109	2001	VOLCANIC MAFIC CARBONATED	AM-12	28,10550000	16,50466667
AA	110	2001	VOLCANIC MAFIC CARBONATED	AM-13	28,10616667	16,50366667
AA	111	2001	MINERALIZATION	AM-14	28,10716667	16,50366667
AA	112	2001	LAPILLI TUFF CARBONATED	AM-17	28,10933333	16,50350000
AA	113	2001	CARBONATE WHITE	AM-19	28,11033333	16,50216667
AA	114	2001	VOLCANIC MAFIC	AM-19	28,11033333	16,50216667
AA	115	2001	TUFF CARBONATED	AM-20	28,11083333	16,50133333
AA	116	2001	VOLCANIC MAFIC MICROPORPHYRIC PILOWED MAGNETIC	20.3	28,10373333	16,59125000
AA	117	2001	VOLCANIC MAFIC MICROPORPHYRIC PILOWED MAGNETIC	20.3	28,10373333	16,59125000

Sample #			Rock description	Stop #	South Co.	East Co.
AA	118	2001	VOLCANIC MAFIC MINERALIZED PYRITE MAGNETIC	20.7	28,10648333	16,59140000
AA	119	2001	VOLCANIC MAFIC MINERALIZED PYRITE MAGNETIC	20.7	28,10648333	16,59140000
AA	120	2001	VOLCANIC MAFIC FELDSPAR-PHYRIC NON-MAGNETIC	20.8	28,10673333	16,56056667
AA	121	2001	VOLCANIC MAFIC FELDSPAR-PHYRIC NON-MAGNETIC PYRITE	20.12	28,10155000	16,59631667
AA	122	2001	VOLCANIC MAFIC AMYGDULAR	20.15	28,09890000	16,59740000
AA	123	2001	VOLCANIC MAFIC AMYGDULAR PYRITE	20.15	28,09890000	16,59740000
AA	124	2001	CARBONATES + GOETHITE	20.18	28,09898333	16,59875000
AA	125	2001	LAPILLI TUFF CARBONATED	20.19	28,09741667	16,59760000
AA	126	2001	CARBONATES WHITE AND GREY	20.21	28,09198333	16,60548333
AA	127	2001	CARBONATES BRECCIA	20.21	28,09198333	16,60548333
AA	128	2001	LEOPAR GABBRO	20.25	28,09631667	16,59400000
AA	129	2001	GABBRO CARBONATED	20.27	28,09556667	16,59398333
AA	130	2001	GABBRO	20.38	28,08281667	16,58123333
AA	131	2001	VOLCANIC MAFIC FELDSPAR-PHYRIC NON-MAGNETIC	20.60	28,09508333	16,58983333
AA	132	2001	TURBIDITE TUFF	21.11	28,11898333	16,60118333
AA	133	2001	GABBRO NON-MAGNETIC	21.16	28,12356667	16,61091667
AA	134	2001	CARBONATES BROWN	21.27	28,12248333	16,62563333
AA	135	2001	CARBONATES WHITE AND GREY	21.27	28,12248333	16,62563333
AA	136	2001	CARBONATES BLUISH-GREY	21.28	28,12205000	16,62605000
AA	137	2001	CARBONATES WHITE	21.28	28,12205000	16,62605000
AA	138	2001	VOLCANIC MAFIC APHANITIC MINERALIZED CARBONATED	21.33	28,11155000	16,61658333
AA	139	2001	MAFIC HYALOCLASTITE LITHOFACIES CARBONATED	21.45	28,12098333	16,62308333
AA	140	2001	MAFIC HYALOCLASTITE LITHOFACIES CARBONATED	21.46	28,11996667	16,62260000
AA	141	2001	CARBONATES	21.50	28,11296667	16,61968333
AA	142	2001	CARBONATES	21.51	28,11273333	16,62053333
AA	143	2001	CARBONATES GREY	21.52	28,11283333	16,61998333
AA	144	2001	CARBONATES BLUISH-GREY	22.4	28,03060000	16,54865000
AA	145	2001	CARBONATES BLUISH-GREY	22.5	28,02838333	16,54680000
AA	146	2001	CARBONATES BLUISH-GREY	22.9	28,01960000	16,54235000
AA	147	2001	PILLOW BRECCIA CARBONATED	22.14	28,02611667	16,53766667
AA	148	2001	TURBIDITE TUFF	22.30	28,04445000	16,54796667
AA	149	2001	APLITE	22.49	28,05715000	16,56096667
AA	150	2001	TURBIDITE TUFF	23.17	28,09068333	16,57948333
AA	151	2001	GABBRO MINERALIZED	23.27	28,08728333	16,59475000
AA	152	2001	VOLCANIC MAFIC APHANITIC VESICULAR NON-MAGNETIC	23.27	28,08728333	16,59475000
AA	153	2001	TURBIDITE TUFF	23.51	28,09398333	16,58231667
AA	154	2001	TURBIDITE TUFF	23.51	28,09398333	16,58231667
AA	155	2001	TURBIDITE TUFF	23.51	28,09398333	16,58231667
AA	156	2001	VOLCANIC MAFIC HORNBLENDE-PHYRIC	23.56	28,09625000	16,58156667

Sample #			Rock description	Stop #	South Co.	East Co.
AA	157	2001	APLITE	24.13	28,05930000	16,56596667
AA	158	2001	VOLCANIC MAFIC APHANITIC PILLOWED NON-MAGNETIC	24.22	28,05613333	16,56696667
AA	159	2001	GABBRO NON-MAGNETIC	25.1	28,07258333	16,57278333
AA	160	2001	VOLCANIC MAFIC APHANITIC VESICULAR	25.7	28,07341667	16,56840000
AA	161	2001	TURBIDITE TUFF	25.10	28,07646667	16,56958333
AA	162	2001	TURBIDITE TUFF	25.10	28,07646667	16,56958333
AA	163	2001	TURBIDITE TUFF	25.11	28,07753333	16,57041667
AA	164	2001	VOLCANIC MAFIC MICROPORPHYRIC NON-MAGNETIC	25.30	28,07411667	16,56366667
AA	165	2001	CARBONATES BLUISH-GREY	26.4	28,03116667	16,55766667
AA	166	2001	CARBONATES BLUISH-GREY	26.5	28,03026667	16,55455000
AA	167	2001	IRON FORMATION	26.20	28,03968333	16,50338333
AA	168	2001	GABBRO FELDSPAR-PHYRIC MAGNETIC	26.42	28,04376667	16,50080000
AA	169	2001	GABBRO FELDSPAR-PHYRIC MAGNETIC	27.1	28,07405000	16,54638333
AA	170	2001	GABBRO FELDSPAR-PHYRIC MAGNETIC	27.1	28,07405000	16,54638333
AA	171	2001	MINERALIZATION	27.33	28,06873333	16,51531667
AA	172	2001	VOLCANIC MAFIC MICROPORPHYRIC VESICULAR MAGNETITE PYRITE	28.23	28,08525000	16,56403333
AA	173	2001	CARBONATES	29.13	28,12965000	16,54475000
AA	174	2001	LAPILLI TUFF	29.13	28,12965000	16,54475000
AA	175	2001	TUFF	29.13	28,12965000	16,54475000
AA	176	2001	LAPILLI TUFF BRECCIA	29.13	28,12965000	16,54475000
AA	177	2001	MINERALIZATION	29.14	28,12776667	16,54333333
AA	178	2001	MINERALIZATION	29.15	28,12805000	16,54331667
AA	179	2001	LAPILLI TUFF BRECCIA	29.16	28,12816667	16,54285000
AA	180	2001	LAPILLI TUFF BRECCIA	29.16	28,12816667	16,54285000
AA	181	2001	TUFF GREY LEACHED	29.16	28,12816667	16,54285000
AA	182	2001	ARGILLIZATION	29.16	28,12816667	16,54285000
AA	183	2001	LAPILLI TUFF CARBONATED	29.16	28,12816667	16,54285000
AA	184	2001	CARBONATES MINERALIZED	29.16	28,12816667	16,54285000
AA	185	2001	SILICIFICATION IRON	29.16	28,12816667	16,54285000
AA	186	2001	CARBONATES BRECCIA BROWN	29.21	28,12658333	16,54073333
AA	187	2001	CARBONATES BRECCIA RED	29.21	28,12658333	16,54073333
AA	188	2001	CARBONATES BRECCIA GOETHITE	29.23	28,12490000	16,53913333
AA	189	2001	GABBRO MAGNETIC	29.24	28,12441667	16,53565000
AA	190	2001	VOLCANIC MAFIC PILLOWED CARBONATED	29.24	28,12441667	16,53565000
AA	191	2001	CARBONATES	29.24	28,12441667	16,53565000
AA	192	2001	LAPILLI TUFF	29.24	28,12441667	16,53565000
AA	193	2001	VOLCANIC MAFIC APHANITIC VESICULAR PILLOWED NON-MAGNETIC	29.25	28,12365000	16,53556667
AA	194	2001	LAPILLI TUFF	29.24	28,12441667	16,53565000
AA	195	2001	LAPILLI TUFF	29.24	28,12441667	16,53565000

Sample #			Rock description	Stop #	South Co.	East Co.
AA	196	2001	ARGILLIZATION	30.1	28,12465000	16,53915000
AA	197	2001	LAPILLI TUFF LEACHED	30.5	28,12295000	16,53770000
AA	198	2001	LIMONITE GOETHITE	30.5	28,12295000	16,53770000
AA	199	2001	LAPILLI TUFF	30.6	28,12551667	16,53650000
AA	200	2001	LAPILLI TUFF BRECCIA	30.6	28,12551667	16,53650000
AA	201	2001	LAPILLI TUFF BRECCIA	30.6	28,12551667	16,53650000
AA	202	2001	LAPILLI TUFF BRECCIA	30.6	28,12551667	16,53650000
AA	203	2001	ZEBRA TUFF	30.14	28,12045000	16,51988333
AA	204	2001	LAPILLI TUFF BRECCIA WHITE	30.14	28,12045000	16,51988333
AA	205	2001	ZEBRA TUFF	30.15	28,11495000	16,51703333
AA	206	2001	BRECCIA MAFIC MATRIX	30.15	28,11495000	16,51703333
AA	207	2001	VOLCANIC MAFIC PILLOWED	31.3	28,12250000	16,53953333
AA	208	2001	VOLCANIC MAFIC PILLOWED	31.3	28,12250000	16,53953333
AA	209	2001	TURBIDITE TUFF	31.3	28,12250000	16,53953333
AA	210	2001	TURBIDITE TUFF	31.3	28,12250000	16,53953333
AA	211	2001	ACCRETIONNARY LAPILLI TUFF	31.4	28,12235000	16,53873333
AA	212	2001	ACCRETIONNARY LAPILLI TUFF	31.4	28,12235000	16,53873333
AA	213	2001	ACCRETIONNARY LAPILLI TUFF	31.4	28,12235000	16,53873333
AA	214	2001	MINERALIZATION MAGNETIC	31.6	28,12245000	16,53916667
AA	215	2001	CARBONATES	31.6	28,12245000	16,53916667
AA	216	2001	ACCRETIONNARY LAPILLI TUFF	31.7	28,12255000	16,53898333
AA	217	2001	ACCRETIONNARY LAPILLI TUFF	31.7	28,12255000	16,53898333
AA	218	2001	MINERALIZATION CARBONATED	31.5	28,12201667	16,53851667
AA	219	2001	ACCRETIONNARY LAPILLI TUFF	31.5	28,12201667	16,53851667
AA	220	2001	LAPILLI TUFF BRECCIA	31.5	28,12201667	16,53851667
AA	221	2001	TUFF CARBONATED	31.8	28,12478333	16,57101667
AA	222	2001	PILLOW BRECCIA	31.8	28,12478333	16,57101667

APPENDIX 2

Microprobe analyses

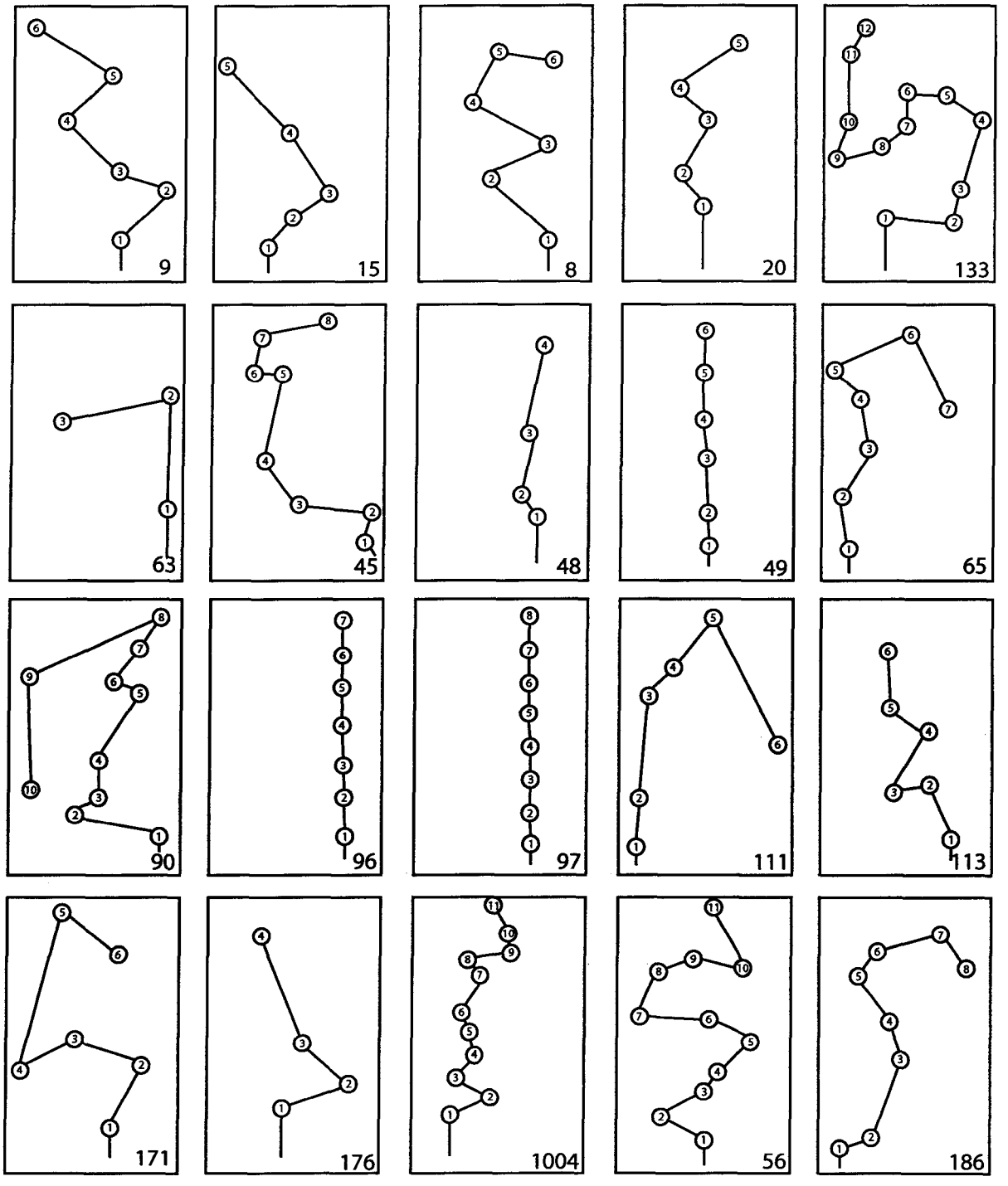

Thin sections zones

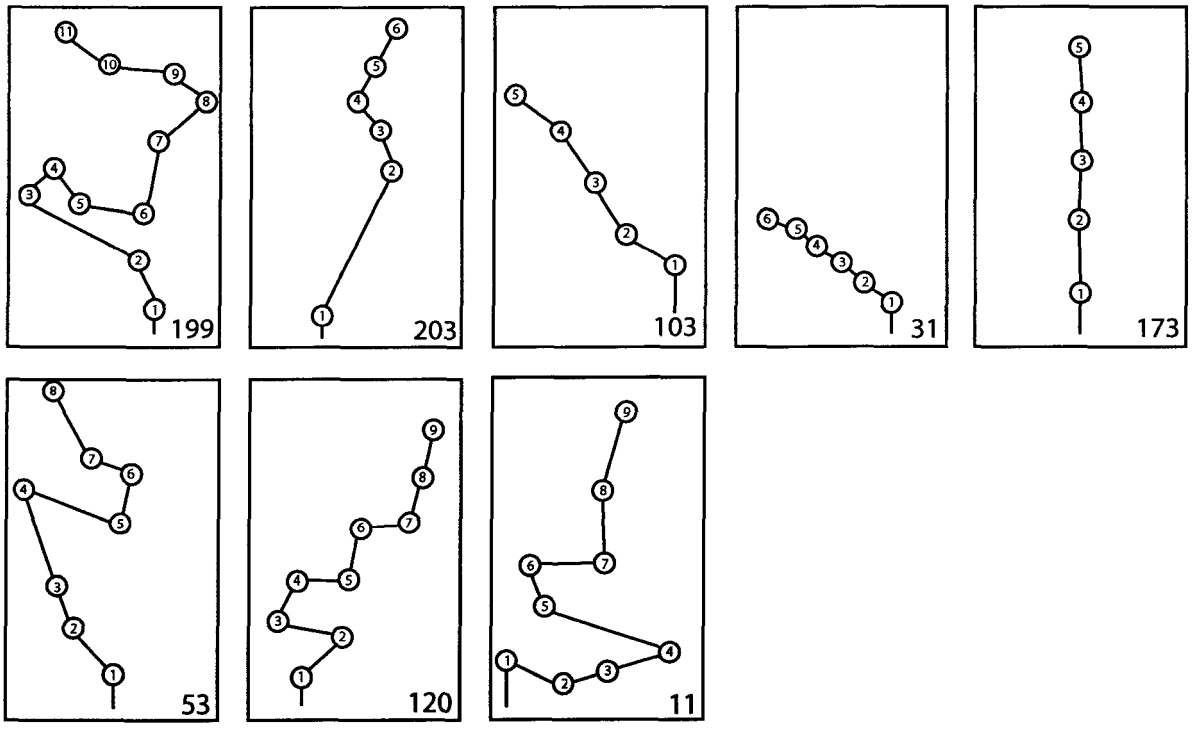

Thin sections zones

Amphiboles

Sample	120	120	120	120	120	120	120	120	133	133	133	133
Zone	2	3	4	5	7	8	9	8	10	9	5	5
SiO2	56,25	55,75	56,75	56,52	55,05	56,62	56,89	54,58	55,20	56,38	54,75	53,78
TiO2	1,04	0,00	0,81	0,00	0,59	0,02	0,00	0,02	0,00	0,02	0,01	0,02
Al2O3	6,48	1,36	1,62	0,76	1,36	0,85	3,89	0,88	1,23	3,39	0,68	1,28
Cr2O3	0,14	0,00	0,00	0,00	0,06	0,02	0,02	0,06	0,00	0,02	0,00	0,03
MgO	14,83	13,23	12,97	13,13	13,57	13,62	11,83	13,61	15,02	14,75	15,63	14,07
CaO	12,84	12,54	12,33	12,45	12,60	12,62	11,18	12,61	12,53	12,56	12,65	12,30
MnO	0,24	0,17	0,25	0,12	0,25	0,19	0,20	0,17	0,24	0,21	0,21	0,21
FeO	13,28	16,61	15,09	16,56	15,53	16,54	15,10	16,52	13,78	13,84	13,79	15,20
Fe2O3	0,00	0,00	0,00	0,00	0,00	0,00	0,00	0,00	0,00	0,00	0,00	0,00
Na2O	0,14	0,13	0,17	0,08	0,11	0,05	1,20	0,09	0,24	0,17	0,11	0,29
K2O	0,08	0,05	0,09	0,03	0,08	0,03	0,11	0,03	0,07	0,08	0,04	0,07
H2O	2,26	2,10	2,13	2,10	2,09	2,12	2,14	2,07	2,09	2,17	2,08	2,05
Total	107,59	101,94	102,19	101,76	101,29	102,68	102,56	100,62	100,40	103,59	99,96	99,29
Si	7,476	7,951	7,999	8,057	7,886	8,005	7,963	7,912	7,915	7,801	7,899	7,866
Ti	0,104	0,000	0,086	0,000	0,064	0,002	0,000	0,002	0,000	0,002	0,001	0,002
Al	1,015	0,229	0,270	0,127	0,230	0,141	0,641	0,150	0,208	0,553	0,116	0,220
Cr	0,015	0,000	0,000	0,000	0,006	0,002	0,002	0,006	0,000	0,003	0,000	0,003
Mg	2,938	2,814	2,725	2,790	2,898	2,870	2,468	2,941	3,211	3,042	3,362	3,069
Ca	1,829	1,916	1,863	1,902	1,935	1,912	1,676	1,959	1,925	1,863	1,956	1,927
Mn	0,027	0,021	0,029	0,014	0,031	0,023	0,024	0,021	0,029	0,025	0,025	0,026
Fe2+	1,476	1,981	1,779	1,975	1,860	1,956	1,767	2,003	1,652	1,602	1,664	1,859
Fe3+	0,000	0,000	0,000	0,000	0,000	0,000	0,000	0,000	0,000	0,000	0,000	0,000
Na	0,037	0,035	0,045	0,023	0,031	0,015	0,327	0,024	0,067	0,045	0,031	0,082
K	0,014	0,009	0,016	0,006	0,014	0,005	0,020	0,006	0,014	0,014	0,006	0,013
OH	2,000	2,000	2,000	2,000	2,000	2,000	2,000	2,000	2,000	2,000	2,000	2,000
Mg/(Mg+Fe)	0,528	0,443	0,462	0,442	0,466	0,451	0,439	0,452	0,522	0,516	0,531	0,481

Apatites

Sample	56	56	56	56	56
Zone	2	2	3	3	8
P2O5	43,56	44,05	43,18	43,60	43,22
SiO2	0,34	0,17	0,43	0,55	0,22
Ce2O3	0,01	0,00	0,08	0,01	0,00
MgO	0,01	0,00	0,00	0,00	0,00
CaO	51,68	52,93	52,18	52,38	52,76
MnO	0,02	0,03	0,03	0,04	0,04
FeO	0,69	0,58	0,51	0,70	0,65
Na2O	0,03	0,02	0,02	0,01	0,05
H2O	0,00	0,00	0,00	0,00	0,00
F	4,86	5,11	5,68	5,05	5,78
Cl	0,00	0,00	0,00	0,00	0,06
Total	101,21	102,88	102,11	102,34	102,77
O=F	2,04	2,15	2,39	2,13	2,43
O=Cl	0,00	0,00	0,00	0,00	0,01
O=F,Cl	2,05	2,15	2,39	2,13	2,45
Total	99,16	100,73	99,72	100,21	100,33
P	3,062	3,051	3,014	3,034	3,006
Si	0,028	0,014	0,035	0,045	0,018
Ce	0,000	0,000	0,003	0,000	0,000
Mg	0,001	0,000	0,000	0,000	0,000
Ca	4,598	4,640	4,611	4,614	4,644
Mn	0,002	0,002	0,002	0,003	0,003
Fe	0,048	0,040	0,035	0,048	0,044
Na	0,005	0,003	0,003	0,002	0,008
OH	0	0	0	0	0
F	1,275	1,321	1,480	1,314	1,500
Cl	0,000	0,000	0,000	0,000	0,008

Carbonates 1

Sample	97	97	97	97	97	173	173	173	173	203	203	203	203
Zone	7	5	4	3	2	1	2	3	5	1	2	3	4
Mg(CO3)	42,49	39,58	42,40	39,71	42,39	41,55	38,44	39,16	41,00	1,38	1,37	1,43	1,93
Ca(CO3)	55,52	51,10	57,19	54,56	57,72	57,44	53,16	53,76	54,78	103,15	101,62	104,92	106,25
Mn(CO3)	0,09	0,00	0,16	0,10	0,00	0,18	0,13	0,27	0,07	0,04	0,00	0,09	0,20
Fe(CO3)	1,07	1,31	0,66	0,43	0,17	1,95	6,57	5,25	3,17	0,27	0,39	0,32	0,53
Sr(CO3)	0,07	0,07	0,00	0,02	0,03	0,03	0,11	0,03	0,05	0,45	0,23	0,27	0,23
Ba(CO3)	0,00	0,01	0,00	0,01	0,00	0,03	0,01	0,03	0,06	0,00	0,00	0,00	0,02
Total	99,23	92,07	100,41	94,83	100,31	101,17	98,43	98,50	99,12	105,29	103,62	107,02	109,16

Sample	203	203	203	103	103	103	103	103	103	31	31	31	31
Zone	4	5	6	1	1	2	3	4	5	1	2	3	4
Mg(CO3)	41,62	1,43	1,29	42,39	42,76	43,66	42,29	41,81	41,87	1,72	1,86	1,55	1,09
Ca(CO3)	54,07	98,03	104,42	54,98	54,31	55,24	55,12	55,20	53,97	102,51	104,16	105,70	105,50
Mn(CO3)	0,04	0,10	0,00	0,52	0,46	0,33	0,28	0,51	0,44	0,07	0,20	0,04	0,00
Fe(CO3)	3,76	0,47	0,23	2,95	2,50	1,83	2,28	3,21	2,55	0,38	0,54	0,66	0,52
Sr(CO3)	0,05	0,27	0,23	0,03	0,07	0,01	0,02	0,00	0,00	0,31	0,36	0,38	0,78
Ba(CO3)	0,03	0,00	0,00	0,00	0,00	0,06	0,06	0,03	0,00	0,00	0,00	0,00	0,00
Total	99,58	100,30	106,17	100,86	100,11	101,13	100,05	100,76	98,83	104,99	107,12	108,34	107,88

Sample	31	31	56	56	56	111	111	111	90	90	90	90	90
Zone	5	6	3	5	10	2	2	3	2	3	5	8	10
Mg(CO3)	1,81	1,79	0,33	0,35	0,01	1,05	0,88	1,52	1,55	1,43	0,30	0,16	1,00
Ca(CO3)	107,28	104,83	102,70	104,42	99,77	100,75	96,67	97,68	97,81	97,52	96,92	99,89	95,92
Mn(CO3)	0,16	0,03	1,22	1,31	0,51	1,34	0,85	0,72	0,92	0,72	1,82	1,69	1,10
Fe(CO3)	0,69	0,66	0,39	0,39	0,21	0,89	0,59	1,38	1,66	0,40	1,15	1,02	1,02
Sr(CO3)	0,33	0,47	0,53	0,25	0,13	0,23	0,11	0,24	0,85	0,39	0,12	0,05	1,10
Ba(CO3)	0,00	0,00	0,00	0,01	0,04	0,01	0,04	0,01	0,07	0,00	0,00	0,03	0,00
Total	110,27	107,79	105,17	106,72	100,67	104,26	99,15	101,55	102,85	100,46	100,31	102,84	100,14

Carbonates 2

Sample	11	11	11	11	11	11	11	11	63	65	199	199	199
Zone	9	8	7	6	5	4	3	2	2	4	3	4	6
Mg(CO3)	40,32	37,24	44,14	35,71	42,83	37,53	46,46	36,89	0,25	1,13	43,61	45,68	44,99
Ca(CO3)	58,03	49,96	54,88	44,45	56,45	52,21	0,31	53,54	101,99	100,85	50,21	49,56	49,98
Mn(CO3)	0,00	0,05	0,02	0,13	0,00	0,15	0,02	0,38	0,22	0,56	0,23	0,18	0,24
Fe(CO3)	0,71	2,18	0,31	1,02	0,35	9,74	31,75	7,79	0,00	0,34	5,62	4,23	3,35
Sr(CO3)	0,00	0,01	0,06	0,04	0,06	0,04	0,03	0,14	0,04	0,12	0,07	0,08	0,08
Ba(CO3)	0,00	0,04	0,00	0,04	0,00	0,09	0,10	0,03	0,14	0,01	0,08	0,06	0,04
Total	99,06	89,49	99,40	81,39	99,69	99,76	78,67	98,76	102,63	103,01	99,82	99,79	98,68

Sample	199	199	199	199	20	20	20	20	20	113	113	113	113
Zone	7	8	9	10	1	2	3	4	5	1	1	2	3
Mg(CO3)	46,13	43,98	43,68	42,73	43,01	45,32	46,00	46,25	42,39	44,65	43,25	44,65	44,65
Ca(CO3)	50,07	51,57	50,01	52,11	57,02	56,23	52,12	53,23	56,66	54,32	56,23	54,44	53,24
Mn(CO3)	0,14	0,31	0,29	0,25	0,00	0,07	0,12	0,09	0,02	0,05	0,01	0,00	0,20
Fe(CO3)	3,21	4,00	4,58	3,98	1,01	0,23	1,03	0,95	0,65	0,89	0,53	0,54	0,32
Sr(CO3)	0,04	0,03	0,06	0,05	0,03	0,02	0,01	0,03	0,05	0,04	0,02	0,06	0,05
Ba(CO3)	0,00	0,01	0,05	0,09	0,00	0,01	0,00	0,01	0,00	0,00	0,00	0,01	0,01
Total	99,59	99,90	98,67	99,21	101,07	101,88	99,28	100,56	99,77	99,95	100,04	99,70	98,47

Sample	113	176	176	176	176	176	176	176	8	8	8	8	186
Zone	4	4	4	3	2	2	1	1	1	3	4	6	1
Mg(CO3)	43,75	43,66	45,71	45,85	45,20	44,18	44,98	44,12	44,35	43,89	44,53	43,25	44,00
Ca(CO3)	55,04	50,98	50,23	49,87	49,96	51,03	51,22	51,66	53,98	54,86	53,83	54,87	49,86
Mn(CO3)	0,02	0,18	0,21	0,15	0,13	0,09	0,28	0,21	0,07	0,02	0,05	0,16	0,16
Fe(CO3)	0,15	4,98	3,65	3,87	4,52	4,26	3,01	3,58	1,32	1,12	1,52	1,24	4,77
Sr(CO3)	0,00	0,06	0,06	0,09	0,06	0,03	0,02	0,03	0,05	0,02	0,05	0,03	0,01
Ba(CO3)	0,01	0,07	0,03	0,02	0,04	0,02	0,00	0,02	0,01	0,01	0,01	0,01	0,05
Total	98,97	99,93	99,89	99,85	99,91	99,61	99,51	99,62	99,78	99,92	99,99	99,56	98,85

Carbonates 3

Sample	186	186	186	186	186	186
Zone	2	3	5	6	7	8
Mg(CO3)	44,85	45,01	45,68	45,39	45,22	44,38
Ca(CO3)	49,98	49,53	49,20	50,02	50,12	50,98
Mn(CO3)	0,28	0,24	0,12	0,21	0,24	0,12
Fe(CO3)	3,28	4,25	3,76	3,77	3,59	4,01
Sr(CO3)	0,02	0,03	0,05	0,05	0,03	0,04
Ba(CO3)	0,05	0,00	0,00	0,01	0,02	0,01
Total	98,46	99,06	98,81	99,45	99,22	99,54

Chlorites

Sample	56	56	56	171	171	49	133	133
Zone	1	1	4	2	4	5	12	11
SiO2	27,24	26,83	26,87	26,42	30,41	26,233	27,95	27,08
TiO2	0,01	0,03	0,00	0,20	0,19	0,03	0,01	0,02
Al2O3	18,59	18,89	18,56	19,57	17,98	21,74	18,85	18,96
Cr2O3	0,07	0,02	0,00	0,06	0,01	0,00	0,95	0,08
MgO	18,51	18,31	18,41	14,72	12,69	18,71	16,31	16,87
CaO	0,04	0,08	0,02	0,03	0,02	0,13	0,01	0,04
MnO	0,45	0,44	0,40	0,15	0,11	0,04	0,29	0,32
FeO	22,74	22,52	22,90	28,20	28,71	22,04	25,58	25,23
Fe2O3	0,00	0,00	0,00	0,00	0,00	0,00	0,00	0,00
Na2O	0,00	0,02	0,01	0,03	0,34	0,01	0,01	0,01
K2O	0,01	0,01	0,00	0,02	0,01	0,00	0,00	0,00
H2O	11,52	11,46	11,44	11,44	11,67	11,78	11,68	11,51
Total	99,18	98,60	98,61	100,84	102,12	100,71	101,64	100,12
Fe/Mg	1,23	1,23	1,24	1,92	2,26	1,18	1,57	1,50
Si	5,671	5,618	5,634	5,53973	6,24851	5,34385	5,740	5,642
Ti	0,002	0,005	0,000	0,032	0,029	0,004	0,001	0,003
Al	4,562	4,661	4,588	4,835	4,355	5,219	4,564	4,657
Cr	0,012	0,003	0,000	0,010	0,001	0,000	0,155	0,014
Mg	5,744	5,714	5,755	4,600	3,886	5,682	4,993	5,239
Ca	0,008	0,019	0,004	0,007	0,005	0,029	0,002	0,008
Mn	0,079	0,079	0,071	0,027	0,019	0,008	0,051	0,056
Fe2+	3,960	3,942	4,017	4,945	4,933	3,755	4,393	4,397
Fe3+	0,000	0,000	0,000	0,000	0,000	0,000	0,000	0,000
Na	0,001	0,006	0,004	0,013	0,135	0,003	0,005	0,004
K	0,002	0,003	0,001	0,005	0,002	0,000	0,001	0,001
OH	16,000	16,000	16,000	16,000	16,000	16,000	16,000	16,000

Epidotes 1

Sample	56	56	56	56	56	56	56	56	56	120	120	120	120
Zone	1	1	5	5	7	7	7	10	10	3	8	9	9
SiO2	36,66	37,35	35,52	37,22	35,33	36,34	36,94	36,09	36,35	39,62	40,50	40,19	40,90
TiO2	0,06	0,15	0,00	0,01	0,06	0,02	0,04	0,01	0,02	0,11	0,03	0,04	0,02
Al2O3	20,37	18,37	16,39	21,06	19,50	18,73	19,84	17,70	20,62	27,05	27,31	26,75	28,69
MgO	0,04	0,00	0,00	0,00	0,02	0,00	0,00	0,00	0,00	0,00	0,03	0,00	0,05
CaO	17,62	22,20	17,62	21,87	16,71	19,35	21,99	20,44	21,61	23,67	23,16	23,50	23,30
MnO	0,21	0,10	0,99	0,23	0,32	0,13	0,11	0,31	0,17	0,11	0,05	0,05	0,00
FeO	0,00	0,00	0,00	0,00	0,00	0,00	0,00	0,00	0,00	0,00	0,00	0,00	0,00
Fe2O3	15,39	19,59	19,88	15,92	16,71	18,90	17,31	19,14	16,38	8,66	8,53	9,29	6,02
Na2O	0,00	0,01	0,00	0,01	0,00	0,00	0,00	0,01	0,03	0,02	0,18	0,24	0,29
K2O	0,00	0,01	0,00	0,00	0,00	0,00	0,00	0,00	0,00	0,03	0,04	0,03	0,00
H2O	1,68	1,75	1,62	1,77	1,63	1,69	1,75	1,68	1,74	1,91	1,93	1,92	1,95
Total	92,02	99,53	92,01	98,07	90,29	95,16	97,98	95,38	96,92	101,19	101,74	102,02	101,23
Si	3,025	2,932	3,009	2,923	2,990	2,957	2,922	2,951	2,898	2,933	2,969	2,954	2,986
Ti	0,004	0,009	0,000	0,000	0,004	0,001	0,002	0,000	0,001	0,006	0,001	0,002	0,001
Al	1,981	1,700	1,637	1,950	1,945	1,796	1,850	1,706	1,937	2,360	2,360	2,317	2,470
Mg	0,004	0,000	0,000	0,000	0,003	0,000	0,000	0,000	0,000	0,000	0,003	0,000	0,006
Ca	1,558	1,867	1,600	1,840	1,515	1,687	1,863	1,791	1,846	1,877	1,820	1,851	1,823
Mn	0,014	0,007	0,071	0,015	0,023	0,009	0,007	0,021	0,011	0,007	0,003	0,003	0,000
Fe2+	0,000	0,000	0,000	0,000	0,000	0,000	0,000	0,000	0,000	0,000	0,000	0,000	0,000
Fe3+	0,955	1,157	1,267	0,941	1,064	1,157	1,030	1,178	0,983	0,483	0,471	0,514	0,331
Na	0,000	0,002	0,000	0,001	0,000	0,000	0,000	0,002	0,004	0,003	0,026	0,035	0,041
K	0,000	0,001	0,000	0,000	0,000	0,000	0,000	0,000	0,000	0,003	0,003	0,002	0,000
OH	0,925	0,917	0,913	0,926	0,920	0,917	0,922	0,916	0,924	0,943	0,944	0,942	0,949

Epidotes 2

Sample	133	133	53	53	53	53	53	53
Zone	10	6	3	4	6	6	7	7
SiO2	39,18	38,54	38,79	36,81	38,15	37,78	38,85	38,70
TiO2	0,00	0,00	0,21	0,55	0,12	0,06	0,18	0,09
Al2O3	22,42	21,36	21,47	20,58	21,55	21,16	19,79	21,43
MgO	0,00	0,00	0,64	0,93	0,00	0,00	0,13	0,01
CaO	22,96	22,12	20,41	18,14	22,17	20,08	21,09	21,89
MnO	0,06	0,08	0,33	0,47	0,17	0,33	0,33	0,14
FeO	0,00	0,00	0,00	0,00	0,00	0,00	0,00	0,00
Fe2O3	14,27	16,29	15,63	15,81	15,12	15,66	16,87	16,01
Na2O	0,00	0,01	0,45	0,04	0,22	0,23	0,28	0,28
K2O	0,00	0,00	0,04	0,86	0,02	0,02	0,02	0,07
H2O	1,84	1,81	1,81	1,73	1,80	1,76	1,79	1,82
Total	100,73	100,20	99,78	95,91	99,31	97,06	99,32	100,43
Si	2,970	2,955	2,973	2,945	2,948	2,977	3,011	2,960
Ti	0,000	0,000	0,012	0,033	0,007	0,003	0,010	0,005
Al	2,003	1,930	1,939	1,941	1,962	1,965	1,807	1,931
Mg	0,000	0,000	0,073	0,110	0,000	0,000	0,014	0,002
Ca	1,865	1,817	1,676	1,555	1,836	1,695	1,751	1,794
Mn	0,004	0,005	0,021	0,032	0,011	0,022	0,021	0,009
Fe2+	0,000	0,000	0,000	0,000	0,000	0,000	0,000	0,000
Fe3+	0,814	0,940	0,902	0,952	0,879	0,929	0,984	0,921
Na	0,000	0,001	0,067	0,006	0,032	0,035	0,042	0,041
K	0,000	0,000	0,004	0,088	0,002	0,002	0,001	0,007
OH	0,930	0,926	0,927	0,925	0,928	0,926	0,924	0,926

Feldspaths 1

Sample	103	56	56	56	56	56	56	56	56	56	120	120	171
Zone	5	1	1	3	3	5	6	6	7	10	5	9	4
SiO2	46,13	67,62	66,82	67,35	67,74	67,93	68,11	67,68	66,79	67,31	68,22	68,60	68,27
TiO2	0,38	0,04	0,02	0,00	0,00	0,02	0,00	0,02	0,00	0,00	0,00	0,06	0,07
Al2O3	36,00	20,45	20,18	20,00	20,09	20,13	19,70	20,51	20,51	20,73	20,19	20,46	20,14
MgO	0,82	0,00	0,02	0,02	0,02	0,00	0,00	0,00	0,05	0,00	0,00	0,01	0,01
CaO	0,12	0,14	0,02	0,17	0,01	0,05	0,07	0,07	0,16	0,10	0,16	0,27	0,01
FeO	0,00	0,00	0,00	0,00	0,00	0,00	0,00	0,00	0,00	0,00	0,00	0,00	0,00
Fe2O3	3,04	0,12	0,09	0,00	0,01	0,01	0,02	0,04	0,15	0,10	0,28	0,04	0,47
BaO	0,06	0,06	0,00	0,07	0,00	0,00	0,03	0,04	0,02	0,01	0,00	0,03	0,03
Na2O	0,26	11,39	11,58	11,36	11,59	11,68	11,62	11,60	11,27	11,26	11,75	11,49	11,72
K2O	9,74	0,09	0,06	0,08	0,07	0,06	0,07	0,06	0,12	0,12	0,08	0,08	0,05
Total	96,56	99,91	98,77	99,05	99,53	99,88	99,62	100,02	99,07	99,63	100,68	101,04	100,78
Si	2,200	2,958	2,958	2,971	2,972	2,971	2,986	2,958	2,948	2,951	2,965	2,966	2,965
Ti	0,014	0,001	0,000	0,000	0,000	0,001	0,000	0,000	0,000	0,000	0,000	0,002	0,002
Al	2,023	1,054	1,053	1,040	1,039	1,038	1,018	1,056	1,067	1,071	1,034	1,043	1,031
Mg	0,059	0,000	0,001	0,001	0,001	0,000	0,000	0,000	0,003	0,000	0,000	0,001	0,001
Ca	0,006	0,007	0,001	0,008	0,001	0,002	0,003	0,003	0,007	0,005	0,007	0,013	0,000
Fe2+	0,000	0,000	0,000	0,000	0,000	0,000	0,000	0,000	0,000	0,000	0,000	0,000	0,000
Fe3+	0,109	0,004	0,003	0,000	0,000	0,000	0,001	0,001	0,005	0,003	0,009	0,001	0,015
Ba	0,001	0,001	0,000	0,001	0,000	0,000	0,000	0,001	0,000	0,000	0,000	0,000	0,001
Na	0,024	0,966	0,994	0,972	0,986	0,991	0,988	0,983	0,964	0,957	0,990	0,963	0,987
K	0,593	0,005	0,003	0,004	0,004	0,003	0,004	0,003	0,007	0,007	0,005	0,004	0,003

Feldspaths 2

Sample	65	133	133	53	53	53	53	53	53	53	53	53	53
Zone	1	10	7	1	2	2	3	3	4	4	6	7	7
SiO2	69,48	68,15	68,70	69,07	68,72	69,36	66,77	63,99	68,40	64,55	64,53	68,79	68,56
TiO2	0,09	0,01	0,00	0,00	0,00	0,03	0,03	0,03	0,03	0,01	0,08	0,00	0,01
Al2O3	20,00	20,41	20,20	19,93	20,16	20,07	19,96	19,27	20,34	19,06	18,84	20,27	20,27
MgO	0,16	0,06	0,01	0,00	0,01	0,00	0,02	0,00	0,04	0,01	0,64	0,01	0,04
CaO	0,01	0,52	0,08	0,10	0,03	0,04	0,05	0,02	0,10	0,02	0,00	0,12	0,13
FeO	0,00	0,00	0,00	0,00	0,00	0,00	0,00	0,00	0,00	0,00	0,00	0,00	0,00
Fe2O3	0,51	0,10	0,08	0,14	0,16	0,21	0,16	0,07	0,24	0,25	0,08	0,07	0,10
BaO	0,02	0,00	0,00	0,05	0,03	0,00	0,28	1,31	0,00	0,56	0,67	0,03	0,02
Na2O	11,86	11,44	11,91	11,72	11,74	11,79	7,50	0,17	11,10	1,13	0,23	11,73	11,82
K2O	0,06	0,05	0,04	0,07	0,45	0,10	5,59	15,83	1,06	14,60	15,59	0,09	0,11
Total	102,19	100,75	101,03	101,08	101,29	101,59	100,35	100,69	101,29	100,18	100,67	101,11	101,06
Si	2,975	2,959	2,973	2,986	2,972	2,983	2,967	2,960	2,963	2,972	2,967	2,973	2,968
Ti	0,003	0,000	0,000	0,000	0,000	0,001	0,001	0,001	0,001	0,000	0,003	0,000	0,000
Al	1,009	1,044	1,030	1,015	1,028	1,018	1,045	1,050	1,038	1,034	1,021	1,033	1,034
Mg	0,010	0,004	0,001	0,000	0,001	0,000	0,001	0,000	0,002	0,001	0,044	0,001	0,003
Ca	0,001	0,024	0,004	0,005	0,001	0,002	0,003	0,001	0,004	0,001	0,000	0,006	0,006
Fe2+	0,000	0,000	0,000	0,000	0,000	0,000	0,000	0,000	0,000	0,000	0,000	0,000	0,000
Fe3+	0,016	0,003	0,003	0,004	0,005	0,007	0,005	0,003	0,008	0,009	0,003	0,002	0,003
Ba	0,000	0,000	0,000	0,001	0,000	0,000	0,005	0,024	0,000	0,010	0,012	0,000	0,000
Na	0,985	0,963	0,999	0,982	0,984	0,983	0,646	0,015	0,932	0,101	0,021	0,983	0,992
K	0,003	0,003	0,002	0,004	0,025	0,005	0,317	0,934	0,058	0,858	0,915	0,005	0,006

Feldspaths 3

Sample	53	53
Zone	7	6
SiO2	68,82	69,47
TiO2	0,00	0,00
Al2O3	20,29	19,83
MgO	0,00	0,01
CaO	0,18	0,07
FeO	0,00	0,00
Fe2O3	0,15	0,20
BaO	0,00	
Na2O	11,72	11,65
K2O	0,10	0,46
Total	101,26	101,68
Si	2,971	2,990
Ti	0,000	0,000
Al	1,032	1,006
Mg	0,000	0,001
Ca	0,008	0,003
Fe2+	0,000	0,000
Fe3+	0,005	0,006
Ba	0,000	0,000
Na	0,981	0,972
K	0,006	0,025

Hematite 1

Sample	56	56	45	45	45	45	45	45	90	90	90	90	90
Zone	3	4	3	4	5	6	7	8	6	6	6	7	7
SiO2	0,98	0,59	0,09	0,19	0,34	0,10	0,14	0,34	0,11	0,35	0,04	0,49	0,22
TiO2	0,46	0,51	0,00	0,00	0,00	0,03	0,00	0,02	0,00	0,02	0,01	0,02	0,39
Al2O3	0,23	0,13	0,02	0,09	0,12	0,04	0,00	0,09	0,02	0,09	0,05	0,06	0,26
V2O3	0,07	0,08	0,06	0,05	0,01	0,00	0,00	0,00	0,00	0,03	0,02	0,03	0,07
Cr2O3	0,00	0,00	0,00	0,00	0,02	0,02	0,00	0,00	0,00	0,00	0,00	0,02	0,03
MgO	0,06	0,02	0,03	0,02	0,03	0,01	0,00	0,03	0,00	0,01	0,03	0,02	0,01
CaO	0,37	0,41	0,00	0,01	0,01	0,01	0,00	0,02	0,10	0,03	0,32	0,37	0,82
MnO	0,02	0,03	0,03	0,01	0,01	0,02	0,02	0,03	0,04	0,04	0,02	0,05	0,05
Fe2O3	100,89	100,04	99,31	98,19	97,61	98,82	98,46	97,03	99,10	98,26	100,02	98,06	96,77
NiO	0,00	0,01	0,00	0,00	0,00	0,02	0,00	0,05	0,01	0,00	0,06	0,04	0,00
Na2O	0,05	0,03	0,00	0,00	0,00	0,02	0,01	0,03	0,00	0,03	0,00	0,02	0,01
K2O	0,01	0,00	0,00	0,00	0,00	0,00	0,00	0,00	0,00	0,00	0,00	0,00	0,00
Total	103,14	101,84	99,53	98,55	98,16	99,07	98,65	97,63	99,39	98,85	100,56	99,18	98,62
Si	0,050	0,031	0,005	0,010	0,018	0,006	0,007	0,018	0,006	0,019	0,002	0,026	0,012
Ti	0,018	0,020	0,000	0,000	0,000	0,001	0,000	0,001	0,000	0,001	0,000	0,001	0,016
Al	0,010	0,006	0,001	0,004	0,006	0,002	0,000	0,004	0,001	0,004	0,002	0,003	0,012
V	0,002	0,003	0,002	0,001	0,000	0,000	0,000	0,000	0,000	0,001	0,001	0,001	0,002
Cr	0,000	0,000	0,000	0,000	0,001	0,001	0,000	0,000	0,000	0,000	0,000	0,001	0,001
Mg	0,002	0,001	0,001	0,001	0,001	0,000	0,000	0,001	0,000	0,000	0,001	0,001	0,001
Ca	0,010	0,011	0,000	0,000	0,000	0,000	0,000	0,001	0,003	0,001	0,009	0,010	0,023
Mn	0,001	0,001	0,001	0,000	0,000	0,000	0,000	0,001	0,001	0,001	0,000	0,001	0,001
Fe3+	2,905	2,927	2,991	2,983	2,973	2,989	2,991	2,972	2,989	2,973	2,983	2,955	2,932
Ni	0,000	0,000	0,000	0,000	0,000	0,000	0,000	0,001	0,000	0,000	0,001	0,001	0,000
Na	0,001	0,001	0,000	0,000	0,000	0,000	0,000	0,001	0,000	0,001	0,000	0,001	0,000
K	0,000	0,000	0,000	0,000	0,000	0,000	0,000	0,000	0,000	0,000	0,000	0,000	0,000

Hematite 2

Sample	90	90	90	90	48	48	65	65	65	53	53	53	53
Zone	7	8	9	10	1	2	7	3	1	1	3	6	7
SiO2	0,16	0,30	0,10	0,38	0,31	0,14	0,20	0,06	0,01	0,27	0,20	2,72	0,97
TiO2	0,47	0,00	0,01	0,01	0,02	0,04	0,24	1,84	3,48	4,74	0,07	0,38	4,11
Al2O3	0,23	0,04	0,02	0,06	0,10	0,05	0,03	0,03	0,04	0,05	0,04	1,45	0,12
V2O3	0,04	0,00	0,00	0,03	0,05	0,00	0,13	0,25	0,10	0,00	0,01	0,00	0,00
Cr2O3	0,00	0,00	0,00	0,00	0,01	0,00	0,09	0,07	0,04	0,00	0,02	0,00	0,00
MgO	0,00	0,02	0,00	0,03	0,04	0,00	0,02	0,01	0,00	0,00	0,03	0,05	0,07
CaO	0,33	0,56	0,02	0,16	0,02	0,00	0,01	0,04	0,02	0,11	0,05	1,22	0,17
MnO	0,04	0,03	0,04	0,01	0,00	0,02	0,01	0,02	0,02	2,97	0,11	0,08	1,53
Fe2O3	98,18	99,49	98,93	98,91	98,42	98,27	99,41	97,32	96,40	90,13	96,84	93,48	90,95
NiO	0,03	0,00	0,02	0,00	0,01	0,00	0,00	0,00	0,04	0,00	0,05	0,00	0,00
Na2O	0,00	0,00	0,00	0,02	0,00	0,00	0,01	0,00	0,03	0,03	0,00	0,02	0,05
K2O	0,00	0,01	0,00	0,00	0,00	0,00	0,01	0,01	0,00	0,01	0,04	0,01	0,02
Total	99,47	100,45	99,13	99,62	99,00	98,53	100,16	99,64	100,17	98,31	97,45	99,41	97,97
Si	0,009	0,016	0,005	0,020	0,017	0,007	0,010	0,003	0,001	0,014	0,011	0,141	0,052
Ti	0,019	0,000	0,000	0,000	0,001	0,002	0,010	0,073	0,137	0,191	0,003	0,015	0,165
Al	0,011	0,002	0,001	0,003	0,005	0,002	0,001	0,002	0,002	0,002	0,002	0,067	0,005
V	0,001	0,000	0,000	0,001	0,002	0,000	0,004	0,008	0,003	0,000	0,000	0,000	0,000
Cr	0,000	0,000	0,000	0,000	0,000	0,000	0,003	0,002	0,001	0,000	0,001	0,000	0,000
Mg	0,000	0,001	0,000	0,001	0,001	0,000	0,001	0,000	0,000	0,000	0,001	0,002	0,003
Ca	0,009	0,016	0,001	0,005	0,001	0,000	0,000	0,001	0,001	0,003	0,002	0,034	0,005
Mn	0,001	0,001	0,001	0,000	0,000	0,001	0,000	0,000	0,000	0,067	0,002	0,002	0,034
Fe3+	2,950	2,965	2,992	2,969	2,973	2,988	2,970	2,910	2,853	2,721	2,977	2,739	2,735
Ni	0,001	0,000	0,000	0,000	0,000	0,000	0,000	0,000	0,001	0,000	0,001	0,000	0,000
Na	0,000	0,000	0,000	0,000	0,000	0,000	0,000	0,000	0,001	0,001	0,000	0,000	0,001
K	0,000	0,000	0,000	0,000	0,000	0,000	0,000	0,000	0,000	0,000	0,001	0,000	0,000

Ilmenite

Sample	120	120	171	171	171
Zone	4	4	2	4	5
SiO2	0,09	0,14	1,49	7,91	0,46
TiO2	50,85	49,41	50,42	43,74	53,92
Al2O3	0,37	0,03	0,10	3,08	0,18
V2O3	0,00	0,00	0,00	0,00	0,00
Cr2O3	0,02	0,01	0,03	0,00	0,00
MgO	0,08	0,09	0,06	1,06	0,10
CaO	0,85	0,33	0,08	0,47	0,04
MnO	4,20	2,99	1,67	1,10	1,46
FeO	33,99	34,70	37,39	31,81	33,81
Fe2O3	6,66	6,80	7,32	6,23	6,62
NiO	0,00	0,00	0,00	0,00	0,02
Na2O	0,02	0,02	0,01	2,11	0,00
K2O	0,00	0,00	0,00	0,01	0,00
H2O					
Total	97,10	94,51	98,55	97,52	96,61
Si	0,004	0,007	0,074	0,377	0,023
Ti	1,947	1,949	1,894	1,570	2,035
Al	0,022	0,002	0,006	0,173	0,011
V	0,000	0,000	0,000	0,000	0,000
Cr	0,001	0,000	0,001	0,000	0,000
Mg	0,006	0,007	0,004	0,075	0,007
Ca	0,046	0,019	0,004	0,024	0,002
Mn	0,181	0,133	0,070	0,044	0,062
Fe2+	1,447	1,522	1,561	1,269	1,419
Fe3+	0,255	0,268	0,275	0,224	0,250
Ni	0,000	0,000	0,000	0,000	0,001
Na	0,002	0,002	0,001	0,195	0,000
K	0,000	0,000	0,000	0,001	0,000
OH	0,000	0,000	0,000	0,000	0,000

Magnetite 1

Sample	56	56	56	45	45	45	45	111	111	111	90	90	90
Zone	2	8	9	3	5	6	7	3	4	4	4	4	5
SiO2	1,93	2,23	3,70	0,20	0,16	0,10	0,29	0,03	0,04	0,09	0,53	0,15	0,18
TiO2	0,57	0,52	0,35	0,00	0,01	0,00	0,04	0,04	0,07	0,04	0,00	0,00	0,03
Al2O3	0,76	0,87	1,52	0,03	0,06	0,05	0,05	0,07	0,01	0,02	0,18	0,06	0,02
V2O3	0,11	0,12	0,16	0,00	0,04	0,00	0,06	0,05	0,11	0,12	0,00	0,00	0,00
Cr2O3	0,06	0,05	0,03	0,00	0,04	0,00	0,00	0,01	0,02	0,02	0,00	0,00	0,02
MgO	0,09	0,29	1,25	0,01	0,02	0,01	0,01	0,00	0,02	0,00	0,04	0,02	0,00
CaO	0,51	0,48	0,35	0,00	0,00	0,00	0,00	0,00	0,00	0,01	2,27	0,00	0,48
MnO	0,03	0,05	0,05	0,03	0,02	0,01	0,04	0,01	0,02	0,03	0,39	0,00	0,06
FeO	29,22	28,92	28,34	30,79	30,51	30,62	30,44	30,32	30,71	30,91	27,92	30,91	30,95
Fe2O3	64,95	64,27	62,99	68,42	67,79	68,04	67,65	67,39	68,25	68,68	62,05	68,68	68,78
NiO	0,05	0,01	0,00	0,00	0,00	0,00	0,00	0,03	0,00	0,00	0,00	0,03	0,00
Na2O	0,15	0,16	0,19	0,01	0,02	0,00	0,01	0,00	0,00	0,00	0,03	0,01	0,00
K2O	0,03	0,03	0,02	0,00	0,00	0,00	0,00	0,00	0,00	0,00	0,01	0,00	0,00
Total	98,45	97,98	98,95	99,50	98,67	98,83	98,58	97,95	99,24	99,92	93,41	99,86	100,52
Si	0,074	0,085	0,137	0,008	0,006	0,004	0,011	0,001	0,001	0,003	0,022	0,006	0,007
Ti	0,016	0,015	0,010	0,000	0,000	0,000	0,001	0,001	0,002	0,001	0,000	0,000	0,001
Al	0,034	0,039	0,066	0,002	0,003	0,002	0,002	0,003	0,000	0,001	0,009	0,003	0,001
V	0,003	0,004	0,005	0,000	0,001	0,000	0,002	0,002	0,003	0,004	0,000	0,000	0,000
Cr	0,002	0,001	0,001	0,000	0,001	0,000	0,000	0,000	0,001	0,001	0,000	0,000	0,001
Mg	0,005	0,016	0,069	0,000	0,001	0,001	0,000	0,000	0,001	0,000	0,002	0,001	0,000
Ca	0,021	0,020	0,014	0,000	0,000	0,000	0,000	0,000	0,000	0,000	0,100	0,000	0,020
Mn	0,001	0,001	0,002	0,001	0,000	0,000	0,001	0,000	0,001	0,001	0,014	0,000	0,002
Fe2+	0,932	0,923	0,877	0,995	0,994	0,997	0,992	0,997	0,996	0,996	0,957	0,996	0,990
Fe3+	1,863	1,845	1,754	1,990	1,988	1,994	1,983	1,993	1,993	1,991	1,913	1,991	1,980
Ni	0,002	0,000	0,000	0,000	0,000	0,000	0,000	0,001	0,000	0,000	0,000	0,001	0,000
Na	0,011	0,012	0,014	0,001	0,001	0,000	0,001	0,000	0,000	0,000	0,002	0,001	0,000
K	0,001	0,001	0,001	0,000	0,000	0,000	0,000	0,000	0,000	0,000	0,000	0,000	0,000

Magnetite 2

Sample	90	90	90	90	48	48	48	48	48	65	65	65	65
Zone	6	7	9	10	1	2	3	3	4	7	7	2	2
SiO2	7,77	0,15	0,14	0,10	0,11	0,10	0,10	0,39	0,18	0,05	4,06	0,06	0,25
TiO2	0,03	0,00	0,01	0,00	0,02	0,01	0,03	4,16	0,02	0,03	0,03	0,03	0,06
Al2O3	0,68	0,02	0,06	0,04	0,02	0,05	0,05	0,48	0,07	0,03	0,20	0,02	0,04
V2O3	0,03	0,09	0,08	0,05	0,07	0,00	0,04	0,06	0,05	0,15	0,00	0,16	0,15
Cr2O3	0,01	0,00	0,05	0,01	0,04	0,04	0,00	0,05	0,01	0,08	0,06	0,03	0,00
MgO	0,11	0,02	0,00	0,01	0,01	0,00	0,02	1,17	0,01	0,01	0,51	0,02	0,02
CaO	0,73	0,29	0,01	0,01	0,03	0,01	0,00	0,13	0,00	0,00	0,08	0,00	0,01
MnO	0,79	0,01	0,01	0,03	0,01	0,00	0,04	0,14	0,05	0,01	0,16	0,02	0,00
FeO	25,83	31,04	30,73	30,76	30,73	30,75	30,87	27,73	30,69	30,93	24,47	30,65	30,00
Fe2O3	57,39	68,97	68,29	68,35	68,30	68,35	68,61	61,63	68,20	68,74	54,39	68,12	66,66
NiO	0,00	0,00	0,00	0,02	0,00	0,00	0,00	0,00	0,00	0,00	0,17	0,00	0,06
Na2O	0,07	0,00	0,03	0,01	0,03	0,00	0,01	0,02	0,00	0,01	0,00	0,03	0,04
K2O	0,07	0,00	0,00	0,00	0,00	0,01	0,00	0,01	0,00	0,00	0,01	0,01	0,00
Total	93,50	100,60	99,41	99,38	99,35	99,32	99,77	95,97	99,27	100,05	84,13	99,15	97,28
Si	0,296	0,006	0,006	0,004	0,004	0,004	0,004	0,015	0,007	0,002	0,177	0,002	0,010
Ti	0,001	0,000	0,000	0,000	0,000	0,000	0,001	0,122	0,001	0,001	0,001	0,001	0,002
Al	0,031	0,001	0,003	0,002	0,001	0,002	0,002	0,022	0,003	0,001	0,010	0,001	0,002
V	0,001	0,003	0,003	0,001	0,002	0,000	0,001	0,002	0,002	0,005	0,000	0,005	0,005
Cr	0,000	0,000	0,001	0,000	0,001	0,001	0,000	0,002	0,000	0,002	0,002	0,001	0,000
Mg	0,006	0,001	0,000	0,001	0,000	0,000	0,001	0,068	0,000	0,001	0,033	0,001	0,001
Ca	0,030	0,012	0,000	0,001	0,001	0,000	0,000	0,005	0,000	0,000	0,004	0,000	0,001
Mn	0,026	0,000	0,000	0,001	0,000	0,000	0,001	0,005	0,002	0,000	0,006	0,001	0,000
Fe2+	0,823	0,992	0,994	0,996	0,996	0,997	0,996	0,902	0,994	0,995	0,894	0,995	0,991
Fe3+	1,646	1,984	1,988	1,992	1,991	1,993	1,991	1,805	1,988	1,990	1,788	1,990	1,981
Ni	0,000	0,000	0,000	0,001	0,000	0,000	0,000	0,000	0,000	0,000	0,006	0,000	0,002
Na	0,005	0,000	0,002	0,000	0,002	0,000	0,001	0,001	0,000	0,001	0,000	0,002	0,003
K	0,003	0,000	0,000	0,000	0,000	0,000	0,000	0,000	0,000	0,000	0,001	0,000	0,000

Magnetite 3

Sample	133
Zone	12
SiO2	0,28
TiO2	0,12
Al2O3	0,02
V2O3	0,19
Cr2O3	1,37
MgO	0,00
CaO	0,03
MnO	0,05
FeO	30,55
Fe2O3	67,90
NiO	0,00
Na2O	0,01
K2O	0,00
Total	100,52
Si	0,011
Ti	0,003
Al	0,001
V	0,006
Cr	0,041
Mg	0,000
Ca	0,001
Mn	0,001
Fe2+	0,974
Fe3+	1,948
Ni	0,000
Na	0,001
K	0,000

Mica

Sample	203	203	203	203	56	56	56	171	171
Zone	2	2	5	5	3	4	6	6	6
SiO2	41,69	41,50	42,87	39,67	36,51	37,73	37,54	36,84	37,24
TiO2	0,38	0,26	0,27	0,27	0,93	1,07	1,09	2,22	2,15
Al2O3	14,10	13,25	13,00	14,77	15,42	14,86	14,60	14,90	14,71
Cr2O3	0,00	0,02	0,02	0,00	0,02	0,04	0,00	0,00	0,00
MgO	24,65	25,48	25,22	25,62	12,56	12,45	12,01	9,92	10,17
CaO	0,09	0,24	0,19	0,49	0,13	0,06	0,22	0,04	0,06
MnO	0,01	0,01	0,00	0,02	0,22	0,26	0,20	0,03	0,06
FeO	3,98	3,58	3,57	3,69	18,71	19,20	18,99	22,91	22,57
Fe2O3	0,00	0,00	0,00	0,00	0,00	0,00	0,00	0,00	0,00
Na2O	0,07	0,05	0,10	0,13	0,08	0,06	0,08	0,04	0,08
K2O	9,60	8,33	9,21	6,64	8,50	8,79	8,01	9,27	9,24
H2O	4,23	4,18	4,25	4,14	3,87	3,92	3,87	3,91	3,92
Total	98,81	96,89	98,70	95,44	96,93	98,42	96,60	100,06	100,20
Si	5,908	5,950	6,049	5,740	5,661	5,767	5,820	5,655	5,696
Ti	0,041	0,028	0,028	0,029	0,108	0,122	0,127	0,256	0,247
Al	2,354	2,239	2,162	2,519	2,818	2,677	2,668	2,696	2,652
Cr	0,000	0,002	0,002	0,000	0,002	0,004	0,000	0,000	0,000
Mg	5,207	5,446	5,306	5,526	2,903	2,836	2,775	2,270	2,318
Ca	0,013	0,037	0,029	0,076	0,021	0,010	0,036	0,006	0,010
Mn	0,001	0,001	0,000	0,002	0,028	0,034	0,027	0,003	0,008
Fe2+	0,472	0,429	0,421	0,447	2,426	2,455	2,463	2,941	2,886
Fe3+	0,000	0,000	0,000	0,000	0,000	0,000	0,000	0,000	0,000
Na	0,019	0,014	0,027	0,037	0,024	0,017	0,023	0,012	0,023
K	1,736	1,523	1,657	1,225	1,681	1,714	1,585	1,816	1,802
OH	4,000	4,000	4,000	4,000	4,000	4,000	4,000	4,000	4,000

Miscellaneous oxides 1

Sample	45	45	45	45	90	90	96	48	48	65	65	65	65
Zone	6	6	7	8	5	6	3	2	2	7	7	6	6
SiO2	1,13	1,64	2,05	1,82	0,24	0,28	3,25	0,65	0,89	4,16	5,12	0,13	0,02
TiO2	0,00	0,01	0,01	0,01	0,00	0,02	0,00	0,02	0,00	0,03	0,03	3,20	2,11
Al2O3	0,01	0,17	0,01	0,32	0,14	1,59	0,34	0,03	0,24	0,43	0,55	0,04	0,06
V2O3	0,00	0,00	0,03	0,01	0,08	0,04	0,57	0,04	0,05	0,01	0,00	0,15	0,21
Cr2O3	0,00	0,00	0,00	0,06	0,00	0,00	0,00	0,00	0,01	0,00	0,00	0,01	0,00
MgO	0,27	0,28	0,35	0,57	0,05	0,04	1,09	0,18	0,26	0,27	0,63	0,02	0,02
CaO	0,02	0,03	0,06	0,19	0,05	0,01	0,86	0,05	0,07	0,41	0,16	0,00	0,00
MnO	0,09	0,05	0,11	0,09	0,02	0,04	0,14	0,04	0,03	0,14	0,25	0,01	0,04
Fe2O3	85,22	83,14	83,71	82,04	87,94	85,88	78,55	85,24	84,71	86,35	77,45	95,83	97,94
NiO	0,00	0,00	0,00	0,01	0,00	0,00	0,05	0,02	0,01	0,21	0,29	0,00	0,00
Na2O	0,01	0,01	0,02	0,00	0,04	0,03	0,02	0,00	0,01	0,03	0,03	0,02	0,00
K2O	0,00	0,00	0,00	0,00	0,02	0,00	0,00	0,00	0,00	0,00	0,06	0,00	0,00
H2O	9,79	9,63	9,74	9,61	9,99	9,92	9,58	9,73437	9,73	10,39	9,54	11,22	11,33
Total	96,54	94,95	96,09	94,73	98,56	97,85	94,46	96,00	96,01	102,42	94,11	110,63	111,74

Sample	65	65	65	65	65	65	65	1004	1004	1004	1004	1004	1004
Zone	4	4	4	3	2	1	1	3	3	3	4	4	4
SiO2	3,96	4,13	3,06	4,03	5,03	4,63	4,81	3,75	3,56	3,27	3,23	3,40	2,80
TiO2	0,00	0,01	0,03	0,04	0,05	0,03	0,05	0,02	0,00	0,01	0,03	0,01	0,00
Al2O3	0,13	0,33	0,33	3,48	0,75	0,73	3,78	0,86	1,05	0,64	0,79	0,62	1,34
V2O3	0,00	0,06	0,07	0,00	0,00	0,10	0,07	0,00	0,00	0,00	0,00	0,00	0,00
Cr2O3	0,00	0,00	0,00	0,02	0,01	0,03	0,03	0,00	0,01	0,00	0,00	0,03	0,00
MgO	0,14	0,27	0,58	0,46	0,18	0,36	0,52	0,25	0,22	0,21	0,22	0,22	0,02
CaO	0,16	0,37	0,35	0,21	0,41	0,42	0,79	0,24	0,20	0,21	0,16	0,21	0,01
MnO	0,23	0,09	0,25	0,09	0,01	0,15	0,20	0,06	0,02	0,06	0,03	0,04	0,08
Fe2O3	83,16	87,25	85,80	77,84	88,76	80,99	74,89	90,12	90,16	90,52	90,39	90,31	81,62
NiO	0,22	0,14	0,20	0,00	0,00	0,20	0,11	0,03	0,00	0,04	0,00	0,03	0,03
Na2O	0,01	0,04	0,06	0,03	0,08	0,05	0,04	0,03	0,04	0,04	0,05	0,05	0,00
K2O	0,00	0,01	0,00	0,01	0,05	0,01	0,01	0,03	0,02	0,01	0,02	0,00	0,02
H2O	9,93	10,46	10,24	9,73	10,76	9,89	9,62	10,76	10,75	10,72	10,71	10,71	9,69
Total	97,94	103,16	100,96	95,91	106,08	97,57	94,91	106,13	106,05	105,72	105,61	105,66	95,60

Miscellaneous oxides 2

Sample	1004	1004	1004	1004	1004	1004	1004	1004	1004	1004	1004
Zone	5	5	6	7	7	8	8	9	10	10	10
SiO2	1,78	1,95	8,21	2,66	2,32	3,34	2,55	2,31	1,81	2,45	1,82
TiO2	0,01	0,00	0,03	0,00	0,04	0,01	0,00	0,04	0,02	0,00	0,00
Al2O3	3,59	2,10	0,54	0,85	1,42	0,39	0,55	0,98	1,16	0,65	1,09
V2O3	0,03	0,02	0,04	0,03	0,00	0,04	0,03	0,01	0,04	0,00	0,02
Cr2O3	0,00	0,03	0,00	0,00	0,00	0,02	0,02	0,00	0,00	0,00	0,01
MgO	0,36	0,06	0,41	0,57	0,38	0,30	0,05	0,14	0,29	0,43	0,68
CaO	0,30	0,04	0,22	0,25	0,23	0,10	0,04	0,08	0,11	0,15	0,22
MnO	0,14	0,13	0,28	0,17	0,13	0,28	0,17	0,10	0,15	0,21	0,17
Fe2O3	76,48	82,02	76,19	79,17	79,49	80,95	81,34	81,00	80,96	80,71	78,94
NiO	0,03	0,00	0,00	0,00	0,01	0,01	0,00	0,02	0,00	0,01	0,00
Na2O	0,15	0,03	0,07	0,02	0,07	0,05	0,02	0,07	0,06	0,02	0,05
K2O	0,00	0,01	0,00	0,00	0,00	0,00	0,00	0,00	0,00	0,00	0,00
H2O	9,35	9,75	9,70	9,45	9,49	9,65	9,56	9,56	9,55	9,55	9,37
Total	92,23	96,12	95,68	93,17	93,58	95,14	94,33	94,32	94,14	94,18	92,36

Mn oxyhydroxide 1

Sample	15	15	15	15	15	15	15	15	15	15	15	15	15
Zone	1	1	1	2	2	3	3	3	3	3	3	4	4
SiO2	0,25	0,57	0,13	2,24	0,19	0,95	1,06	1,86	0,66	0,84	0,64	0,10	0,43
TiO2	0,00	0,01	0,00	0,01	0,00	0,04	0,01	0,00	0,00	0,01	0,00	0,01	0,00
Al2O3	2,51	6,19	0,38	4,85	1,88	5,15	5,09	6,05	3,94	4,50	4,54	0,84	5,42
V2O3	0,00	0,00	0,00	0,08	0,00	0,00	0,00	0,00	0,02	0,02	0,05	0,00	0,08
Cr2O3	0,00	0,01	0,00	0,09	0,00	0,05	0,00	0,00	0,00	0,03	0,03	0,02	0,00
MgO	0,14	0,52	0,04	0,53	0,10	0,69	0,71	0,71	0,64	0,73	0,89	0,21	0,35
CaO	0,34	0,53	0,37	0,76	0,29	0,63	0,69	0,72	0,65	0,61	0,77	0,45	0,42
MnO	2,93	2,61	3,06	2,61	2,98	2,64	2,61	2,48	2,68	2,65	2,62	2,81	2,59
MnO2	79,16	70,50	82,53	70,45	80,42	71,17	70,39	66,92	72,38	71,46	70,75	75,77	70,00
Fe2O3	0,00	0,00	0,00	0,00	0,00	0,00	0,00	0,00	0,00	0,00	0,00	0,00	0,00
NiO	0,10	0,66	0,00	0,55	0,00	0,57	0,68	0,62	0,70	0,66	0,79	0,01	0,41
Na2O	0,97	0,88	1,40	1,33	0,85	1,48	1,32	1,24	1,13	1,25	1,64	2,00	1,09
K2O	4,11	3,40	3,45	3,09	4,28	2,95	2,81	2,96	3,03	3,04	2,44	1,64	3,07
H2O	4,38	4,16	4,42	4,19	4,40	4,18	4,13	4,04	4,15	4,15	4,12	4,06	4,06
Total	94,89	90,03	95,78	90,79	95,38	90,50	89,49	87,62	89,97	89,96	89,30	87,92	87,93

Mn oxyhydroxide 2

Sample	15	15	15	15	15	9	9	9	9	9	9	9	9
Zone	5	5	5	5	5	1	1	1	2	3	3	3	3
SiO2	0,34	0,32	0,11	0,30	0,39	0,67	0,69	0,48	0,51	0,22	0,23	0,31	0,28
TiO2	0,02	0,00	0,02	0,01	0,00	0,01	0,01	0,01	0,03	0,00	0,00	0,00	0,02
Al2O3	4,20	4,38	0,65	4,10	4,94	8,74	7,91	5,43	4,04	2,73	3,04	3,76	2,76
V2O3	0,00	0,03	0,07	0,15	0,06	0,00	0,00	0,03	0,03	0,00	0,00	0,00	0,10
Cr2O3	0,00	0,00	0,00	0,03	0,00	0,01	0,02	0,00	0,03	0,01	0,00	0,00	0,03
MgO	0,35	0,38	0,08	0,41	0,33	0,20	0,21	0,11	0,21	0,11	0,16	0,16	0,12
CaO	0,52	0,45	0,44	0,47	0,48	0,24	0,31	0,19	0,22	0,17	0,21	0,22	0,25
MnO	2,70	2,78	3,04	2,75	2,71	2,58	2,58	2,78	2,56	2,89	2,86	2,84	2,86
MnO2	72,76	74,97	81,95	74,30	73,08	69,58	69,69	75,14	68,99	77,89	77,07	76,67	77,21
Fe2O3	0,00	0,00	0,00	0,00	0,00	0,00	0,00	0,00	4,66	0,00	0,00	0,00	0,00
NiO	0,32	0,27	0,00	0,32	0,31	0,21	0,20	0,19	0,04	0,05	0,08	0,08	0,09
Na2O	1,21	1,17	1,45	1,41	1,24	1,61	1,61	0,71	1,00	0,81	0,69	0,68	0,68
K2O	3,33	3,28	3,25	3,16	3,35	3,05	3,08	4,58	3,44	4,49	4,25	4,29	4,52
H2O	4,15	4,26	4,41	4,23	4,21	4,21	4,18	4,34	4,15	4,33	4,29	4,31	4,30
Total	89,89	92,28	95,46	91,64	91,09	91,10	90,49	93,99	89,91	93,69	92,87	93,33	93,22

Mn oxyhydroxide 3

Sample	9	9	9	9
Zone	4	6	6	6
SiO2	0,76	0,36	0,28	0,30
TiO2	0,00	0,00	0,01	0,00
Al2O3	7,08	2,90	3,24	3,19
V2O3	0,03	0,09	0,01	0,02
Cr2O3	0,00	0,00	0,00	0,01
MgO	0,08	0,11	0,08	0,05
CaO	0,24	0,11	0,13	0,15
MnO	2,49	2,91	2,88	2,89
MnO2	67,07	78,54	77,73	78,03
Fe2O3	3,16	0,00	0,00	0,00
NiO	0,05	0,06	0,02	0,02
Na2O	1,37	0,25	0,21	0,21
K2O	3,26	4,99	4,88	5,19
H2O	4,14	4,37	4,33	4,36
Total	89,72	94,69	93,80	94,44

Titanite

Sample	120	120	120	120	120	171	133	133	133	53
Zone	4	4	5	5	6	5	11	12	7	3
SiO2	32,13	31,16	32,09	32,12	31,96	31,52	32,24	30,46	32,99	31,02
TiO2	39,95	39,54	39,81	39,39	39,13	34,32	39,17	34,59	34,95	31,45
Al2O3	0,56	0,70	0,66	0,70	0,84	1,99	0,47	1,69	1,60	2,87
V2O3						0,11		0,00	0,00	0,00
Cr2O3						0,17		0,69	0,03	0,02
MgO	0,00	0,00	0,00	0,00	0,00	0,15	0,00	0,75	0,34	0,05
CaO	28,07	27,71	28,18	28,10	28,01	26,31	28,04	25,76	27,06	26,49
MnO	0,07	0,06	0,00	0,06	0,00	0,01	0,00	0,03	0,03	0,08
FeO	0,00	0,00	0,00	0,00	0,00	0,00	0,00	0,00	0,00	0,00
Fe2O3	0,48	0,83	0,34	0,37	0,38	2,52	0,48	6,16	2,27	4,60
NiO						0,03		0,00	0,00	0,00
Na2O	0,01	0,01	0,02	0,01	0,00	0,03	0,05	0,00	0,06	0,08
K2O	0,00	0,01	0,00	0,00	0,01	0,03	0,00	0,00	0,01	0,09
H2O	0,00	0,00	0,00	0,00	0,00	0,00	0,00	0,00	0,00	0,00
Total	101,28	100,02	101,09	100,73	100,33	97,17	100,46	100,13	99,34	96,75
Si	1,029	1,014	1,030	1,034	1,033	1,052	1,041	0,999	1,074	1,046
Ti	0,963	0,967	0,961	0,954	0,951	0,861	0,951	0,853	0,856	0,798
Al	0,021	0,027	0,025	0,026	0,032	0,078	0,018	0,065	0,062	0,114
V						0,003	0,000	0,000	0,000	0,000
Cr						0,004	0,000	0,018	0,001	0,000
Mg	0,000	0,000	0,000	0,000	0,000	0,007	0,000	0,037	0,017	0,002
Ca	0,964	0,966	0,969	0,969	0,970	0,941	0,970	0,905	0,944	0,957
Mn	0,002	0,002	0,000	0,001	0,000	0,000	0,000	0,001	0,001	0,002
Fe2+	0,000	0,000	0,000	0,000	0,000	0,000	0,000	0,000	0,000	0,000
Fe3+	0,012	0,020	0,008	0,009	0,009	0,063	0,012	0,152	0,056	0,117
Ni						0,001	0,000	0,000	0,000	0,000
Na	0,001	0,001	0,001	0,001	0,000	0,002	0,003	0,000	0,004	0,005
K	0,000	0,000	0,000	0,000	0,000	0,001	0,000	0,000	0,000	0,004
OH	0,000	0,000	0,000	0,000	0,000	0,000	0,000	0,000	0,000	0,000